

SC5056.4FR

LEVEL

III
A059 946

12

SC5056.4FR

COPY NO. 9

AD A068810

MECHANICAL BEHAVIOR OF TITANIUM ALLOYS

FINAL REPORT

Submitted to:

Office of Naval Research

Prepared by:

C.G. Rhodes and N.E. Paton

DDC FILE COPY

DDC
RECEIVED
MAY 21 1979
RECEIVED
47
D

Approved for Public Release; Distribution Unlimited.



Rockwell International
Science Center

05 18 001

Unclassified

SECURITY CLASSIFICATION OF THIS PAGE (When Data Entered)

REPORT DOCUMENTATION PAGE		READ INSTRUCTIONS BEFORE COMPLETING FORM
1. REPORT NUMBER	2. GOVT ACCESSION NO.	3. RECIPIENT'S CATALOG NUMBER
4. TITLE (and Subtitle) Mechanical Behavior of Titanium Alloys.		5. TYPE OF REPORT & PERIOD COVERED Final Report 2/1/76 through 1/31/79
6. AUTHOR(s) C.G. Rhodes and N.E. Paton		7. PERFORMING ORG. REPORT NUMBER SC5056.4FR
8. CONTRACT OR GRANT NUMBER(s) N00014-76-C-0598		9. PROGRAM ELEMENT, PROJECT, TASK AREA & WORK UNIT NUMBERS NR 031-790 Project No. 471
10. CONTROLLING OFFICE NAME AND ADDRESS Dr. Bruce MacDonald Office of Naval Research 800 N. Quincy, Arlington, VA 22217		11. REPORT DATE April, 1979
12. MONITORING AGENCY NAME & ADDRESS (if different from Controlling Office) 12-127 P.		13. NUMBER OF PAGES 124
14. DISTRIBUTION STATEMENT (of this Report) Approved for public release; distribution unlimited.		15. SECURITY CLASS. (of this report) Unclassified
15a. DECLASSIFICATION/DOWNGRADING SCHEDULE		
16. DISTRIBUTION STATEMENT (of the abstract entered in Block 20, if different from Report) Final rept. 1 Feb 76 - 31 Jan 79		
17. SUPPLEMENTARY NOTES		
18. KEY WORDS (Continue on reverse side if necessary and identify by block number) Titanium alloys, fracture toughness, fatigue crack growth rate, hydrogen effects.		
19. ABSTRACT (Continue on reverse side if necessary and identify by block number) Conditions for the formation of the alpha-beta interface phase in Ti-6Al-4V have been determined, and the influence of this phase on mechanical properties examined. In previously reported work, it was shown that tensile yield strength could be increased by increasing the interface phase width. In the current work, it was found that fatigue crack propagation (FCP) resistance can also be improved by heat treatments which increase interface phase width. The		

DD FORM 1 JAN 73 1473 EDITION OF 1 NOV 65 IS OBSOLETE

Unclassified 389 949
SECURITY CLASSIFICATION OF THIS PAGE (When Data Entered)

05 10 00

Unclassified

SECURITY CLASSIFICATION OF THIS PAGE(When Data Entered)

improved FCP resistance was associated with an increase in secondary cracking, which propagated predominantly along alpha-beta interfaces, especially at higher stress levels. Fracture toughness was found to be relatively insensitive to interface phase width, so that treatments which improve both tensile yield strength and FCP resistance do not degrade fracture toughness. An influence on fracture toughness found in this study was banding of primary alpha particles parallel to the rolling direction. This type of microstructure exhibited a high fracture toughness for cracks propagating normal to the bands, and such effects appear to be larger than effects due to interface phase or volume fraction alpha. In a second part of the program, some effects of hydrogen in titanium alloys were studied. Hydrogen was observed to suppress the formation of omega phase in Ti-20V, and the presence of hydrogen altered the omega particle morphology from cuboidal to ellipsoidal in the early stages of growth. In an attempt to determine the solubility of hydrogen in beta titanium, a Ti-40V alloy was found to absorb 19,700 ppm by weight of hydrogen without the formation of hydride particles. The beta phase lattice parameter was increased by about 7% with the addition of 16,000 ppm hydrogen. Finally, it was also found that the addition of hydrogen to Ti-6Al-4V resulted in an improvement in room temperature tensile elongation from 11% for no hydrogen to 16% for 1000 ppm hydrogen. This result indicates a potential for hydrogen-assisted forming.

Unclassified

SECURITY CLASSIFICATION OF THIS PAGE(When Data Entered)



SC5056.4FR

PREFACE

This document is the final report on Contract N00014-76-C-0598 sponsored by the Office of Naval Research entitled, "Mechanical Behavior of Titanium Alloys". During the course of the program, extensive investigations of the α/β interface phase in Ti-6Al-4V and the behavior of hydrogen in β -phase alloys have been accomplished. Several technical reports and papers have resulted from the work and are included in Appendix I. For details of the earlier work, the reader is referred to these documents. The body of this report describes the results of research conducted in the final year of the contract during the period February 1978 through February 1979, which has not otherwise been published. The program was monitored by Dr. Bruce MacDonald of ONR and was conducted at the Rockwell International Science Center by Mr. Cecil Rhodes, Dr. Otto Buck, and Dr. Neil Paton, with technical assistance from Mr. Robert Spurling, Dr. John Wert, and Mr. Lloyd Ahlberg. Experimental assistance was provided by Mr. J.C. Chesnutt, Mr. M.W. Mahoney, Mr. P.Q. Sauer, and Ms. J.F. Wugalter. Dr. R. Jewett of the Rocketdyne Division of Rockwell International conducted the high pressure hydrogen tensile tests.

ACCESSION BY	
DTIC	White Section <input checked="" type="checkbox"/>
DDC	Dark Section <input type="checkbox"/>
UNANNOUNCED	<input type="checkbox"/>
JUSTIFICATION	
BY	
DISTRIBUTION/AVAILABILITY CODES	
Dist.	AVAIL. and/or SPECIAL
A	



SC5056.4FR

TABLE OF CONTENTS

	<u>Page</u>
PREFACE	i
LIST OF FIGURES.....	iv
1.0 INTRODUCTION.....	1
2.0 EXPERIMENTAL.....	4
3.0 RESULTS, PART I. THE INFLUENCE OF INTERFACE PHASE ON MECHANICAL PROPERTIES.....	6
3.1 Microstructural Considerations.....	6
3.2 Fracture Toughness.....	7
3.2.1 Alpha-Beta Processed.....	7
3.2.2 Beta Processed.....	15
3.3 Fatigue Crack Growth Rate.....	19
PART II. HYDROGEN EFFECTS.....	30
3.4 Omega Phase.....	30
3.5 Solubility of Hydrogen in Beta Phase.....	34
3.6 Influence of Hydrogen on Ductility in an α/β Alloy.....	34
3.7 Tensile Properties of Beta Titanium in High Pressure Hydrogen.....	35
4.0 DISCUSSION, PART I. THE INFLUENCE OF INTERFACE PHASE ON MECHANICAL PROPERTIES.....	39
4.1 Fracture Toughness.....	39
4.2 Fatigue Crack Growth Rate.....	40
PART II. HYDROGEN EFFECTS.....	42
4.3 Omega Phase.....	42
4.4 Solubility of Hydrogen in Beta Phase.....	42
4.5 Influence of Hydrogen on Ductility in an α/β Alloy.....	43



SC5056.4FR

TABLE OF CONTENTS (Cont'd)

	<u>Page</u>
4.6 Tensile Properties of Beta Titanium in High Pressure Hydrogen.....	43
5.0 CONCLUSIONS.....	44
6.0 REFERENCES.....	45
7.0 APPENDIX	46
7.1 Formation Characteristics of the α/β Interface Phase in Ti-6Al-4V.....	47
7.2 The Influence of α/β Interface Phase on Tensile Properties in Ti6-Al-4V.....	76
7.3 Effects of Hydrogen on Anisotropic Elastic Properties of FCC Ti Alloys.....	110



SC5056.4FR

LIST OF FIGURES

<u>Figure</u>		<u>Page</u>
1	Isometric view of Ti-6Al-4V used in Part I of the program. Note banding of primary alpha particles parallel to rolling plane (LT plane).....	9
2	Pole figures for Ti-6Al-4V plate used in Part I of the program. (a) [0002] poles; (b) [1010] poles.....	10
3	Scanning electron micrographs of fracture surface of Charpy bars. (a) perpendicular crack, moving in S direction; (b) parallel crack, moving in T direction. Crack direction is from left to right in both micrographs.....	13
4	Fracture toughness, K_Q , as a function of volume percent primary alpha in α/β processed Ti-6Al-4V.....	14
5	Fracture toughness, K_Q , as a function of interface phase width in α/β processed Ti-6Al-4V.....	16
6	Light micrograph of Ti-6Al-4V showing a band of several contiguous alpha grains (between arrows).....	17
7	Scanning electron micrographs of fracture surfaces of Charpy bars. (a) parallel crack, moving in T direction; (b) perpendicular crack, moving in S direction. Crack direction is from left to right in both micrographs. A portion of the fracture surface has been polished and etched to reveal the underlying microstructure in each micrograph.....	18
8	Fracture toughness, K_Q , as a function of interface phase width in β treated Ti-6Al-4V. Line drawn is linear least squares fit of data.....	22
9	Light micrographs of β treated Charpy bars illustrating variation in alpha phase plate size. (a) Test specimen #5; (b) Test specimen #1.....	23
10	Scanning electron micrographs of fracture surface of beta treated Charpy bars. (a) Test specimen #5; (b) Test specimen #1. Note the larger void size in (a).....	24
11	Fatigue crack propagation rate as a function of applied stress for three microstructural conditions of Ti-6Al-4V. The band is a typical scatter band for Ti-6Al-4V in RA condition.....	25



SC5056.4FR

LIST OF FIGURES (Cont'd)

<u>Figure</u>		<u>Page</u>
12	Fatigue crack propagation rate as a function of interface phase width (and volume percent primary alpha) for several applied stress levels.....	27
13	Scanning electron micrographs of fracture surfaces of FCP Ti-6Al-4V specimens at a stress level of 15 ksi/ $\sqrt{\text{in}}$. (a) Test specimen #1; (b) Test specimen #3. Crack direction is horizontal.....	28
14	Scanning electron micrographs of fracture surfaces of FCP Ti-6Al-4V specimens. (a) Test specimen #2, $\Delta K = 30$ ksi/ $\sqrt{\text{in}}$; (b) Test specimen #3, $\Delta K = 30$ ksi/ $\sqrt{\text{in}}$; (c) Test specimen #2, $\Delta K = 40$ ksi/ $\sqrt{\text{in}}$; (d) Test specimen #3, $\Delta K = 40$ ksi/ $\sqrt{\text{in}}$. Crack direction is horizontal.....	29
15	Micro hardness of Ti-20V as a function of aging time at 350°C for various levels of hydrogen.....	31
16	Dark field transmission electron micrographs showing omega phase particles in Ti-20V with various levels of hydrogen aged at 350°C for 28 hours. (a) No H; (b) 500 ppm H; (c) 1000 ppm H; (d) 2000 ppm H.....	32
17	Dark field transmission electron micrographs showing omega phase particle morphologies in Ti-20V aged for 20 minutes at 350°C with different levels of hydrogen. (a) No H; (b) 500 ppm H.....	33
18	Scanning electron micrographs of fracture surfaces of Beta-III titanium alloy solution treated at 745°C and tensile tested in (a) 5000 psi He, and (b) 5000 psi H ₂	38



SC5056.4FR

1.0 INTRODUCTION

The properties of titanium alloys are such that frequently the most severely loaded parts of a vehicle structure can most advantageously be fabricated from titanium, making a detailed understanding of the mechanical properties of titanium alloys of great importance. Although much has already been accomplished in recent years to further our understanding of the mechanical behavior of these materials, there are still several important areas where our knowledge is lacking. This report describes the results of a study in two such areas. Part I is directed at a specific aspect of the effect of microstructure of a two phase $\alpha + \beta$ Ti alloy on mechanical properties, while Part II is concerned with the effect of hydrogen on properties of β Ti alloys.

Part I of the program was a detailed study of the effect of some specific aspects of microstructure on the properties of the $\alpha + \beta$ Ti alloy Ti-6Al-4V. Ti-6Al-4V, when initially developed, was intended to be used in the solution treated and aged conditions. However, in the interests of higher fracture toughness, more and more material is being used in the "annealed" condition. Very little is known about the effects of annealing temperature and cooling rate on mechanical properties, and it is this void in our current knowledge at which Part I of this program was aimed. A wide variety of annealing treatments is used in the industry at present, some of which can give less than optimum performance.

Heat treatment is one technique available to alter mechanical properties in α/β titanium alloys such as Ti-6Al-4V. A change in properties is generally brought on by a change in the microstructure which occurs as a result of the heat treatment. Frequently, 6-4 is subjected to heat treatments during processing, or fabrication, where such heat treatments, which are not designed to improve properties may, in fact, be deleterious to properties. In particular, processes such as diffusion bonding require slow cooling from high in the α/β phase field. Studies performed in the preceding year of this program¹ have shown that slow cooling has a significant effect on the microstructure of 6-4 and an effect on tensile properties.



SC5056.4FR

The previous year's work under this program² showed that interface phase, which occurs in the α/β interfaces, does not grow isothermally, but grows only during cooling and the width of the interface phase is dependent upon cooling rate. Cooling rate also affects the volume fraction and, when cooled from above the beta transus, the morphology of primary alpha particles. The effects of both primary alpha and interface phase on tensile properties of Ti-6Al-4V were studied previously in this program.¹ The general trend observed was one of increasing tensile strength and decreasing tensile ductility with increasing volume fraction of primary alpha. There was, however, a fairly wide scatter band which was the result of a variation in interface phase width. The results indicate that yield strength can be increased by increasing the interface phase width, but that ductility is sacrificed.

The correlation of interface phase width and volume fraction primary alpha with tensile properties implies that other mechanical properties may also be affected by these microstructural features. Properties such as fatigue crack propagation and fracture toughness are important design parameters for structural materials such as Ti-6Al-4V. Part I of this report presents a summary of the results of a study of the influence of interface phase width and volume fraction primary alpha on fatigue crack propagation rate and fracture toughness. A more detailed account of previous work may be found in the published papers included in Appendix I.

In the past year, considerable progress has been made toward understanding the influence of hydrogen on mechanical properties of beta Ti alloys. Two alloy systems have been studied, Ti-V and Ti-Mo, and both are of interest on account of their ability to retain high concentrations of hydrogen in solid solution; as much as 10 atom percent hydrogen or more is soluble without resulting in hydride precipitation.

The significant observation which has been made in the past³ was that hydrogen in solid solution in certain beta Ti alloys decreases both the strength and the modulus, while increasing the lattice parameter. These observations could be attributed to either electronic interaction of the hydrogen with the host lattice, or a suppression of omega phase formation by



SC5056.4FR

addition of hydrogen. The latter argument is based on the observation that hydrogen is a beta stabilizer⁴ much like V or Mo and would, therefore, tend to reduce the tendency to form athermal omega phase in a given alloy. Omega phase precipitation causes larger increases in strength⁵ so that suppression of its formation might be expected to cause softening for this reason. Based on the recent results obtained in this program, the latter explanation appears to correlate with the observation most satisfactorily.

The data appear to indicate that the main influence of hydrogen additions is to stabilize the beta phase, decrease the tendency to form omega phase and, in doing so, lower the strength and decrease the modulus. Although there is probably an electronic contribution also, its magnitude is certainly smaller than the former effects. This observation raises the question as to whether hydrogen additions might be useful to lower the strength of commercial beta Ti alloys, and thereby improve their formability by reducing their tendency to form omega phase either at room temperature or at temperatures slightly above room temperature.

Part II of the program was a study of the effect of internal hydrogen on $\beta \rightarrow \omega$ transformation and on mechanical properties in β -Ti alloys. The former was intended to provide a confirmation of the explanation proposed in the preceding paragraphs and the latter was a preliminary examination of possible effects of hydrogen on formability. In addition, a limited number of tensile tests of a commercial beta Ti alloy, Beta III, were conducted in high pressure hydrogen to see if the tolerance of the beta phase to high hydrogen contents could be translated into good mechanical properties in hydrogen.



SC5056.4FR

2.0 EXPERIMENTAL

The alloy used in Part I of the program had a nominal composition of Ti-6Al-4V; the chemical analysis of this alloy is given in Table 1. The as-received microstructure consisted of ~90% equiaxed primary alpha particles, having approximately a 12 μ m diameter, in a continuous beta matrix. The Part II alloys were Ti-6Al-4V, Ti-20V and Ti-40V, all nominal compositions. The heat treatments were carried out with the samples, either in a dynamic inert gas atmosphere or encapsulated in evacuated ampoules. A programmable controller supplying power to the furnace was used for controlled-cooling-rate treatments. Hydrogen charging was accomplished using a conventional Sievert's apparatus.

Fracture toughness was measured by notched, precracked Charpy bars tested in slow bend. Compact tension specimens were used for fatigue crack growth rate measurements, which were carried out at 10 Hz and $R = 0.1$ in an MTS machine. Crack length was determined optically with the specimen removed from the testing machine. Tensile tests were conducted on an Instron testing machine equipped with a furnace. The samples were in the form of flat, strip specimens and elongation was determined by measuring the distance between fiducial marks under a travelling microscope.

Thin foils for transmission electron microscopy were prepared by conventional electropolishing techniques⁶ or by ion milling.⁷ The foils were examined in either a Philips EM300 or a Philips EM400 electron microscope, both equipped with double tilt goniometer stages. Fractography was carried out using an ETEC Autoscan scanning electron microscope.



SC5056.4FR

Table I
Composition by Weight of Ti-6Al-4V

Ti	Al	V	Fe	C	O	H	N
Bal	6.15	4.09	0.18	0.011	0.129	0.0067	0.019



SC5056.4FR

3.0 RESULTS

Part I. The Influence of Interface Phase on Mechanical Properties

3.1 Microstructural Considerations

The fracture toughness and fatigue crack propagation (FCP) tests were limited in the number of test specimens available and essentially represent a survey of the influence of interface phase and volume fraction primary alpha on these properties. Because of the limited number of specimens, a wide variation in interface phase width with all other microstructural features held constant was not attainable, unlike the previously reported¹ segment of this program studying the influence of interface phase on tensile properties.

The objective of this work was to examine the influence of interface phase width on toughness and FCP rate. In order to do this, samples must be treated so that only the interface phase width is varied and other microstructural features which can influence properties are held constant. Among these features which can influence properties is volume fraction of primary alpha phase. Since the interface phase only grows during slow cooling,² treatments which vary the interface phase width will also alter the volume fraction of primary alpha, and so this microstructural feature is not easily controlled.

Another feature which can affect properties is ordering in the primary alpha grains. The slow cooling treatments used to produce various interface phase widths are conducive to ordering in this alloy. Indeed, in two out of the ten fracture toughness test specimens, superlattice reflections were observed in the selected area electron diffraction (SAD) patterns, indicating the presence of Ti_3Al (α_2) particles within the primary alpha grains. In three additional fracture toughness specimens, very faint superlattice reflections were observed, indicating few α_2 particles in the primary alpha. For the remainder of the toughness test specimens and the FCP test specimens, no superlattice reflections were observed in the SAD patterns. However, the absence of superlattice reflection does not preclude the existence of some degree of order of the alpha phase; indeed, some order would be expected in an



SC5056.4FR

alloy with 6% Al given slow cooling treatments from high in the α/β phase field. Marcincowski and co-workers⁸ showed, some time ago, that dislocations moved in pairs through an ordered lattice and that the spacing of the pairs was a function of the degree of order of the lattice in which they were moving. Dislocation pairs were observed in the ECP samples and those toughness samples which did not show α_2 reflections and they were confirmed to be pairs of the same sign (i.e. dislocations moving in an ordered lattice) by $\pm g$ experiments.⁹ The spacings of the dislocations pairs was approximately constant in all the specimens, and it was therefore concluded that the degree of order was approximately the same in those samples.

Another microstructural feature which can influence mechanical properties is decomposition of the beta phase. That is, if the beta phase decomposes on cooling to fine alpha phase precipitates in the beta phase, properties can be affected. For the results presented in this report, there have been various degrees of β -phase decomposition and, although the results would indicate that the amounts of decomposition have not significantly influenced properties, the degree of decomposition will be pointed out for each of the tests specimens.

The foregoing remarks in this section indicate that microstructural features other than interface phase widths have not been held constant in all the test specimens. Because of the limited number of test specimens available, elimination from evaluation of test results from those specimens containing either superlattice reflections in the primary alpha or decomposed beta phase is not practical. Therefore, all test results will be included in the report and, although care must be taken in drawing detailed conclusions, some generalizations can be gleaned from the results.

3.2 Fracture Toughness

3.2.1 Alpha-Beta Processed

Charpy bars were machined from the Ti-6Al-4V rolled plate starting material and notched so that the crack ran in the ST plane, i.e., the plane normal to the rolling direction. For the α/β processed condition, the bars



SC5056.4FR

were notched such that the crack ran in the S direction in one-half the tests and in the T direction in the other half of the tests.

The bars were heat treated to produce a variation in interface phase width, which will also generally produce a variation in volume fraction primary alpha.² Examination of the microstructure after heat treatment revealed a banded appearance of the primary alpha, as shown in Fig. 1. The banding which is a resistance of the primary alpha particles in the band to the stain etch used to reveal the microstructure is parallel to the rolling plane. Examination of these banded regions by polarized light indicates that they are composed of alpha particles of a similar crystallographic orientation, different from the regions surrounding the bands. Texture analysis of the plate reveals [0001] poles concentrated in the rolling direction and in the transverse direction, Fig. 2a, and [1010] poles concentrated approximately 45° to L, T and S directions, Fig. 2b. It is not unambiguously clear whether the texture effects can be related to the banded regions or to the surrounding regions, but nevertheless the results indicate a concentration of basal planes parallel to the crack plane and an additional concentration of c-directions either parallel or perpendicular to the crack direction. It can be seen in Fig. 1 that a crack running in the S direction moves perpendicular to the bands of primary alpha and a crack moving in the T direction moves parallel to the bands. The former condition will be called a perpendicular crack and the latter condition will be called a parallel crack in subsequent discussion.

The test results of the α/β processed 6-4 are presented in Table II. The fracture toughness is considerably greater for a perpendicular crack orientation than for the parallel crack orientation. Fractography of the various samples revealed that the fracture topography was strongly influenced by the underlying banded microstructure, Fig. 3. The interface phase widths vary from 635A to 5235A, while the volume fractions of primary alpha vary from 0.68 to 0.86. A plot of toughness as a function of primary alpha is shown in Fig. 4, where it can be seen that, for a parallel crack orientation, there is no influence of volume fraction primary alpha on K_Q . It can also be seen that there is no influence of the higher degree of order in test samples numbers 8 and 10, and no influence of beta phase decomposition on K_Q in these samples.



Rockwell International
Science Center
SC5056.4FR

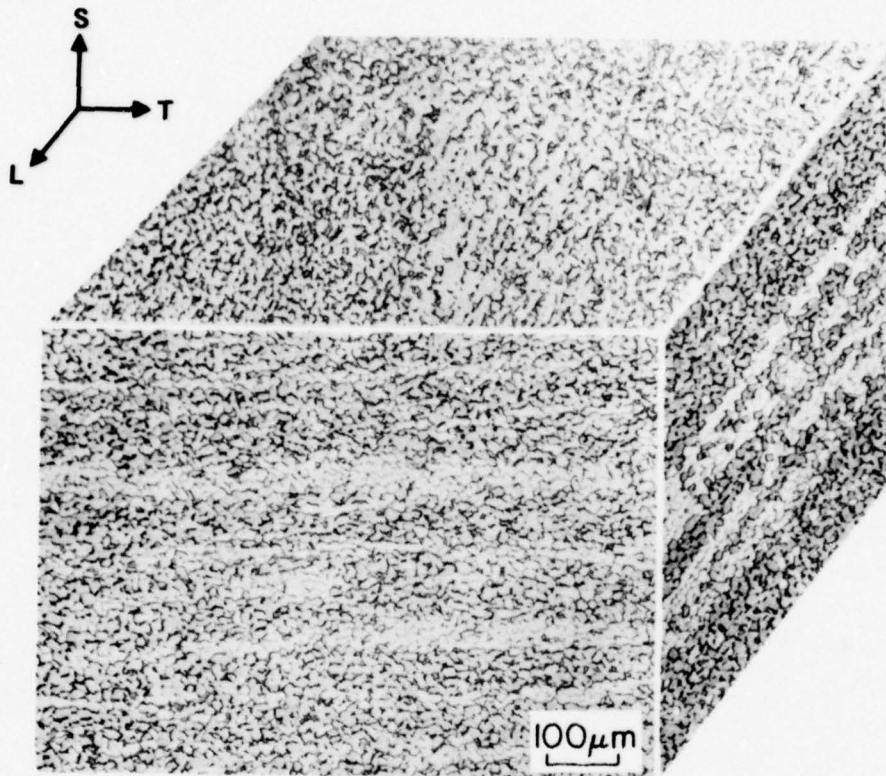


Fig. 1 Isometric view of Ti-6Al-4V used in Part I of the program.
Note banding of primary alpha particles parallel to rolling
plane (LT plane).



Rockwell International
Science Center

SC5056.4FR

PROGRAM TECOL1
VERSION COL1B1
RUN DATE 02/05/79

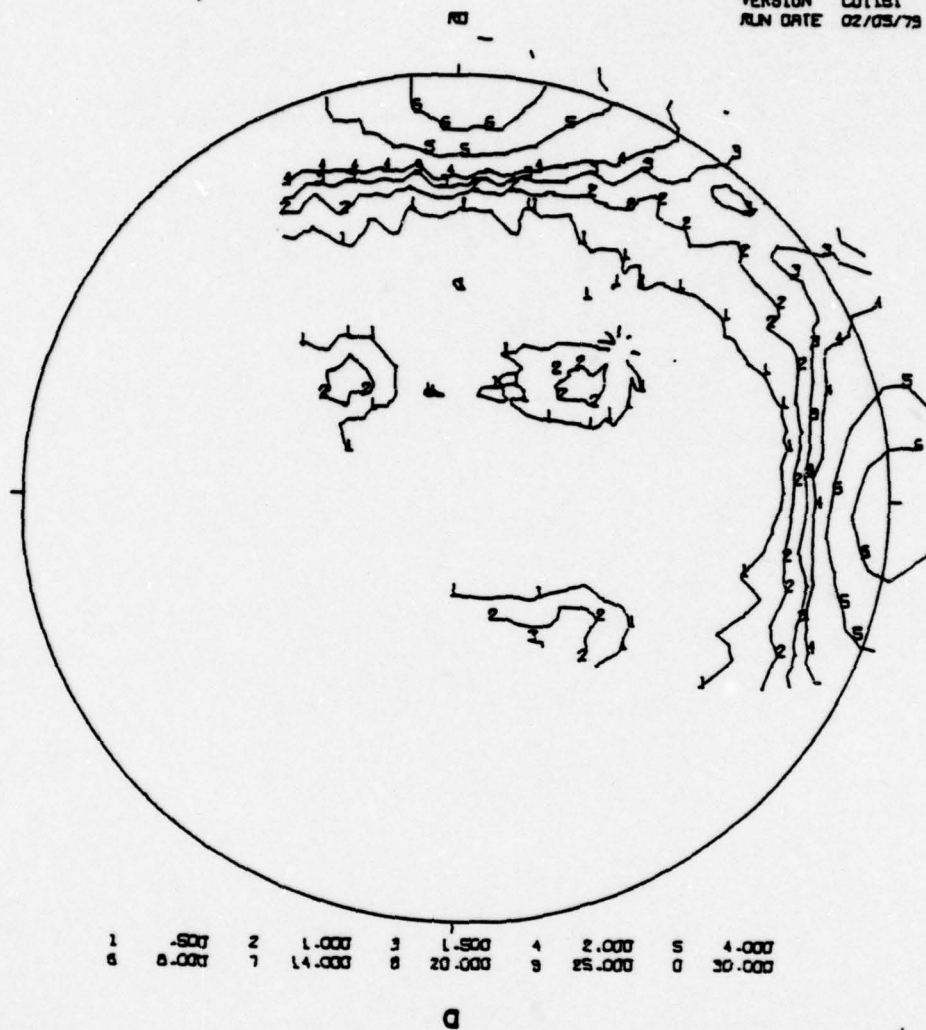


Fig. 2 Pole figures for Ti-6Al-4V plate used in Part I of program
(a) [0002] poles; (b) [10T0] poles.



SC5056.4FR

PROGRAM	TECOLL
VERSION	COLLBI
RUN DATE	02/05/79

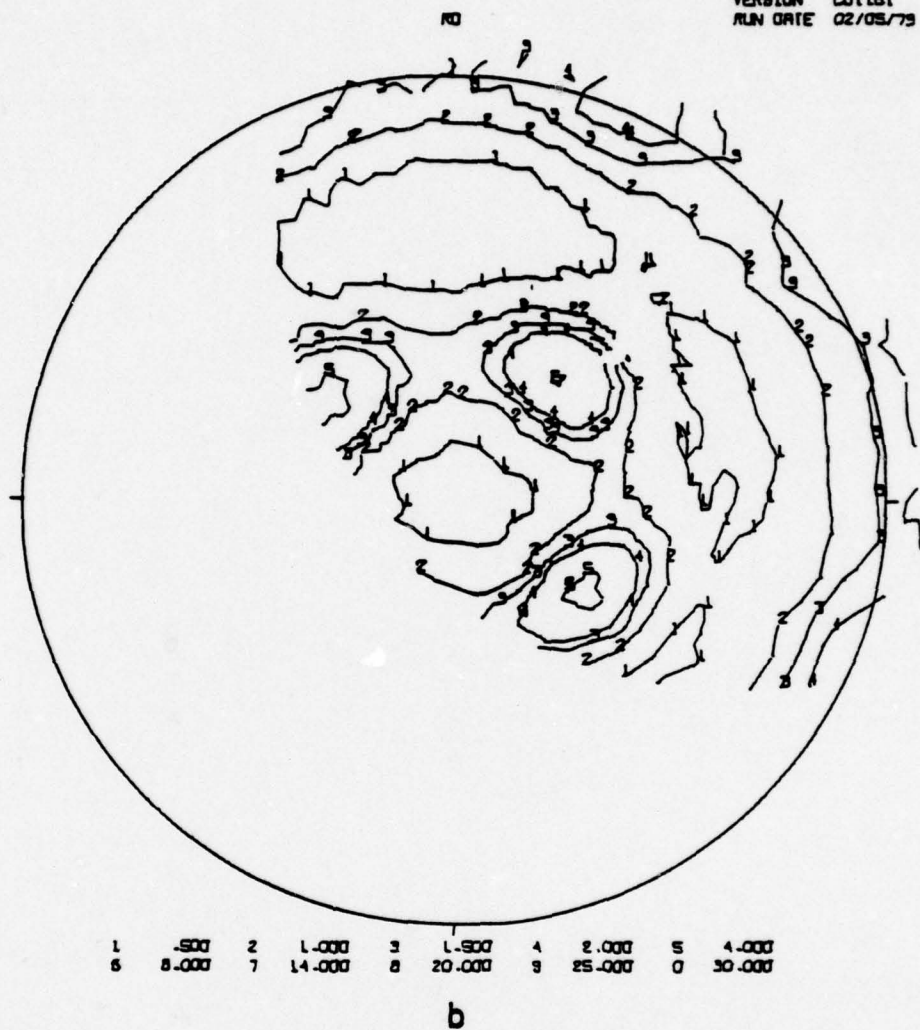


Figure 2



Table II

Charpy Bar Slow Bend Test Results for α/β Processed Ti-6Al-4V

Test #	Crack Orientation	KQ (ksi $\sqrt{\text{in}}$)	Volume Fraction Primary Alpha	Interface Phase Width (Å)	Superlattice Reflections in α	Beta Phase Decomposition
1	Perpendicular	140	0.85	3295	Yes	None
2	Perpendicular	130	0.84	2930	Yes	None
3	Perpendicular	107	0.83	3760	No	Considerable
4	Perpendicular	103	0.82	2225	No	None
5	Perpendicular	96	0.84	5235	Faint	None
6	Parallel	73	0.78	920	No	Slight
7	Parallel	72	0.83	5050	No	Considerable
8	Parallel	70	0.86	3825	Faint	None
9	Parallel	69	0.68	635	No	Slight
10	Parallel	67	0.81	1785	Faint	None

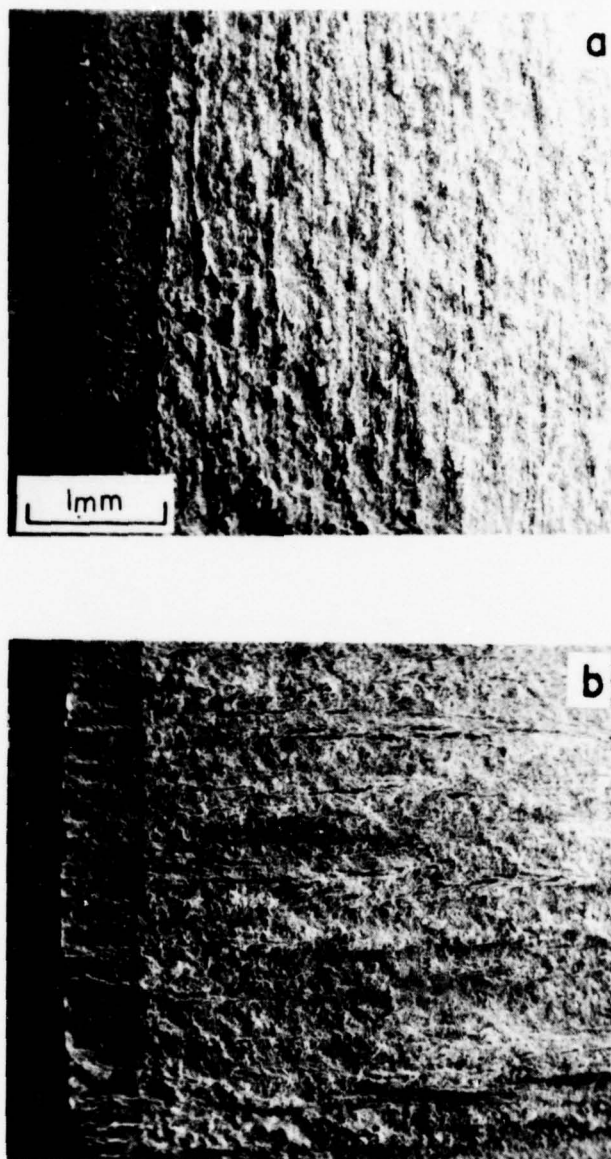


Fig. 3 Scanning electron micrographs of fracture surface of Charpy bars. (a) perpendicular crack, moving in S direction; (b) parallel crack, moving in T direction. Crack direction is from left to right in both micrographs.

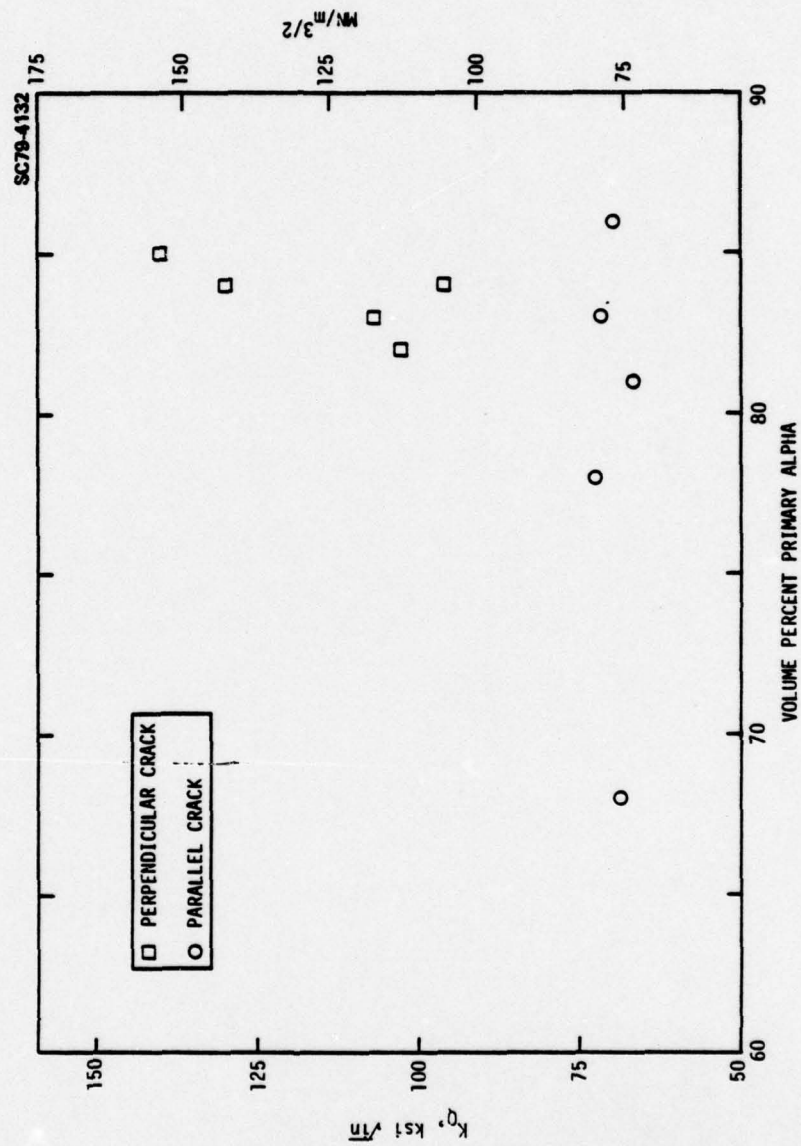


Fig. 4 Fracture toughness, K_Q , as a function of volume percent primary alpha in α/β processed Ti-6Al-4V.



SC5056.4FR

For the perpendicular crack orientation, the volume fraction of primary alpha does not vary significantly, but there is a large variation in K_Q . The two tests having the greatest toughness values also exhibited strong superlattice reflections indicating the high degree of order in these samples has likely influenced toughness. There is no influence of β -phase decomposition on toughness as can be seen by comparing test samples #3 and 4.

The same data can be plotted as a function of interface phase width, Fig. 5. For the parallel crack orientation, there is no dependence of K_Q on interface phase width for a wide variation in widths (635 to 5050Å). Similarly, there is essentially no influence of interface phase width on K_Q of samples oriented for a perpendicular crack.

Although neither interface phase width nor volume fraction primary alpha influence K_Q , there is a significant effect of microstructure as manifested by sample orientation. The presence of the bands of alpha grains, which have grown in a similar crystallographic orientation, has clearly influenced the crack extension. Closer inspection of the bands of alpha grains reveals that frequently several grains contact without the presence of β -phase between them, Fig. 6. When this occurs, the crack propagates by void coalescence (hole growth) along these several grains, with the growth uninterrupted by the presence of a grain boundary devoid of β -phase. This results in large elongated voids in the fracture face, as shown in Fig. 7. The wavy lines within the large voids are serpentine glide resulting from the intersection of slip with the void surface; they are seen to be related to the crystallographic orientation of the underlying α particle and not a function of crack direction. The serpentine glide within the large voids is indicative of deformation prior to the void joining the crack and opening up.

3.2.2 Beta Processed

Notched Charpy bars were solution treated above the beta transus (at 1015°C) for 15 minutes and water quenched in order to produce a fine acicular alpha microstructure. The bars were then heat treated to generate various interface phase widths. These treatments involve heating high in the α/β



SC5056.4FR

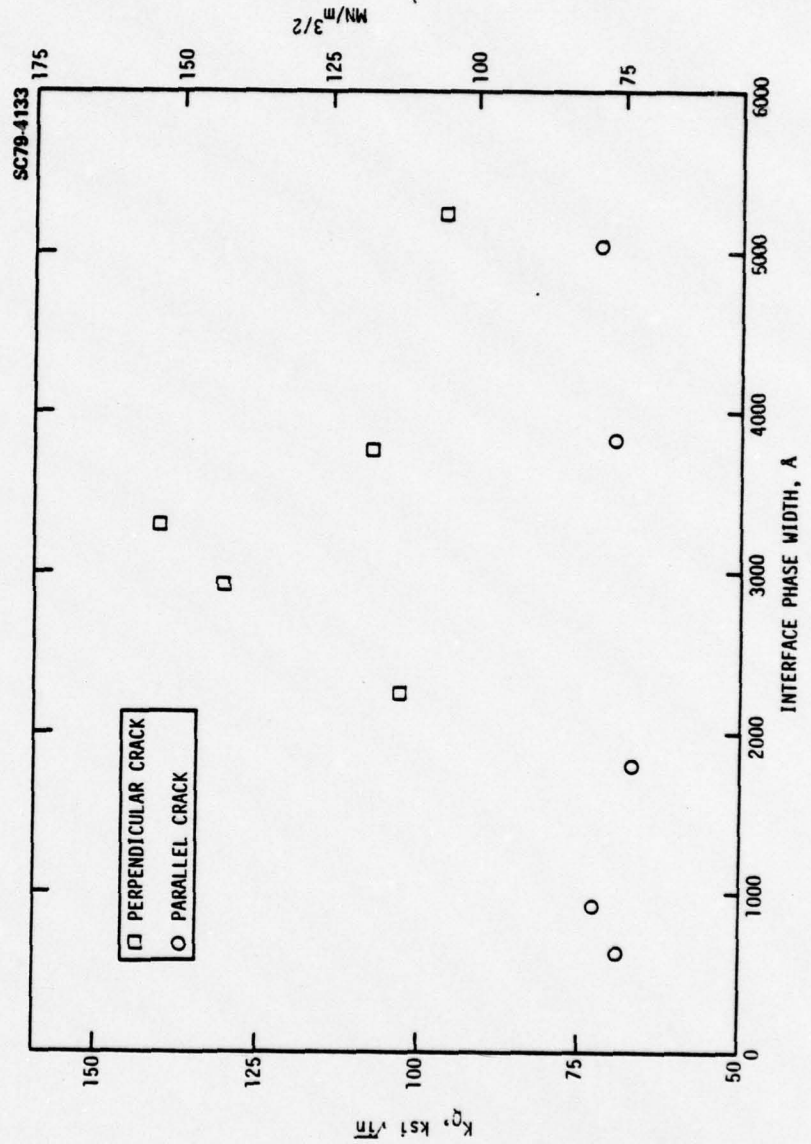


Fig. 5 Fracture toughness, K_Q , as a function of interface phase width in α/β processed Ti-6Al-4V.



Rockwell International
Science Center
SC5056.4FR

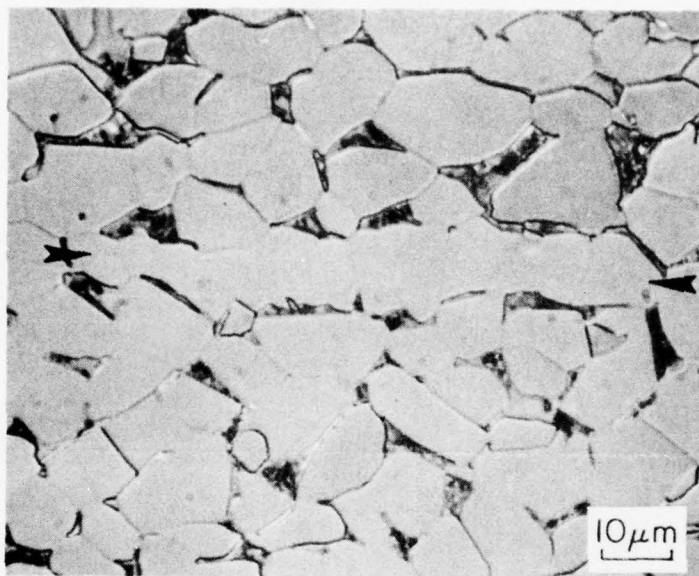


Fig. 6 Light micrograph of Ti-6Al-4V showing a band of several contiguous alpha grains (between arrows).

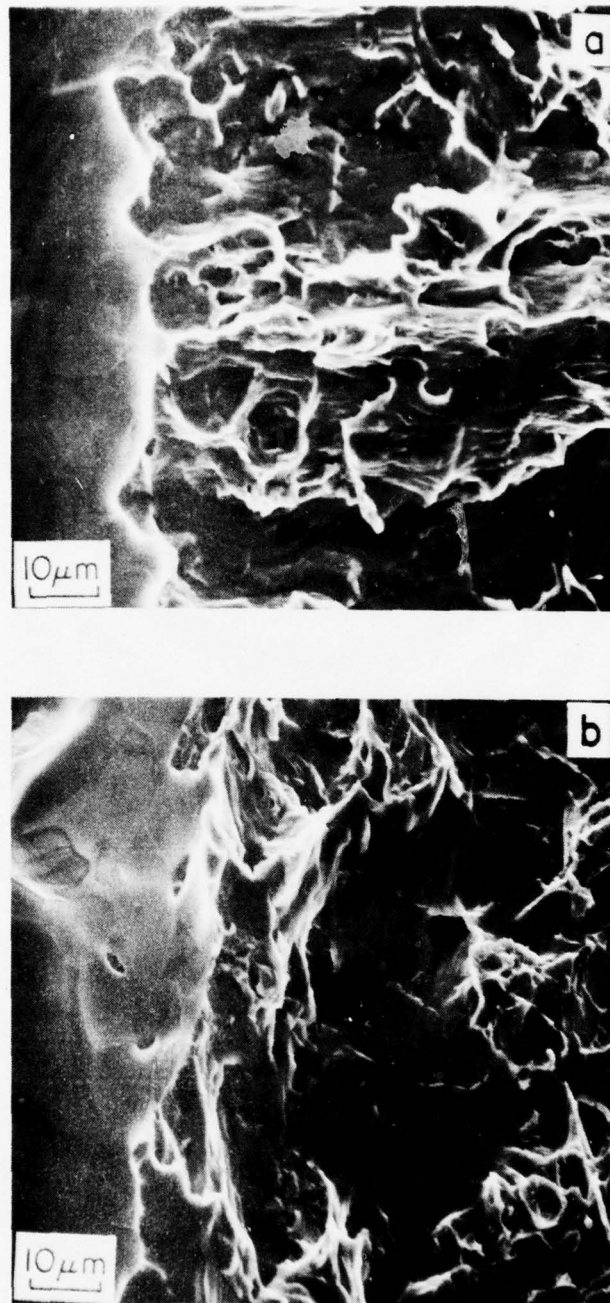


Fig. 7 Scanning electron micrographs of fracture surfaces of Charpy bars. (a) parallel crack, moving in T direction; (b) perpendicular crack, moving in S direction. Crack direction is from left to right in both micrographs. A portion of the fracture surface has been polished and etched to reveal the underlying microstructure in each micrograph.



SC5056.4FR

phase field followed by slow cooling; consequently the resulting microstructures not only show a variation in interface phase width, but there is also a variation in the aspect ratio of the acicular alpha phase particles.

The test results of the β processed 6-4 are presented in Table III. The aspect ratios of the alpha particles in each of the test specimens is listed in Table III; however, no measurements of volume fraction of alpha phase were made. The toughness is plotted as a function of interface phase width in Fig. 8, in which the curve drawn is a linear least squares fit. The curve indicates a positive correlation of K_Q with interface phase width, but there is considerable scatter. The variation in alpha phase particle size is illustrated in Fig. 9, where the samples with the largest and smallest K_Q are shown. Fractography revealed that the fracture surfaces of the high toughness samples were more tortuous with extensive secondary cracking than the fractures of lower toughness samples, which showed no secondary cracking. The fracture surfaces of the high and low toughness samples are shown at high magnification in Fig. 10. It can be seen that the void size is much smaller in the high toughness sample, 10b, than in the low toughness sample, 10a.

3.3 Fatigue Crack Growth Rate

Compact tension specimens were given sub-transus heat treatments intended to produce a wide variation in interface phase widths. This portion of the program was essentially an investigatory examination of the influence of interface phase width on fatigue crack propagation (FCP) rates in equiax primary alpha microstructures. Only three samples were tested, but these were heat treated so that the interface phase widths varied considerably. As expected, the volume fraction of primary alpha phase also varied. These parameters are listed in Table IV. For these results, then, it will be difficult to separate out the influence of interface phase on FCP, since volume fraction primary alpha also varies significantly.

The results of the tests, which were run at 20°C in dry laboratory air, are presented in Fig. 11. It can be seen that at the low ΔK region ($\Delta K \approx 10 \text{ ksi}/\sqrt{\text{in}}$) there is little difference in FCP rate among the three



Table III

Charpy Bar Slow Bend Test Results for β Processed Ti-6Al-4V

Test #	K_{IC} (ksi \sqrt{in})	Interface Phase Width (\AA)	Alpha Phase Aspect Ratio	Superlattice Reflections in α	Beta Phase Decomposition
1	136	2670	20	No	None
2	122	3700	20	No	None
3	90	2510	22	No	None
4	85	2685	22	No	None
5	81	410	36	No	None



SC5056.4FR

Table IV
Microstructural Parameters of Fatigue Specimens

Test #	Volume Fraction Primary α	Interface Phase Width, A	Superlattice Reflections	Beta Phase Decomposition
1	0.71	640	No	Considerable
2	0.82	2070	No	Slight
3	0.92	4135	No	None



SC5056.4FR

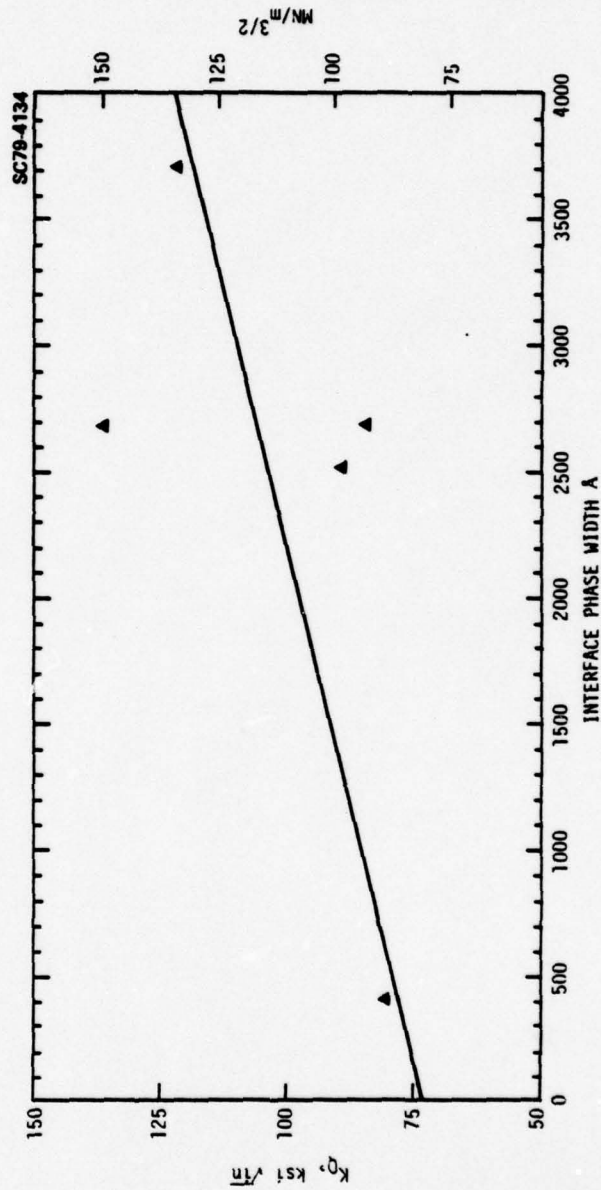


Fig. 8 Fracture toughness, K_Q , as a function of interface phase width in β treated Ti-6Al-4V. Line is linear test squares fit of data.

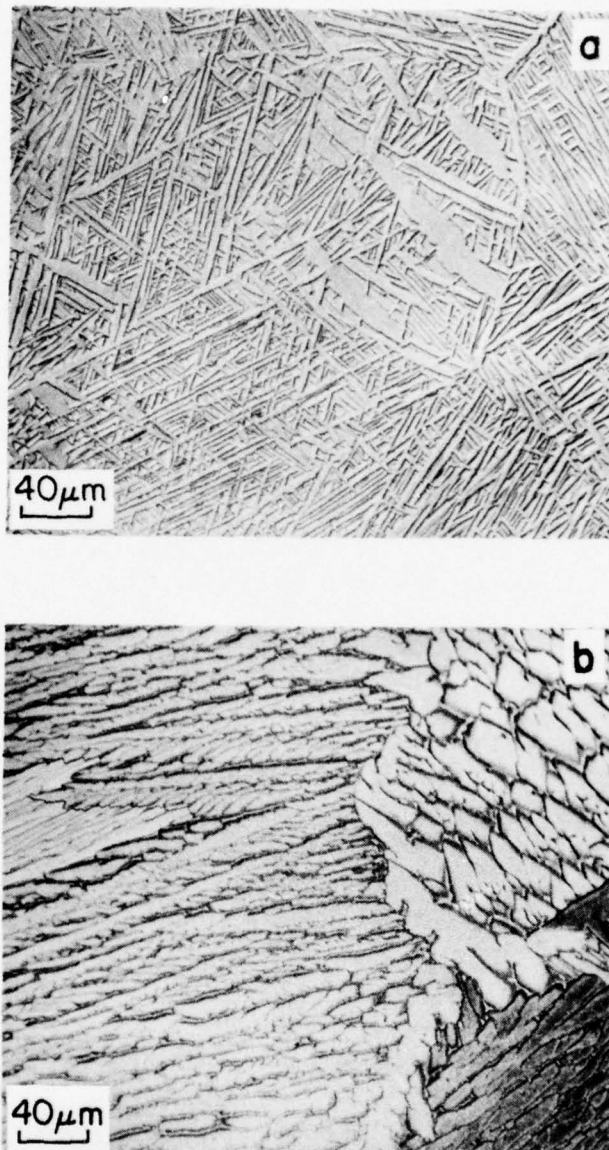


Fig. 9 Light micrographs of β treated Charpy bars illustrating variation in alpha phase plate size. (a) test specimen #5, (b) test specimen #1.

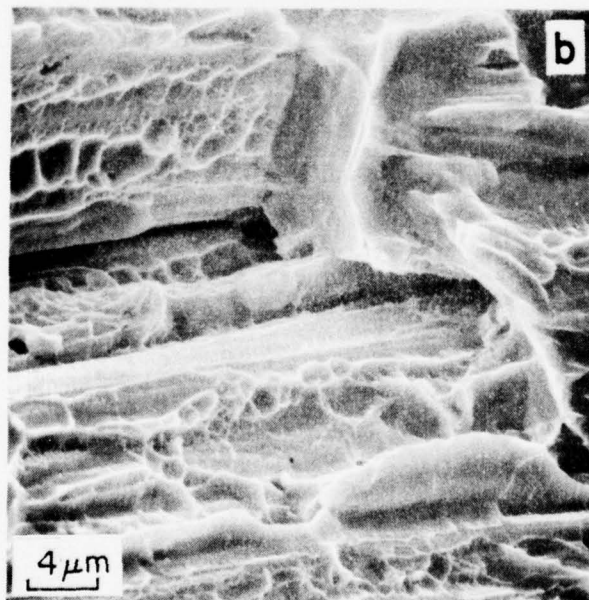
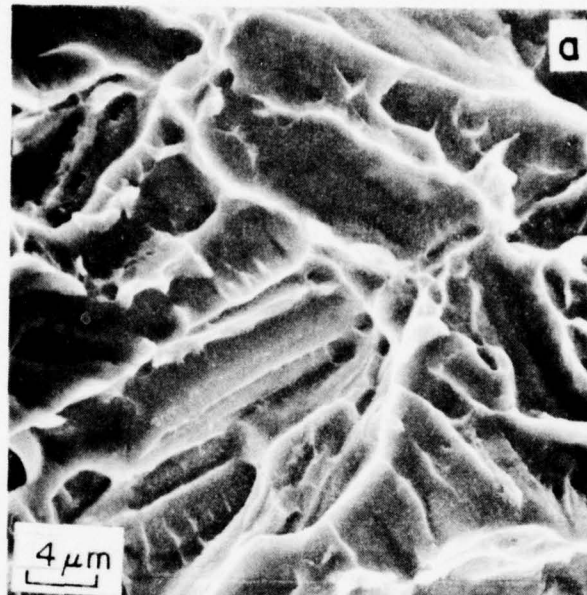


Fig. 10 Scanning electron micrographs of fracture surfaces of beta treated Charpy bars. (a) test specimen #5; (b) test specimen #1. Note the larger void size in (a).



SC5056.4FR

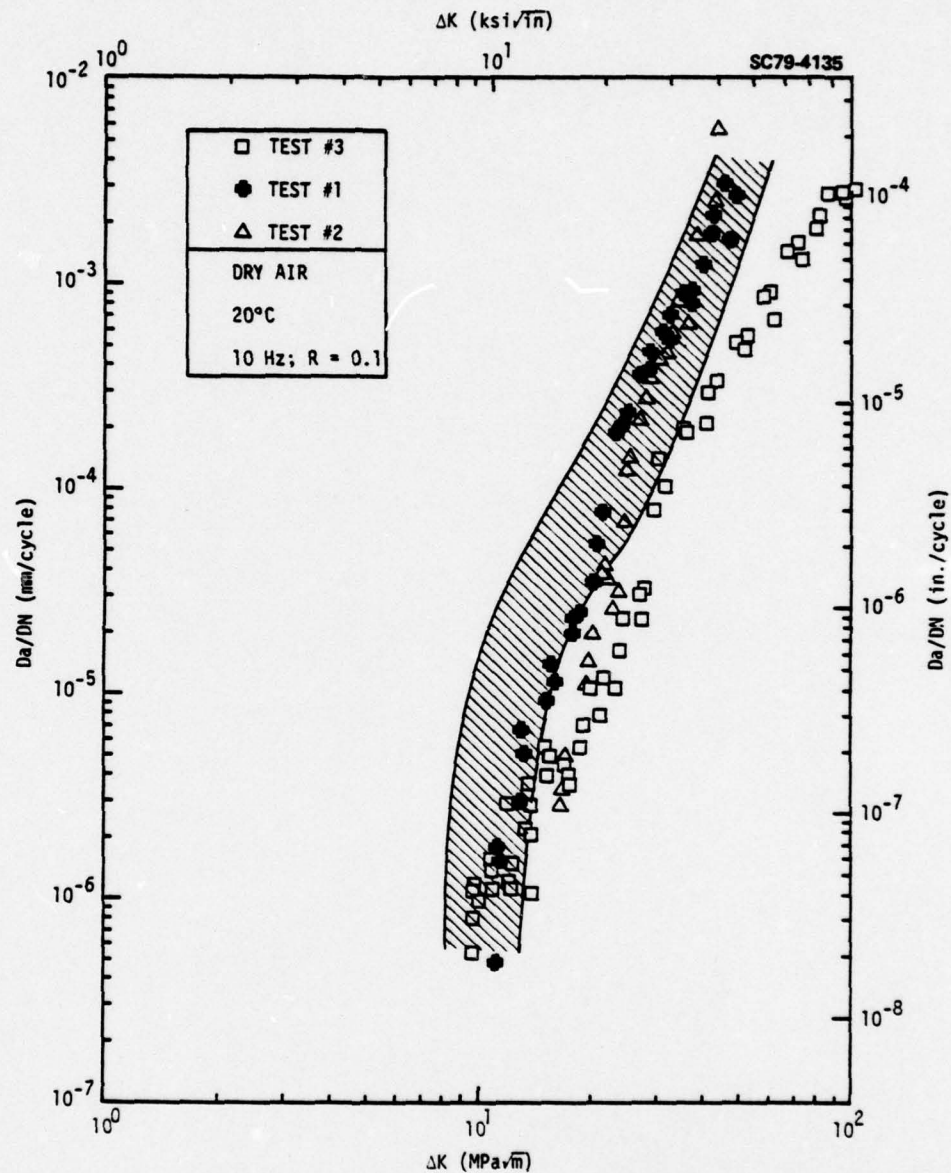


Fig. 11 Fatigue crack propagation rate as a function of applied stress for three microstructural conditions of Ti-6Al-4V. The band is a typical scatter band for Ti-6Al-4V in R-A condition.



SC5056.4FR

conditions. However, at about $\Delta K = 15 \text{ ksi}/\sqrt{\text{in}}$, the curves begin to separate with test sample #3 exhibiting better FCP resistance than samples #1 and #2. As the stress level increases, the separation between #3 and the other two samples becomes increasingly larger, reaching a difference of an order of magnitude at the high stress levels. Figure 12 presents plots of FCP rates as a function of interface phase width (and volume fraction primary alpha) for several stress levels. At low stress levels, there is little influence of these microstructural features on FCP rate, but as the stress level increases, there is generally an increasing dependence of da/dN on interface phase width and/or volume fraction primary alpha.

Fractography reveals that at the low stress levels, fracture is predominantly by cleavage through the alpha phase in all three test specimens, Fig. 13. Striations are not detected until the FCP rate reaches about 10^{-5} inches/cycles; for samples #1 and #2, this is at a stress level of about $20 \text{ ksi}/\sqrt{\text{in}}$, while for sample #3, a rate of 10^{-5} inches/cycle is achieved at a stress level of about $30 \text{ ksi}/\sqrt{\text{in}}$, Fig. 14. The change in mode appears to be gradual with the transition region showing cleavage of some α particles and striations in other α particles, Fig. 13b. There is extensive secondary cracking over the entire range of stress levels in sample #3. The secondary cracks extend both across alpha grains and along alpha-beta interfaces. As the stress level is increased, the occurrence of interface cracking increases, becoming predominant at the higher stress levels. Samples #1 and #2 exhibit little secondary cracking.



SC5056.4FR

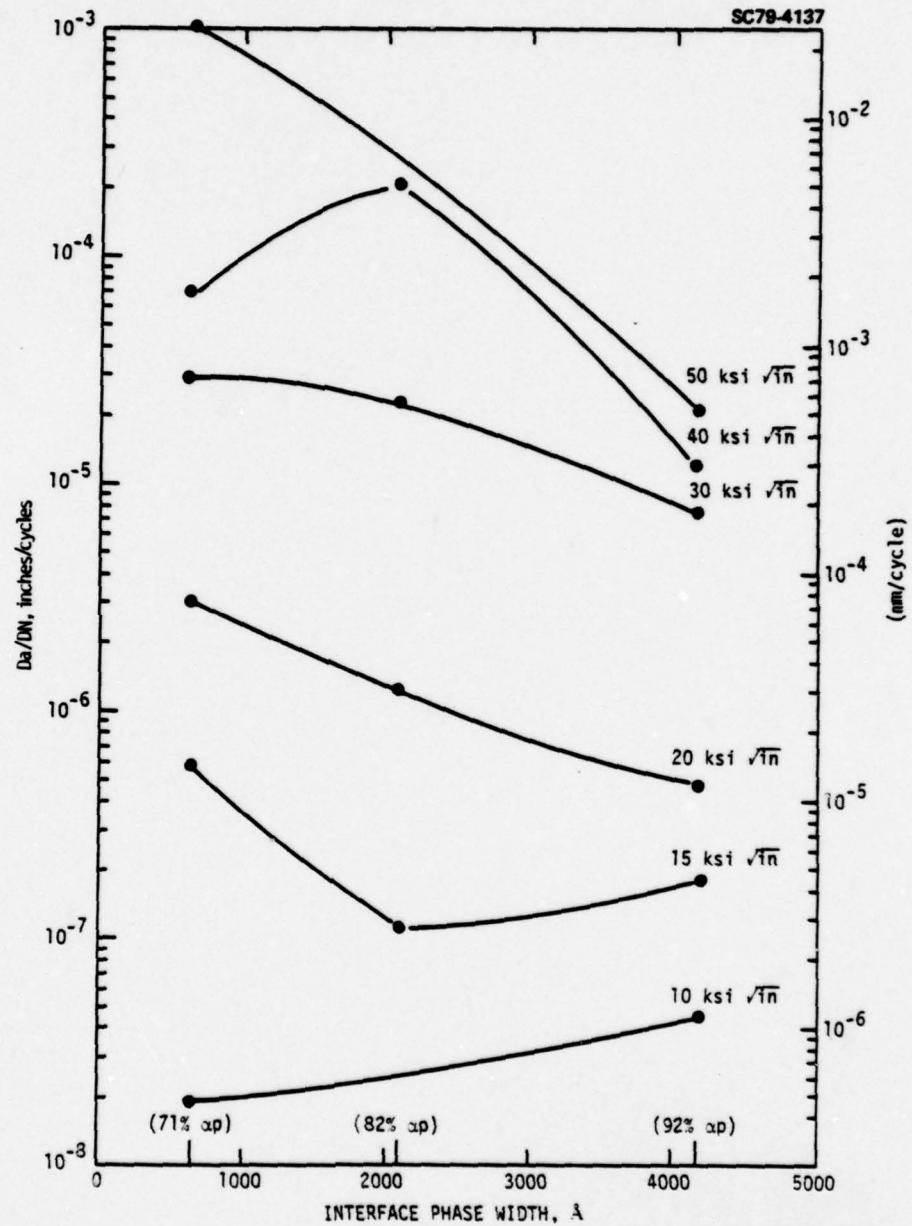


Fig. 12 Fatigue crack propagation rate as a function of interface phase width (and volume percent primary alpha) for several applied stress levels.

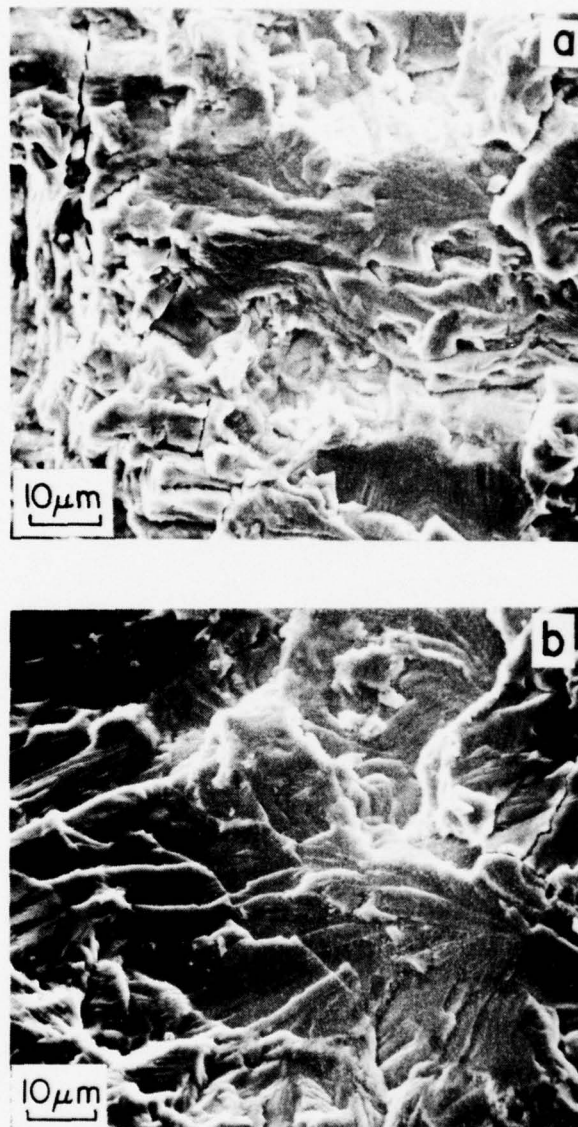


Fig. 13 Scanning electron micrographs of fracture surfaces of FCP Ti-6Al-4V specimens at a stress level of 15 Ksi $\sqrt{\text{in}}$. (a) test specimen #2; (b) test specimen #3. Crack direction is horizontal.

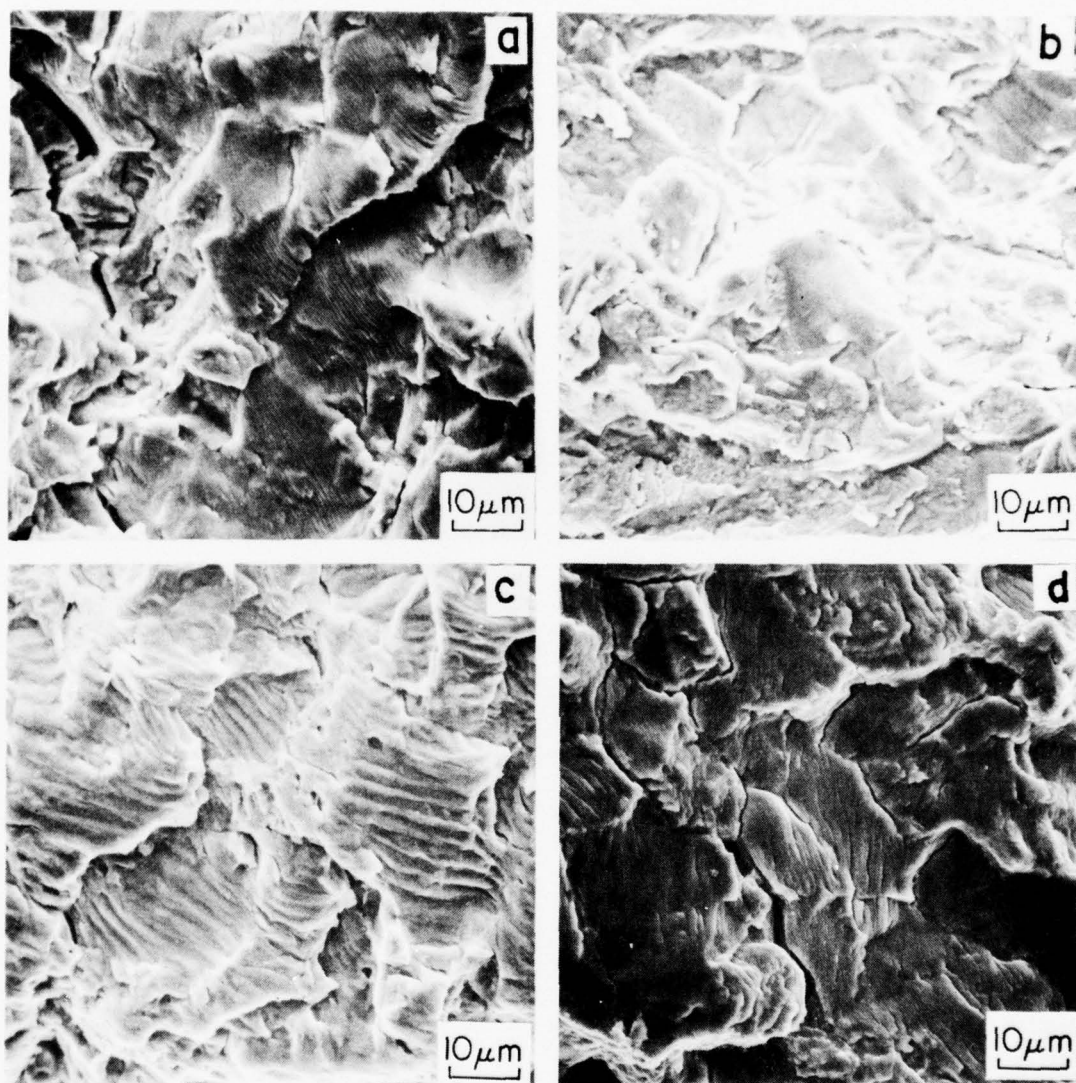


Fig. 14 Scanning electron micrographs of fracture surfaces of FCP Ti-6Al-4V specimens. (a) test specimen #2, $\Delta K = 30 \text{ Ksi } \sqrt{\text{in}}$; (b) test specimen #3, $\Delta K = 30 \text{ Ksi } \sqrt{\text{in}}$; (c) test specimen #2, $\Delta K = 40 \text{ Ksi } \sqrt{\text{in}}$; (d) test specimen #3, $\Delta K = 40 \text{ Ksi } \sqrt{\text{in}}$.



SC5056.4FR

Part II. Hydrogen Effects

3.4 Omega Phase

The influence of hydrogen on omega phase nucleation and growth was studied in Ti-20 wt. pct. V. For this study, the alloy was charged with various levels of hydrogen up to 4000 ppm by weight. The samples were then aged at 350°C for various times up to 28 hours and examined by hardness measurements, light microscopy and transmission electron microscopy. The hardness results are presented in Fig. 15 in which it can be seen that the hardness is reduced by increasing hydrogen content. TEM reveals that the reduction in hardness corresponds to a reduction in the volume fraction of omega phase; for example, Fig. 16 is a series of electron micrographs illustrating the distribution of omega phase in samples having four different levels of hydrogen aged for 28 hours. Not only does the volume fraction of omega phase decrease with increasing hydrogen content, but the number of particles is also significantly reduced with increasing hydrogen. The nucleation of omega phase is retarded by the presence of hydrogen as evidenced by the observation that omega phase is observed in the 'as solution treated' condition in the sample with no hydrogen, is first detected after 40 minutes of aging in the sample with 1000 ppm hydrogen, and is not present after 28 hours of aging in the sample with 2000 ppm hydrogen.

Another interesting effect of hydrogen on omega phase is its influence on omega particle morphology. In the alloy with no hydrogen, omega forms cuboidal particles, but when 500 ppm hydrogen is added, the particles are ellipsoidal, as illustrated in Fig. 17. It is well known that the omega phase morphology is a function of the misfit between the parent β -phase lattice and the omega phase lattice.¹⁵ The result shown in Fig. 17 would indicate that the presence of hydrogen in the β lattice alters its lattice parameter towards that of the omega phase. Precision lattice parameter measurements, which were beyond the scope of this program, would assist in resolving this point. Finally, it was also observed that the omega particles, which form initially as ellipsoidal particles, eventually grow into a more nearly cuboidal form, c.f. Figs. 17b and 16b. This effect is not the result of a loss of hydrogen



SC5056.4FR

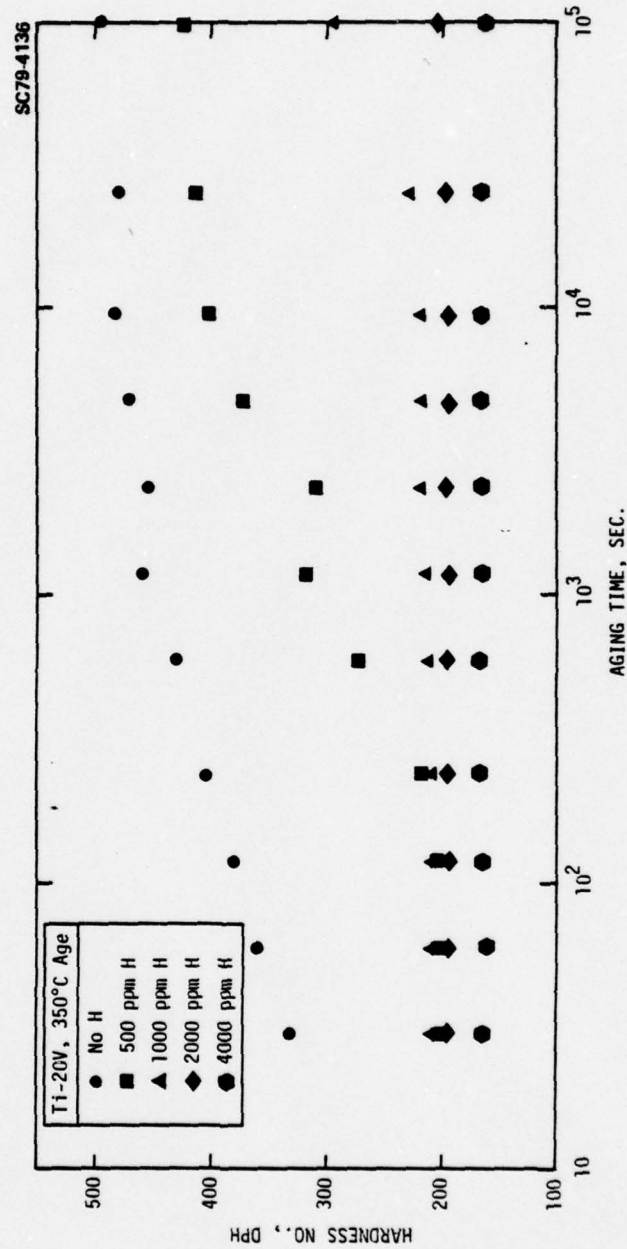


Fig. 15 Microhardness of Ti-20V as a function of aging time at 350°C for various levels of hydrogen.

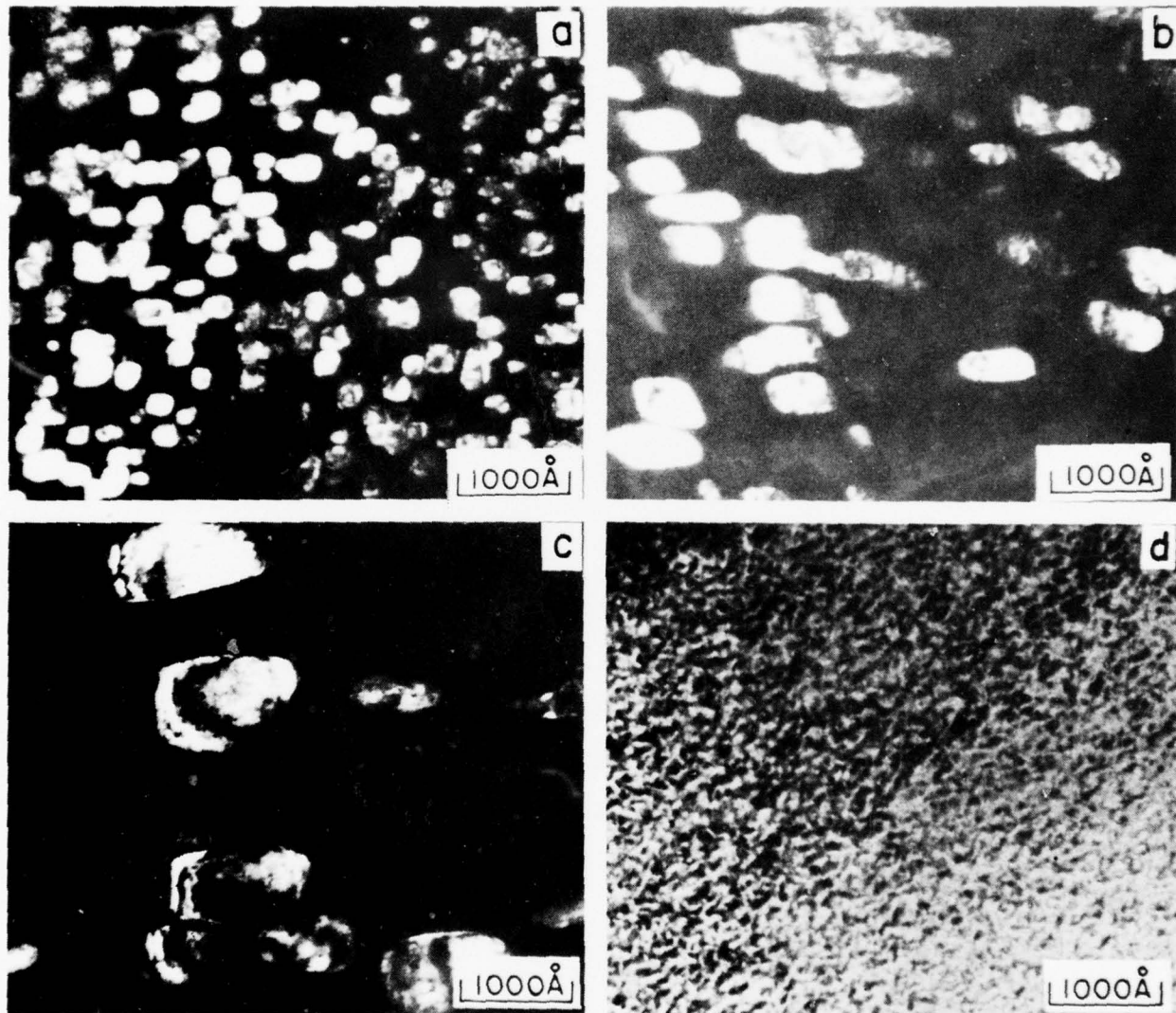


Fig. 16 Dark field transmission electron micrographs showing omega phase particles in Ti-20V with various levels of hydrogen aged at 350°C for 28 hours. (a) no H; (b) 500 ppm H; (c) 1000 ppm H; (d) 2000 ppm H.

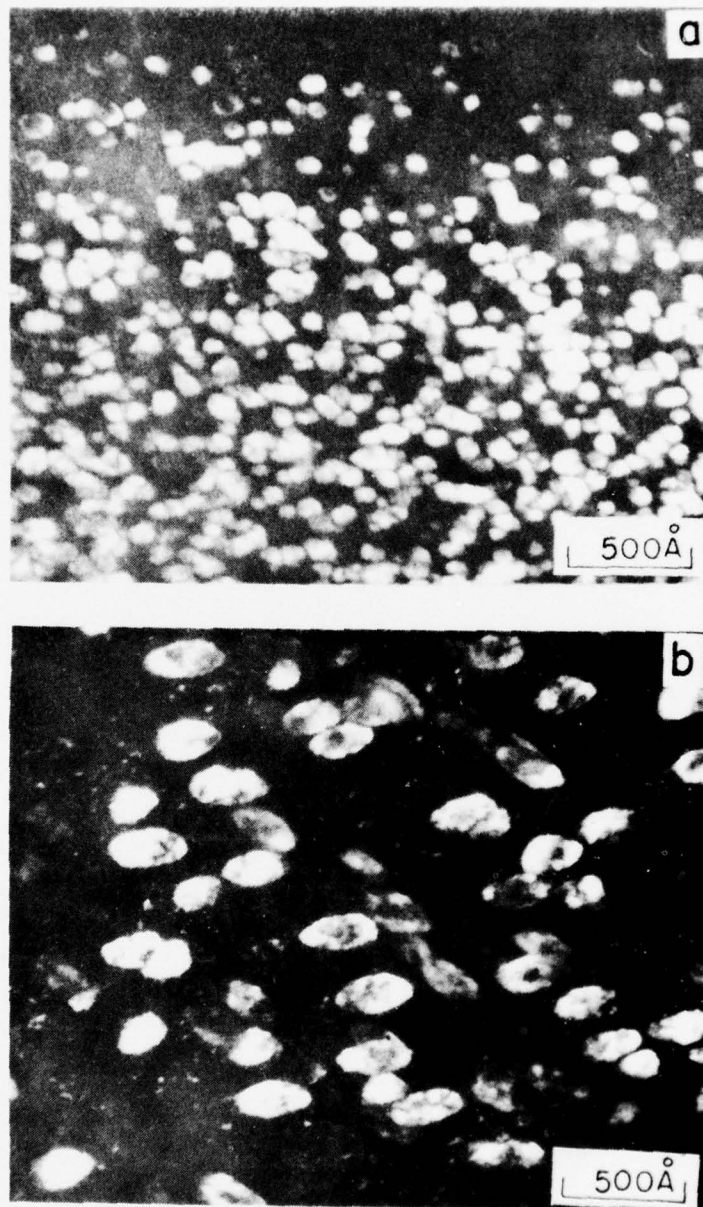


Fig.17 Dark field transmission electron micrographs showing omega phase particle morphologies in Ti-20V aged for 20 minutes at 350°C with different levels of hydrogen. (a) no H; (b) 500 ppm H.



SC5056.4FR

during aging because analysis of samples before and after aging treatments showed no loss of hydrogen. Again, precise lattice parameter measurements would lend insight into this effect.

3.5 Solubility of Hydrogen in Beta Phase

This portion of the program was aimed at establishing the solubility limit of hydrogen in a beta stabilized alloy. Ti-40 wt.pct.V was selected for this study and hydrogen was added by the Sieverts method at 800°C. Hydrogen levels of from 7000 to 19,782 ppm by weight were examined. The presence of hydrides was monitored by x-ray diffraction and by TEM.

No evidence of hydrides was seen in the x-ray diffraction patterns from all hydrogen levels. TEM revealed only beta phase in samples with hydrogen up to 12,884 ppm. The samples with 16,413 and 19,782 ppm H showed unusual linear features which dominated the microstructure and which gave a face centered cubic diffraction pattern. The structure had the appearance of the thinning artifact, designated spontaneous relaxation,⁷ common to beta stabilized titanium alloys. The x-ray diffraction patterns from this alloy exhibited only a bcc fracture, not fcc. Although precision lattice parameter measurements were not made, it could be estimated from the x-ray patterns that the lattice parameter increased from about 3.18Å to about 3.42Å as the hydrogen level increased from zero to 16,413 ppm.

3.6 Influence of Hydrogen on Ductility in an α/β Alloy

This portion of the program was a preliminary investigation into the potential use of hydrogen to promote ductility in α/β titanium alloys. Since hydrogen is a beta stabilizer, the possibility exists to introduce large amounts of hydrogen into a conventional α/β alloy-like Ti-6Al-4V which has a fairly low volume fraction of beta phase in order to stabilize larger amounts of the more ductile beta phase. The alloy could then be formed and the hydrogen subsequently pumped out.

The approach here was to charge sheet tensile samples with 1000 ppm by weight of hydrogen and to pull the specimens at two strain rates and two



SC5056.4FR

temperatures. The results are presented in Table V. The ultimate strength is increased by the presence of 1000 ppm hydrogen, but the yield strength is not significantly increased, except for the 350°C test at a strain rate of 0.05. The ductility, as measured by total elongation, has been increased at room temperature at both strain rates. The elongation is not effected at 350°C.

3.7 Tensile Properties of Beta Titanium in High Pressure Hydrogen

In recognition of the fact that beta titanium alloys appear to have an exceptional tolerance for high levels of hydrogen in solution, it was decided that the tensile properties of a commercial titanium alloy tested in high pressure hydrogen would be worthy of investigation. Round tensile bars of a commercially available Beta III titanium alloy, the composition of which was Ti-11.5Mo-6Zr-4.5Sn, were tested in various heat treatment conditions in an atmosphere of 5,000 psi hydrogen and, for comparison, 5,000 psi helium. The results of these tests are shown in Table VI, and it can be seen that the high pressure hydrogen environment caused a definite degradation in the ductility of this titanium alloy. The degradation in ductility was particularly evident in the results of the fractography performed on the fracture specimens of the failed tensile samples. An example of this fractographic evidence is shown in Fig. 18, where the classical ductile-dimple rupture found in the high pressure helium environment is shown in Fig. 18a, contrasted with the very brittle cleavage-like fracture found in high pressure hydrogen environments shown in Fig. 18b. These results show that, although beta titanium alloys can dissolve large amounts of hydrogen, and in some cases, without severely damaging tensile properties, high pressure hydrogen environments apparently introduce sufficiently large quantities of hydrogen into solution to cause severe degradation in mechanical properties.



SC5056.4FR

Table V
Influence of Hydrogen on Tensile Properties of Ti-6Al-4V

Hydrogen Content	Yield Strength (ksi)			
	Room Temperature		350°C	
	Strain Rate		Strain Rate	
	.005	.05	.005	.05
0	126.8	129.5	95.6	93.6
1000 ppm	126.8	132.7	87.4	101.5

Hydrogen Content	Ultimate Tensile Strength (ksi)			
	Room Temperature		350°C	
	Strain Rate		Strain Rate	
	.005	.05	.005	.05
0	138.0	139.1	104.9	100.5
1000 ppm	154.0	155.1	114.6	112.7

Hydrogen Content	Total Elongation (percent)			
	Room Temperature		350°C	
	Strain Rate		Strain Rate	
	.005	.05	.005	.05
0	11.1	12.1	9.9	9.9
1000 ppm	16.5	16.2	10.2	9.4



SC5056.4FR

Table VI
Tensile Properties of Beta III in High Pressure Helium and Hydrogen

Specimen No.	Gas	Test Pressure PSIA	Yield Strength ksi	Ultimate Tensile Strength ksi	R.A. %	Elong. %
<u>ST 745°C /5 min/W.Q.</u>						
1	H ₂	5000	78.8	97.5	13.1	4.0
2	He	5000	79.8	113.7	63.4	22.0
<u>ST 745°C /5 min/W.Q. + Age 540°C/8 hrs</u>						
4	H ₂	5000	143.4	154.0	6.7	4.0
5	He	5000	143.1	152.3	16.6	7.2
<u>ST 815°C /5 min/W.Q.</u>						
1	H ₂	5000	80.5	96.8	6.3	3.8
2	He	5000	85.4	110.7	72.9	31.6
<u>ST 815°C /5 min/W.Q. + Age 540°C/8 hrs</u>						
4	H ₂	5000	143.4	150.4	7.1	6.6
5	He	5000	137.6	147.2	13.8	8.8

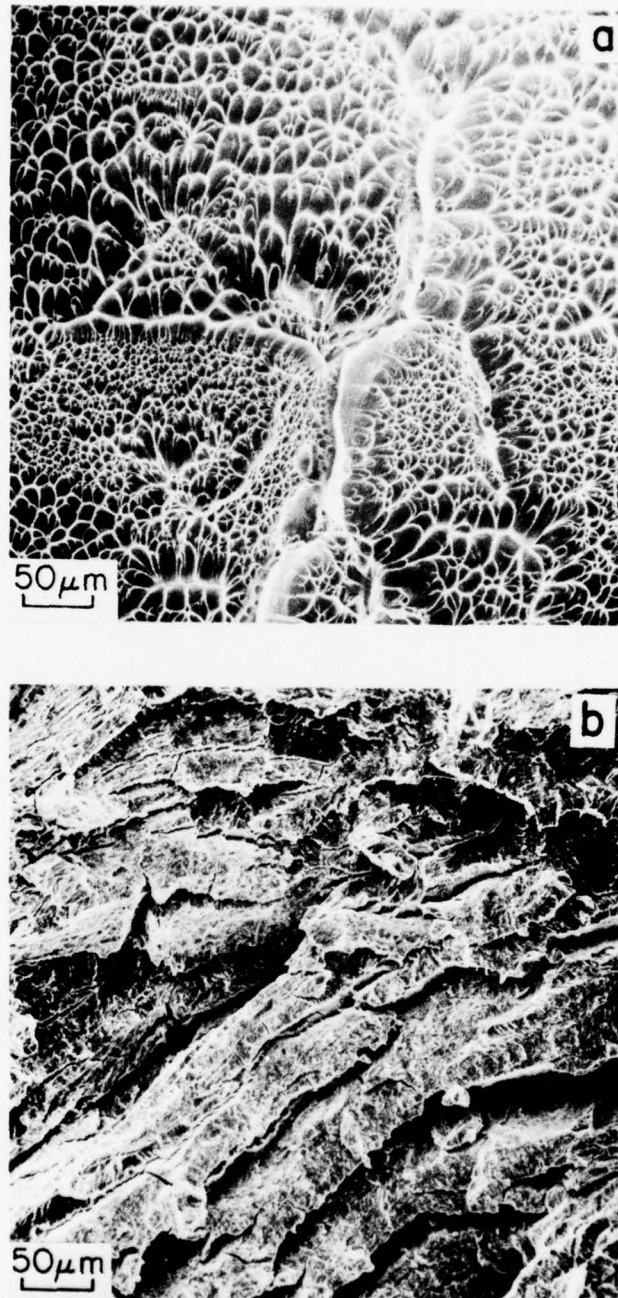


Fig. 18 Scanning electron micrographs of fracture surfaces of β -III titanium alloy solution treated at 1375^oF and tensile tested in (a) 5000 psi He, and (b) 5000 psi H₂.



SC5056.4FR

4.0 DISCUSSION

Part I. The Influence of Interface Phase on Mechanical Properties

4.1 Fracture Toughness

Any influence that volume fraction primary alpha or interface phase might have on fracture toughness is overshadowed in the α/β processed material by the presence of the bands of primary α phase. The fracture surface is characterized by large elongated voids which correlate with the presence of several alpha grains of a similar orientation having no beta phase separating them. When these bands of alpha grains are parallel to the crack propagation direction, lower toughness values are observed because the crack proceeds as the elongated holes open up. This mechanism operates whether there is 68% or 86% primary alpha and whether the interface phase is 600Å or 5000Å. Similarly, when the bands of alpha grains are perpendicular to the crack propagation direction, higher toughness values are observed because the crack moves normal to its propagation direction as it encounters elongated holes opening up. Again, this delaying mechanism operates regardless of volume fraction primary alpha or interface phase width.

The moderate texture of [0001] poles eight times random in the T (transverse) direction is fairly typical of rolled plate, but the eight times random [0001] poles parallel to the rolling directions is somewhat unusual. It is possible that the banded structure is associated with this latter texture. The decrease or absence of beta phase in these banded regions would also suggest microsegregation of vanadium, although no evidence for this was obtained. At any rate, the presence of the banded microstructure leads to directionality in fracture toughness of 6-4.

For the beta processed material, directional effects were not examined based on studies reported in the literature showing that texture is destroyed by beta processing.¹⁰ Correlation of the toughness values with interface phase width is somewhat tenuous inasmuch as alpha phase particle size, aspect ratios, and spacing are varying among the samples as well as



SC5056.4FR

interface phase width. However, examination of the fracture surface shows that fracture basically advances by microvoid coalescence and that the crack appears to follow along the alpha-beta interfaces. The voids are considerably smaller in the tougher samples leading to the conclusion that a broad interface phase can inhibit microvoid coalescence and thereby improve toughness.

4.2 Fatigue Crack Growth Rate

The fatigue results indicate that microstructure influences crack growth rates, especially at higher stress levels. The fracture mode is essentially the same among the fatigue samples: cleavage-like fracture through the primary alpha particles at low ΔK ($<15\text{ksi}\sqrt{\text{in}}$), gradually changing to striation type fracture, seemingly less structure sensitive, as the stress level is increased. The mechanism by which the condition having the broadest interface phase (and the highest volume fraction of primary alpha) improves the FCP resistance is the formation of numerous secondary cracks.

The influence of microstructure on FCP then, is to promote additional cracking to absorb applied energy rather than impart resistance, per se, to an advancing crack. From the limited data obtained here, it is not clear whether the interface phase or volume fraction primary alpha (or some other parameter such as amount of transformed beta regions) dominates the effect. The most likely way in which increased volume fraction of primary alpha could improve crack resistance would be through an increase in the strength of the beta phase rather than any effects of larger alpha particle or increased α grain boundary surface area. Increasing the volume fraction of primary alpha from .71 to .92 increases the particle size from about 9 to $10\mu\text{m}$ and the particle surface area by about 20%. Such minor changes in these parameters would not seem likely to cause such significant effects as are observed. On the other hand, the beta phase will be markedly enriched in vanadium as the volume fraction of primary alpha phase increases, and the solid solution strengthening thus afforded could provide increased crack resistance, forcing the crack to branch along interfaces. (The presence of decomposition of the beta phase in the sample with the lowest volume fraction of primary alpha detracts from this possibility, since the actual amount of beta phase was not established.)



SC5056.4FR

Alternatively, one way in which interface phase could promote crack branching is to nucleate cracks ahead of the advancing crack front in the plastic zone. If a broad interface phase inhibits the transfer of slip between the alpha and beta phases, stress concentrations could arise at the interface and cracks could form at more than one boundary position within the plastic zone. As these link up to the main crack, energy is absorbed and crack branches result. Further work is needed to determine which, if either, of these mechanisms speculated upon here is operative.



SC5056.4FR

Part II. Hydrogen Effects

4.3 Omega Phase

This study has confirmed that hydrogen suppresses omega phase formation. The hardness curves in Fig. 15 indicate that nucleation of omega phase is retarded by hydrogen and the TEM results support this observation. In this respect, hydrogen acts in a manner similar to other beta stabilizers, even though hydrogen is an interstitial, rather than substitutional, alloying addition.

The effect of hydrogen on omega phase particle morphology is similar to that observed for Zr additions in which it was shown that increasing the Zr content of a Ti-10V alloy altered the omega morphology from cuboidal to ellipsoidal.¹¹ In that case, it was shown the Zr expanded the beta phase lattice parameters, thereby reducing the misfit between the beta and omega phases. Hydrogen is known to increase the beta lattice parameter.¹³ The reversion of the omega morphology in the hydrogen bearing alloys from ellipsoidal to cuboidal with aging time is somewhat curious. As noted earlier, this is not the result of a loss of hydrogen during the aging treatments. It is possible that 500 ppm hydrogen is sufficient to expand the beta lattice parameter an amount such that there is near zero misfit between the omega and beta phases. With continued aging, however, as the volume fraction of omega phase increases (and rejects hydrogen), the beta matrix becomes further enriched in hydrogen and the lattice parameter expands such that the misfit is beyond zero, or a negative misfit, using Hickman's designation.⁵ Previous work³ showed that hydrogen additions to the Ti-Mo system significantly increased the beta phase lattice parameter and extrapolation of that data to the current Ti-V system indicates the above speculation is reasonable.

4.4 Solubility of Hydrogen in Beta Phase

Hydrides were not detected in a Ti-40V alloy containing up to 19,789 ppm hydrogen. The fact that TEM samples with high hydrogen contents underwent spontaneous relaxation during thinning by ion milling indicates the



SC5056.4FR

material contains a high residual stress due to the presence of the hydrogen. The observed increase in lattice parameter from 3.18Å to 3.42Å represents a 7% increase as the hydrogen level increased from zero to ~16,000 ppm. The large amounts of interstitial hydrogen causing large expansion of the bcc lattice could result in the high residual stresses. This likely means there is a limit to the 'softening' effect of hydrogen observed earlier,³ and that there is some optimum level of hydrogen for "hydrogen assisted" forming.

4.5 Influence of Hydrogen on Ductility in an α/β Alloy

The exploratory tests run to examine the influence of hydrogen on ductility in Ti-6Al-4V indicate some promise for this approach. The room temperature tensile elongation was improved from 11-12% to 16% with the addition of 1000 ppm hydrogen. However, the 350°C tests showed no improvement in ductility. Further tests of this kind are needed to determine if this will be a viable forming technique.

4.6 Tensile Properties of Beta Titanium in High Pressure Hydrogen

The finding that high pressure hydrogen seriously degrades the mechanical properties, and in particular the ductility, of beta titanium indicates that the tolerance that these alloys have for hydrogen is distinctly limited. Earlier results on Ti-Mo alloys also showed that at very high hydrogen levels, ductility was severely limited.¹² This present result would indicate that high levels of hydrogen are, in fact, reached in these room temperature high pressure hydrogen tensile tests, probably by dislocation transport of hydrogen into the interior of the specimen as has been suggested by previous workers.¹³ These tests indicate that beta titanium alloys are probably not useful as containment vessels for high pressure hydrogen or for service in high pressure hydrogen environment.



SC5056.4FR

5.0 CONCLUSIONS

1. Fracture toughness of Ti-6Al-4V, having an equiaxed primary alpha structure, is more strongly influenced by microstructure developed as a result of processing than by the presence or absence of interface phase.
2. Fatigue crack propagation resistance in Ti-6Al-4V, having an equiaxed primary alpha structure, can be improved by heat treatments which increase the interface phase width. The FCP resistance is increased by the promotion of extensive secondary cracking.
3. Hydrogen suppresses omega phase formation in Ti-20V.
4. Ti-40V will take at least 19,700 ppm by weight of hydrogen into solution without hydrides forming. The beta lattice parameter is increased significantly by hydrogen.
5. The commercial beta titanium alloy, Beta III, suffers severe ductility loss in 5000 psi hydrogen as compared to 5000 psi helium.



SC5056.4FR

6.0 REFERENCES

1. C.G. Rhodes and N.E. Paton, "The Influence of the α/β Interface Phase on Tensile Properties in Ti-6Al-4V," ONR Annual Report, SC5056-2TR, 1979.
2. C.G. Rhodes and N.E. Paton, *Met. Trans.*, Vol. 10A, 1979, pp. 209-16.
3. N.E. Paton, O. Buck and J.C. Williams, *Scr. Met.*, Vol. 9, 1975, pp. 687-91.
4. A.D. McQuillan, *Proc. Roy. Soc. (London)*, Vol. 204A, 1950, pp. 309-23.
5. B.S. Hickman, *J. Mat. Sci.*, Vol. 4, 1969, pp. 554-63.
6. R.A. Spurling, *Met. Trans.*, Vol. 6A, 1975, pp. 1660-61.
7. R.A. Spurling, C.G. Rhodes and J.C. Williams, *Met. Trans.*, Vol. 5A, 1975, pp. 2597-600.
8. M.J. Marcinkowski and D.S. Miller, *Phil. Mag.*, Vol. 6, 1961, pp. 871-93.
9. P.B. Hirsch, A. Howie, R.B. Nicholson, D.W. Pashley and M.J. Whelan, Electron Microscopy of Thin Crystals, Butterworths, London, 1971, p. 188.
10. T.S. Baker, C.A. Stubbington and G.I. Lewis, "The Effect of Heat Treatment and Texture on the Fracture Toughness of Ti-6Al-4V Alloy Bars," R.A. E. Technical Report, TR77075, May 1977.
11. J.C. Williams, B.S. Hickman and D.H. Leslie, *Met. Trans.* Vol. 2A, 1971, pp. 477-84.
12. N.E. Paton and O. Buck, Effect of Hydrogen on Behavior of Materials, A.W. Thompson and I.M. Bernstein, eds., AIME, New York, 1976, p. 83.
13. J. Tien, A.W. Thompson, I.M. Bernstein and R.J. Richards, *Met. Trans.*, Vol. 7A, 1976, pp. 821-29.



SC5056.4FR

APPENDIX I

The following reports have been submitted under the subject contract and cover details of technical accomplishments in previous years of the program.

SC5056.1TR	Technical Report	1/13/78
SC5056.2TR	Technical Report	6/23/78
SC5056.3TR	Technical Report	8/23/78

In addition to the above reports, the following technical papers have been written for publication:

1. C.G. Rhodes and N.E. Paton, "Formation Characteristics of the α/β Interface Phase in Ti-6Al-4V," Met. Trans., Vol. 10A, 1979, pp. 209-16.
2. C.G. Rhodes and N.E. Paton, "The Influence of α/β Interface Phase on Tensile Properties in Ti-6Al-4V," submitted for publication.
3. L.A. Ahlberg, O. Buck and N.E. Paton, "Effects of Hydrogen on Anisotropic Elastic Properties of Bcc Ti-Alloys," Scr. Met., Vol. 12, 1978, pp. 1051-54.
4. L.A. Ahlberg, O. Buck, N.E. Paton and E.S. Fisher, "Note on Effects of Hydrogen on Anisotropic Elastic Properties of Bcc Ti-Alloys," submitted for publication.
5. N.E. Paton and R.A. Spurling, "Effects of Hydrogen in Two Titanium Alloys," in preparation.

Included in this appendix are complete copies of the three technical reports submitted previously under this contract.



7.1 FORMATION CHARACTERISTICS OF THE α/β INTERFACE
PHASE IN Ti-6Al-4V

C. G. Rhodes and N. E. Paton
Science Center, Rockwell International
Thousand Oaks, California

ABSTRACT

The conditions for formation of the interface phase, or interfacial layer, in Ti-6Al-4V have been studied systematically. The interface phase does not grow during isothermal treatments, but rather grows only during cooling from elevated temperatures to about 650°C. The width of the interfacial layer is a function of the cooling rate, having a maximum of about 4000Å at 28°C/hr. The interface phase forms initially with an fcc structure which subsequently transforms to hcp α phase. A theoretical description of the mechanisms of interface phase formation is presented.



INTRODUCTION

The microstructural feature which occurs under certain conditions at the interphase boundaries of alpha and beta phases in titanium alloys has been called alternatively "interface phase"⁽¹⁾ or "interfacial layer."⁽²⁾ This feature is most easily studied by transmission electron microscopy because it grows to a maximum width of about one micron and generally is considerably less than that. The role of interface phase in the $\beta \rightleftharpoons \alpha$ phase transformation and its potential effect on mechanical properties are two areas which warrant further study.

The α/β boundaries have been shown to be an important factor in the fracture of two-phase titanium alloys in the cases of tensile⁽³⁾ and fatigue⁽⁴⁾ testing. The presence of an interfacial layer may influence the fracture process by providing an easy crack path or by providing crack initiation sites. Strength and ductility may be affected if the presence of the interface phase inhibits the transfer of slip between the α and β phases. Margolin et al.⁽⁵⁾, on the other hand, have recently suggested that interface phase would have only minor effects on ductility.

Previous work^(1,2) indicated that the interfacial layer could form either with an fcc structure or with an hcp structure, and evidence was presented that the interface phase was α phase in a "non-Burgers" orientation⁽¹⁾ or in a Burgers orientation different from that of the adjacent primary α .⁽⁵⁾ This paper reports the results of a study undertaken to establish systematically the conditions for interface phase formation and its crystallography in Ti-6Al-4V.



EXPERIMENTAL

Two heats of Ti-6Al-4V were used in this work, the chemical analyses are listed in Table I. The "as-received" microstructure of both heats consisted of ~90% equiaxed primary alpha particles, having approximately a $12\mu\text{m}$ diameter in a continuous β matrix. The heat treatments were carried out with the samples either in a dynamic inert gas atmosphere or encapsulated in evacuated ampoules. The isothermal reaction treatments were accomplished by quenching samples directly from an inert-atmosphere furnace held above the beta transus into a fluidized bed held at the reaction temperature. A programmable controller supplying power to the furnace was used for controlled-cooling-rate treatments.

Thin foils for transmission electron microscopy were prepared by conventional electropolishing techniques⁽⁶⁾ or by ion milling.⁽⁷⁾ The foils were examined in a Philips EM-300 electron microscope equipped with a double tilt goniometer stage.

Since the projected width of the interfacial layer in an electron micrograph is dependent upon the angle which the interface makes with the electron beam, a standard geometric-crystallographic condition was established for all interface phase measurements. This condition calls for the interface to be parallel to the electron beam within 5° and for the α phase to be in a two-beam diffracting condition with $g = 0002$. The standard condition can be achieved in the following manner. When 6-4 is cooled from above the beta transus, the alpha phase which results from the $\beta \rightarrow \beta + \alpha$ transformation forms as elongated plates. The rate of cooling generally controls the aspect ratio



of the plates. Previous work^(8,9) has shown that these nucleation-and-growth plates have a $\{334\}$ β habit plane which corresponds through the Burgers relation to a $\{41\bar{5}0\}$ α phase plane⁽⁸⁾ and is identical to the martensite habit plane.⁽¹⁰⁾ The plates grow with the long direction of the plate parallel to $[0001]$ α and $[011]$ β . The $\{41\bar{5}0\}$ α habit plane lies 11° from $\{10\bar{1}0\}$ α about the $[0001]$ α . The standard condition for electron microscope observations can then be achieved by a 15° tilt about the $[0001]$ α from the $\langle 10\bar{1}0 \rangle$ α zone; the standard condition lies halfway between the $\langle 10\bar{1}0 \rangle$ and $\langle 11\bar{2}0 \rangle$ α zones.

RESULTS

I. Layer Formation Behavior

The interfacial layer has been shown previously^(1,2) to occur either with a dense internal structure (called a striated layer) or with no internal structure (called a monolithic layer). The striated layer was interpreted as having the hcp structure of the alpha phase, but in a different orientation from the adjacent primary alpha. The monolithic layer was shown to have an fcc structure.

In order to establish the conditions under which the interface phase will grow, two heat treat schedules were devised. The first was a series of isothermal reaction treatments aimed at establishing a T-T-T diagram for interface phase growth. Samples of 6-4 were solutionized above the beta transus (at 1030°C) and then quenched directly to one of several temperatures below the β transus. The samples were held at the reaction



temperature for times from 1 minute to 24 hours. Electron microscopy of the samples revealed that there was no growth of the interface phase during isothermal treatments. For example, Figure 1 shows the alloy held for 1 minute (a) and 24 hours (b) at 704°C (1300°F). The 704°C (1300°F) reaction temperature is above the martensite start temperature (M_s) for Ti-6Al-4V(11) and the beta to alpha transformation, which is approximately 25% complete after 2 minutes, is complete after about 4 hours. Isothermally reacting below the M_s does not alter the observed result of negligible layer growth during isothermal treatment, as illustrated in Figure 2. In all cases the layer was so narrow that the nature of the layer (striated or monolithic) could not be determined either by selected area diffraction (SAD) or by imaging.

The second heat treat schedule was a series of controlled cooling treatments in two parts: cooling from above the β transus and cooling from below the β transus. The samples were cooled to temperatures in the range of 472°C (800°F) to 927°C (1700°F) at rates ranging from 2.8°C/hr (50°F/hr) to 555°C/hr (1000°F/hr) and were water quenched immediately upon reaching the lower temperature. Samples were also cooled to room temperature. These treatments produced interfacial layers of varying thicknesses. The widths of the layers were measured for all of the treatments and the results obtained from the samples cooled from above the β transus are presented in Figure 3. Samples cooled to temperatures below 760°C (1400°F) appear to fall on a single curve which shows a maximum layer width at 28°C/hr (50°F/hr). The samples cooled to 760°C (1400°F) exhibit a narrower layer width than those cooled further, and also appear to have a



maximum around 28°C/hr (50°F/hr). Samples cooled to 816°C (1500°F) and above had no interfacial layer in the α - β interfaces.

The interface phase was predominantly the striated type in all cases. Although the monolithic type layer could be observed in most samples, it rarely, if ever, was present in more than 50% of the interfacial area, and more generally was observed in 25% or less of the interfaces. No systematic correlation of the amount of monolithic interface phase with cooling rate or lower temperature could be discerned. The monolithic layer was generally on the order of one-half the width of the striated layer in any one sample. The values in Figure 3 are the mean values of measurements of both striated and monolithic layers and the fairly large error bars (which are 95% confidence intervals) reflect the large difference in widths of the two types of layers. Examples of the interface phase in these samples are shown in Figures 4 and 5. Those layers in samples cooled to 649°C (1200°F), Figure 4, have a well-developed striated structure, while those in samples cooled to 760°C (1400°F), Figure 5, have a less developed internal structure.

A series of samples was controlled cooled from below the β transus. These samples were cooled from an upper temperature of 982°C (1800°F), 927°C (1700°F) or 871°C (1600°F) at rates of 28°C/hr (50°F/hr), 56°C/hr (100°F/hr) and 112°C/hr (200°F/hr). As was the case for samples cooled from above the β transus, no interface phase was formed on cooling to 816°C (1500°F) and higher. Those cooled to 760°C (1400°F) and lower showed mainly striated layers similar to the results observed for samples cooled from above the β transus.



II. Crystallography of Interfacial Layer

The monolithic layer has an fcc structure, as reported previously^(1,2) with a lattice parameter approximately 4.26Å. Figure 6 is a sequence illustrating the fcc monolithic layer. The orientation relation between the fcc monolithic layer and the bcc beta phase is $(110)\beta \parallel (1\bar{1}1) \text{ fcc}$ and $[\bar{1}11] \beta \parallel [110] \text{ fcc}$, which is the Kurdjumov-Sachs relationship. The orientation relation between the fcc monolithic layer and the hcp alpha phase is $(0002) \alpha \parallel (1\bar{1}\bar{2}) \text{ fcc}$ and $[11\bar{2}0] \alpha \parallel [110] \text{ fcc}$. This relationship has close packed planes parallel, and close packed directions parallel in the two phases.

Occasionally, a monolithic layer can be found with a few internal striations such as shown in Figure 7. Trace analysis of these striations reveals that they lie in a (111) plane, suggesting that these features may be twins or stacking faults, both of which lie on (111) planes in fcc structures.

A striated layer is composed of a densely packed series of planar features which appear to be extending into the alpha phase, Figure 8. Trace analysis of the striations shows that they lie parallel to the basal plane of the alpha phase. The SAD pattern from a striated layer such as that in Figure 8 is composed of arced reflections as illustrated in Figure 9. This pattern is similar to that observed for Type 2 alpha⁽⁹⁾ but in this case can be indexed as fcc with both twinned and untwinned zones present. Figure 9 illustrates the relationship $[111]\beta \parallel [11\bar{2}0] \alpha \parallel [110] \text{ fcc}$. To confirm this relationship and that the striated layer is mainly composed of twinned and untwinned fcc structure, Figure 10 shows another orientation of the α and β phases. In



SC5056.1TR

Figure 10, the β zone normal is $[100]$ and, in agreement with the Burgers relation, the adjacent α phase is near a $[11\bar{2}0]$ zone normal.

The interface orientation for plate-shaped alpha phase was confirmed to be $\{334\}\beta \parallel \{41\bar{5}0\}\alpha$. Additionally, several interfaces in samples having equiaxed alpha particles were analyzed. It was found that many of the noncurved interfaces had the same orientation as that observed for the plate-shaped α , namely $\{334\}\beta \parallel \{41\bar{5}0\}\alpha$. Another interface orientation observed was $\{10\bar{1}2\}\alpha$. The orientations held whether the interface phase was monolithic or striated.

DISCUSSION

The results have shown that the interfacial layer forms only during a continuous change in temperature and is not formed by isothermal treatments. This would indicate that the interface phase is a consequence of composition shifts and/or volumetric constraints which occur during the change in relative amounts of alpha and beta phases present. During slow cooling, there is a continuous increase in the equilibrium volume fraction of α phase and a corresponding decrease in volume fraction of β phase which occurs principally as growth of the primary α particles rather than nucleation of new α particles. Since the equilibrium α phase in 6-4 contains $<1.2\%$ vanadium,⁽¹²⁾ there is continual diffusion of vanadium from the newly formed α into the β phase as the α - β interface advances into the β phase. The composition gradient thus established may influence the formation of interface phase as described later.



The observations that the monolithic (fcc) layer exists in 50% or less of the interface area and always in conjunction with the striated form suggests that the monolithic is a transient form of the interface phase. Figure 11 illustrates that the fcc layer is frequently observed adjacent to the beta but in combination with the striated interface phase which in turn is adjacent to the growing primary α particle. The fact that growth is taking place into the beta suggests that the monolithic fcc phase forms first, as a nonequilibrium transition phase. Another point which would appear to support the view that monolithic is a transient form is that the fcc layer occurs most frequently on curved boundaries convex into the beta phase. Since boundary curvature might be expected to be a measure of the driving force for boundary motion, this suggests that the most rapidly moving boundaries (those farthest from chemical equilibrium) are the ones with the most monolithic fcc interface phase. On the other hand, straight boundaries were found to be frequently associated with the striated interface phase, as might be expected if these were closer to equilibrium.

We believe that the bcc β phase transforms initially to an fcc structure as a result of the composition gradients described above. As reported earlier,⁽²⁾ the fcc structure is an intermediate atomic arrangement in the $\beta \rightarrow \alpha$ transformation. Calculations show that the expected lattice parameter of the fcc structure would be 1.4 times that of the β phase. The lattice parameter which we observe for the monolithic layer is 4.26Å, which is approximately 1.3 times larger than the β parameter. The high vanadium content apparently influences the $\beta \rightarrow \alpha$ transformation such that the fcc transition structure is stabilized.



SC5056.1TR

The transition from fcc interface phase to the striated form was, as noted earlier, frequently associated with $\{111\}$ twin formation in the fcc structure. That is, the initial form of interface phase is a narrow fcc monolithic layer which is subsequently modified by the formation of $\{111\}$ twins. The heavily twinned fcc layer then transforms to equilibrium hcp alpha phase resulting in thin plates of alpha phase. Inspection of the crystallography of the fcc to hcp transformation reveals that both the twinned and untwinned plates will transform to an identical alpha phase orientation, which is the Burgers orientation. Thus the primary alpha particle grows during cooling with its original orientation in spite of the complex transformation sequence. The newly formed α phase plates in the interface region appear to retain a high density of the prior fcc dislocations, while the twin boundaries seem to persist as internal boundaries in the α phase. Although most of this debris appears to eventually anneal out, many basal plane "faults" are present in the primary alpha particles and are probably remnants of the fcc twin boundaries, Figure 12.

This representation of interface phase formation precludes the presence of Type 2 alpha.⁽⁹⁾ The SAD patterns from interface phase had previously^(1,2) been compared to those arising from Type 2 α and their similarity led to the conclusion that the striated interface phase was hcp α phase of an orientation different from the adjacent alpha. However, this work shows that the interface phase patterns are, in fact, from twinned fcc structures. It is not surprising that twinned fcc and twinned hcp (Type 2 α) having the $(110) \parallel (11\bar{2}0)$ and $[\bar{1}\bar{1}1] \parallel [0001]$ relationship (with d-spacings of parallel planes within 5%) would generate similar diffraction patterns with respect to the parent β phase.



SC5056.1TR

In order for the above description of interface phase formation to be acceptable, the possible driving forces involved in the reactions should be examined. The metastable condition which exists during cooling was described earlier. As the α/β interface advances into the β phase, the β phase becomes more enriched in V and more vanadium must be rejected by newly formed α phase. A potential chemical driving force for the formation of interface phase results from the nonequilibrium, high vanadium content of the α/β interface region.

The influence of diffusion of vanadium and aluminum in the vicinity of the interface is difficult to assess quantitatively under these conditions where the interface is moving, the temperature is changing constantly, and the equilibrium volume fractions and compositions of the two phases are changing. However, a qualitative description of the composition and composition profile in the vicinity of the interface can be made. This has been done schematically in Figure 13. In Region I, which corresponds to the very slow cooling rates in Figure 3, equilibrium conditions obtain producing the sharp composition gradient depicted in the figure. This holds because the $\beta \rightarrow \alpha$ transformation will be slow, allowing vanadium to diffuse from the interface into the β phase. In Region III, which corresponds to the very fast cooling rates in Figure 3, a sharp composition gradient develops because the $\beta \rightarrow \alpha$ transformation is rapid. In this case, the α phase forms with a maximum (critical) vanadium content, which is higher than the equilibrium content, because the rapid cooling rate inhibits vanadium diffusion. Region II, which corresponds to the mid-region of Figure 3, exhibits a broad composition gradient in the α/β interface region. If vanadium diffusion is slightly



slower than beta transformation, the composition gradient will develop as depicted in the figure. The fcc layer will exist at the β phase side of the interface corresponding to a high vanadium content, while the hcp layer forms on the α phase side of the interface corresponding to a lower vanadium content.

In addition to the chemical change during cooling noted above, there is approximately a 5% volume expansion coincident with the $\beta \rightarrow \alpha$ transformation. This expansion, together with the larger coefficient of thermal expansion of the β phase, will place the alpha phase in compression. Since the β phase in Ti-6Al-4V has a higher yield strength than the α phase,⁽¹³⁾ the compressive stresses may be relieved by deformation in the vicinity of the α/β interface where the stresses will be highest. The twins observed in the monolithic fcc layer can provide the necessary stress relief. These stresses thus account for the deformation of the monolithic layer and provide a mechanical driving force for the completion of the bcc to hcp transformation.

This model of interface phase formation predicts that the initial product of the β phase decomposition will be an fcc phase having a vanadium content higher than that of the equilibrium α phase. With continued cooling, as the monolithic (fcc) layer enlarges, the compressive stresses on the α phase are relieved by deformation of the fcc layer. The subsequent diffusion of vanadium from the twinned fcc layer allows it to complete the transformation to hcp alpha phase. The process continues during cooling, thus producing broad striated layers.

A final comment regarding the similarities and differences of Type 2 α ⁽⁹⁾ and interface phase seems appropriate. Type 2 α is generally



SC5056.1TR

observed in the isothermal decomposition of metastable β phase alloys, which are characterized by lower volume fractions of α phase (compared to $\alpha+\beta$ alloys). Since the fcc structure does not form to any significant degree during isothermal treatments, the alpha phase particles form with the hcp structure in the metastable β phase alloys. Thus the original alternatives⁽⁹⁾ of nucleation and growth or mechanical twinning (which was subsequently supported by Margolin et al.⁽⁵⁾) mechanisms are not negated by the observation of fcc structures in nonisothermal transformations.

CONCLUSIONS

1. The α/β interface phase does not grow during isothermal treatments.
2. The interphase phase grows during slow cooling and its final thickness is a function of cooling rate.
3. The monolithic morphology of interface phase has a face centered cubic structure and obeys the crystallographic relationship:
 $(110)\beta \parallel (111) \text{ fcc} \parallel (0002)\alpha$ and $[111]\beta \parallel [110] \text{ fcc} \parallel [\bar{1}120]\alpha$.
4. The fcc monolithic interface phase may be a transition structure in the $\beta \rightarrow \alpha$ transformation.
5. The interface phase may result from sluggish beta stabilizer (vanadium) diffusion away from the transforming ($\beta \rightarrow \alpha$) interface region.



Rockwell International
Science Center

SC5056.1TR

ACKNOWLEDGEMENTS

We are pleased to acknowledge the assistance of R. A. Spurling, P. Q. Sauers, and E. H. Wright. This work was supported by the Office of Naval Research (Contract N00014-76-C-0598).



REFERENCES

1. C. G. Rhodes and J. C. Williams, Met. Trans., Vol. 6A, 1975, pp 1670-71
2. C. G. Rhodes and N. E. Paton, Proceedings of 3rd Intern. Conf. on Ti, Moscow, 1976, in press
3. J. C. Chesnutt and J. C. Williams, Scanning Electron Microscopy/1974 (Part IV), p 895, ITT Research Institute, Chicago, 1974
4. C. A. Stubbington and A. W. Bowen, J. Mater. Sci., Vol. 9, 1974, pp 941-47
5. H. Margolin, E. Levine, and M. Young, Met. Trans., Vol. 8A, 1977, pp 373-77
6. R. A. Spurling, Met. Trans., Vol. 6A, 1975, pp 1660-61
7. R. A. Spurling, C. G. Rhodes, and J. C. Williams, Met. Trans., Vol 5, 1974, pp 2597-600
8. G. Hahn, Senior Thesis, New York Univ., cited by P. A. Albert, Trans. TMS-AIME, Vol. 197, 1953, pp 1449-50
9. C. G. Rhodes and J. C. Williams, Met. Trans., Vol. 6A, 1975, pp 2103-14
10. D. J. Maykuth, F. C. Holden, D. N. Williams, H. R. Ogden, and R. I. Jaffee, DMIC Report 136B, Battelle Memorial Institute, Columbus, Ohio, May 1961
11. L. E. Tanner, DMIC Report 46G, Battelle Memorial Institute, Columbus, Ohio, Oct. 1959
12. F. A. Shunk: Constitution of Binary Alloys, Second Supplement, p 703 McGraw-Hill Book Co., New York, 1969
13. N. E. Paton, Science Center, Rockwell International, Thousand Oaks, California, unpublished research, 1977



TABLE I
COMPOSITION BY WEIGHT OF Ti-6Al-4V

Heat	Ti	Al	V	Fe	C	O	H	N
#1	Bal	6.15	4.09	0.18	0.011	0.129	0.0067	0.019
#2	Bal	6.1	4.0	0.19	0.02	0.122	0.0088	0.018



FIGURE CAPTIONS

- Fig. 1 TEM of Ti-6Al-4V isothermally reacted at 704°C (1300°F) for (a) 1 minute, (b) 24 hours.
- Fig. 2 TEM of Ti-6Al-4V isothermally reacted at 593°C (1100°F) for (a) 2 minutes, (b) 24 hours.
- Fig. 3 Interfacial layer width as a function of cooling rate from 1030°C (1885°F) in Ti-6Al-4V.
- Fig. 4 TEM of Ti-6Al-4V cooled 28°C/hr (50°F/hr) from 1030°C (1885°F) to 649°C (1200°F) and water quenched.
- Fig. 5 TEM of Ti-6Al-4V cooled 28°C/hr (50°F/hr) from 1030°C (1885°F) to 760°C (1400°F) and water quenched.
- Fig. 6 TEM of Ti-6Al-4V illustrating fcc structure of monolithic interface phase: (a) SAD of interface phase in [011] fcc orientation and adjacent beta phase in [001] orientation, (b) dark field image of beta phase, (c) dark field image of interfacial layer, (d) dark field of interfacial layer.
- Fig. 7 TEM of Ti-6Al-4V illustrating internal striations in monolithic layer.
- Fig. 8 TEM of Ti-6Al-4V illustrating detailed structure of striated interfacial layer: (a) bright field, (b) dark field.
- Fig. 9 Selected area electron diffraction pattern from striated interfacial layer.
- Fig. 10 Selected area electron diffraction patterns confirming orientation relation among beta phase, interface phase, and alpha phase.
- Fig. 11 TEM of Ti-6Al-4V illustrating monolithic (white) and striated (dark) interfacial layers in α/β boundary.
- Fig. 12 TEM of Ti-6Al-4V demonstrating basal plane faults in primary alpha phase.
- Fig. 13 Schematic description of vanadium concentration gradient in three regions of Figure 3 corresponding to (I) very slow cooling rate, (II) intermediate cooling rate, and (III) rapid cooling rate.

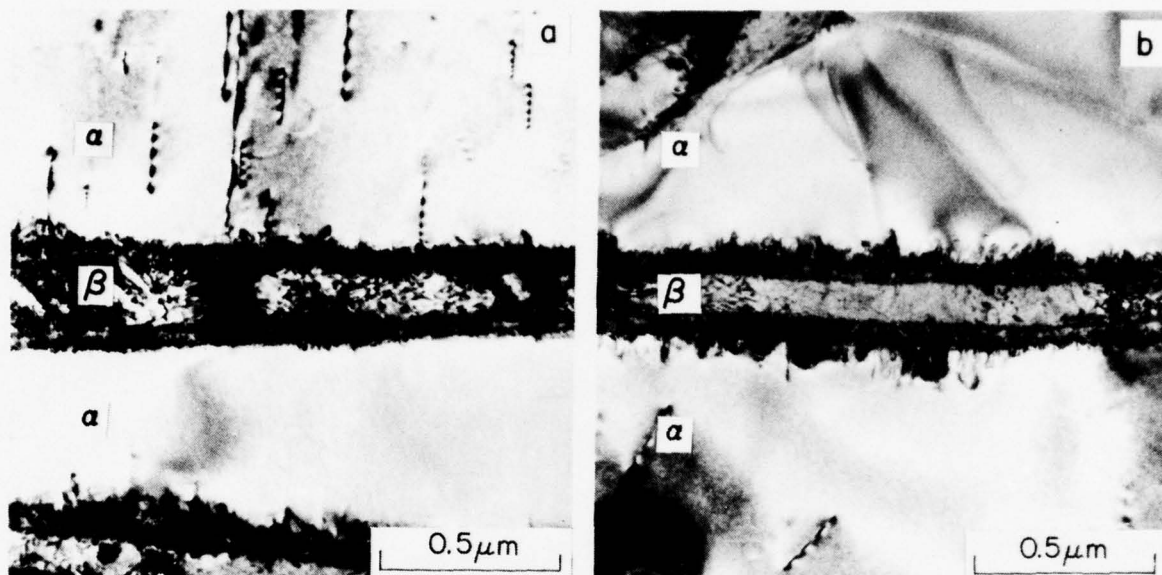


Fig. 1 TEM of Ti-6Al-4V isothermally reacted at 704°C (1300°F) for (a) 1 minute, (b) 24 hours.

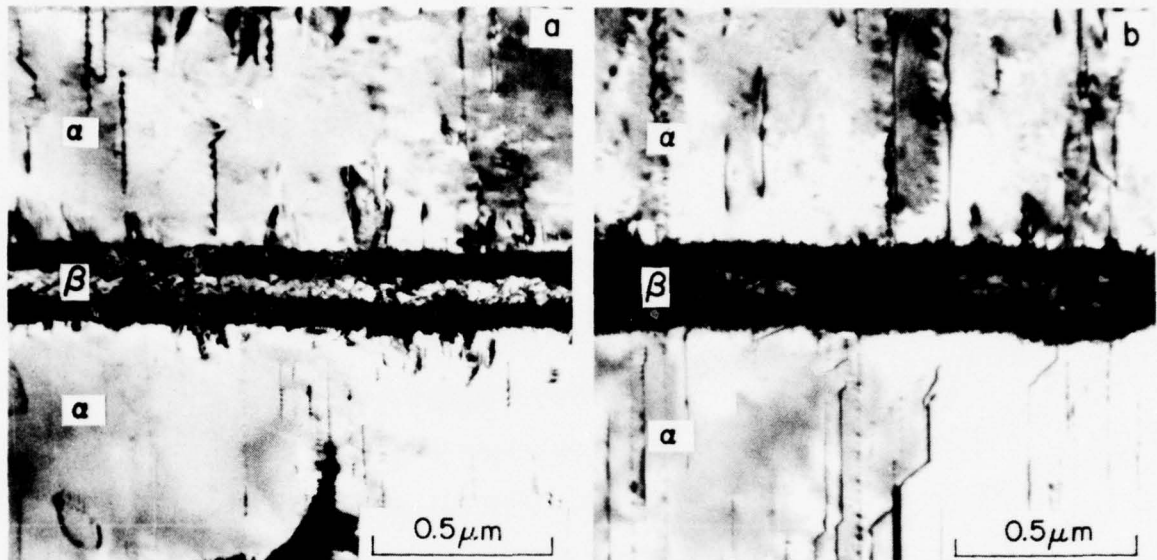


Fig. 2 TEM of Ti-6Al-4V isothermally reacted at 593⁰C (1100⁰F) for (a) 2 minutes, (b) 24 hours.



SC5056.1TR
20

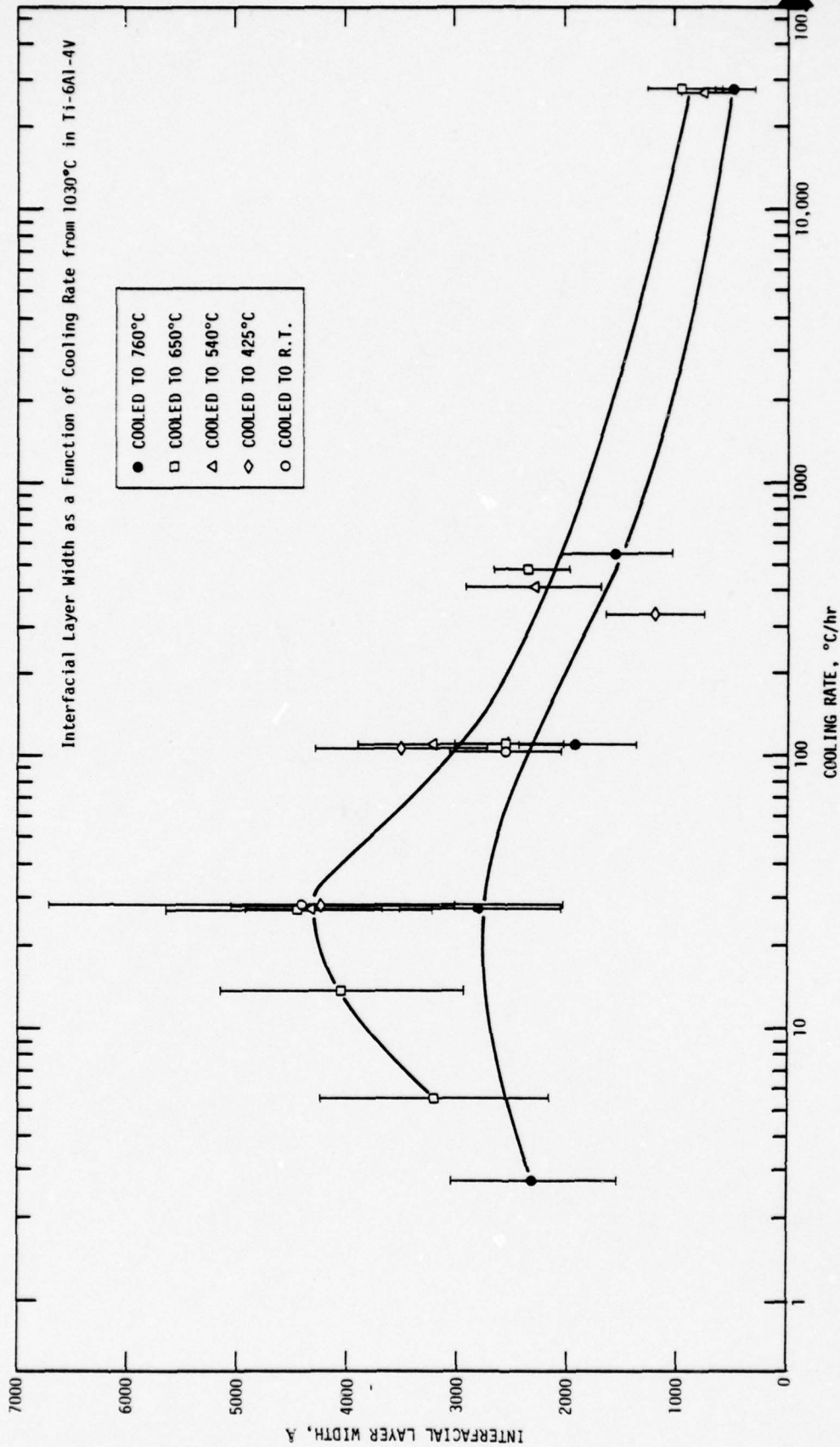


Fig. 3 Interfacial layer width as a function of cooling rate from 1030°C (1885°F) in Ti-6Al-4V.

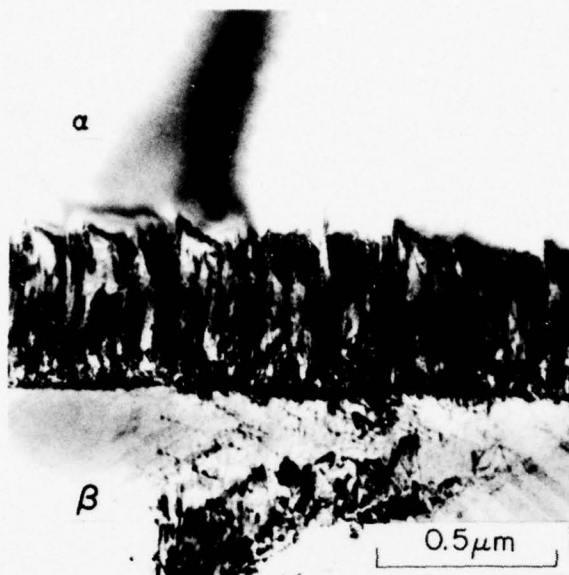


Fig. 4 TEM of Ti-6Al-4V cooled 28°C/hr (50°F/hr) from 1030°C (1885°F) to 649°C (1200°F) and water quenched.

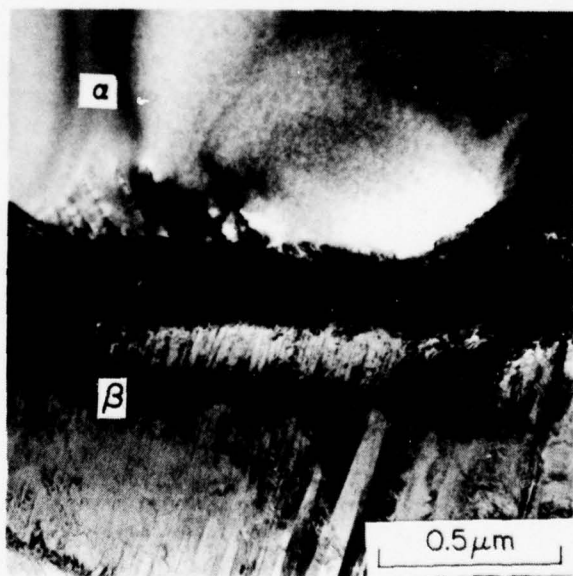


Fig. 5 TEM of Ti-6Al-4V cooled 28°C/hr (50°F/hr) from 1030°C (1885°F) to 760°C (1400°F) and water quenched.

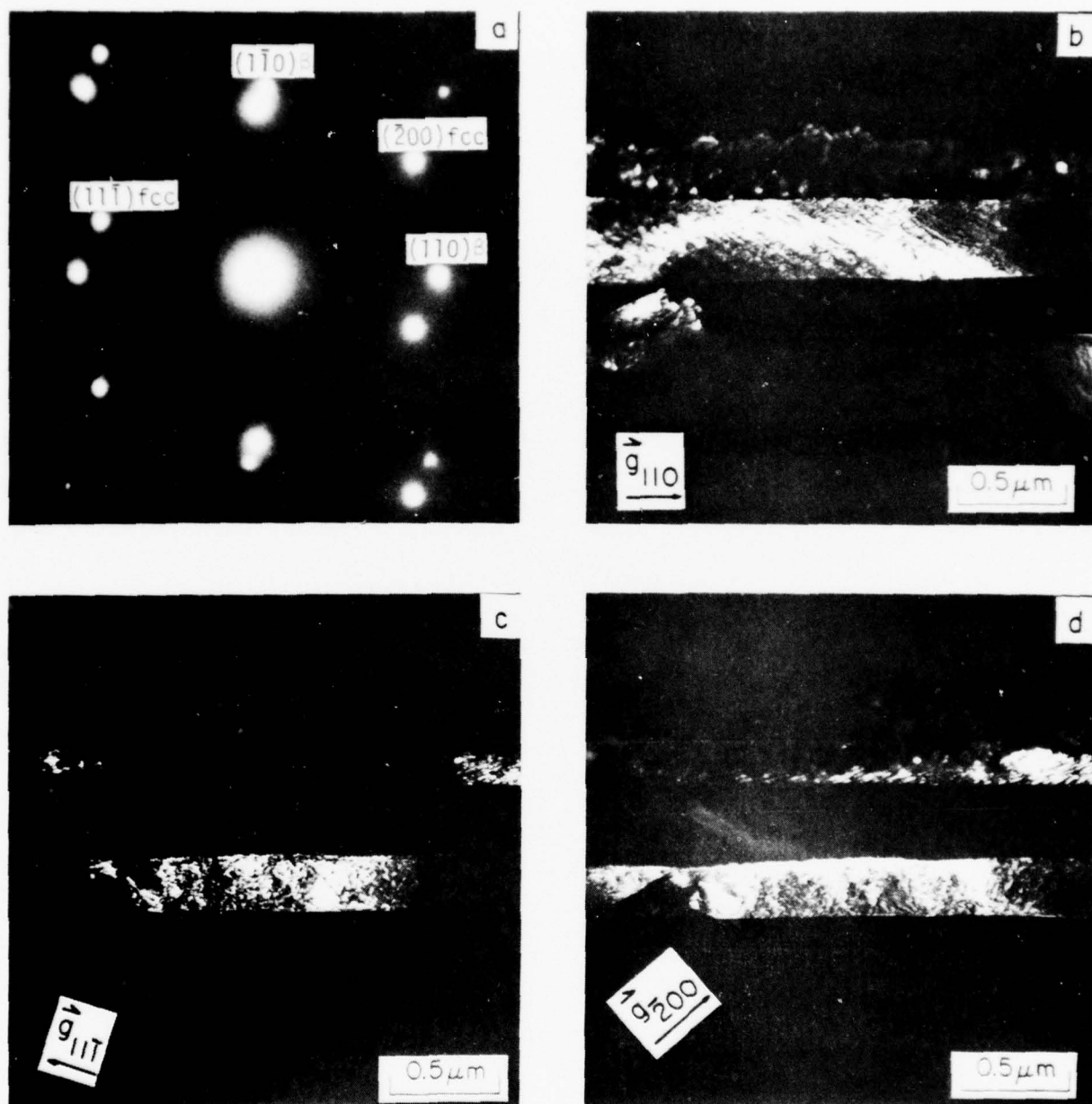


Fig. 6 TEM of Ti-6Al-4V illustrating fcc structure of monolithic interface phase: (a) SAD of interface phase in $[011]$ fcc orientation and adjacent beta phase in $[001]$ orientation, (b) dark field image of beta phase, (c) dark field image of interfacial layer, (d) dark field of interfacial layer.

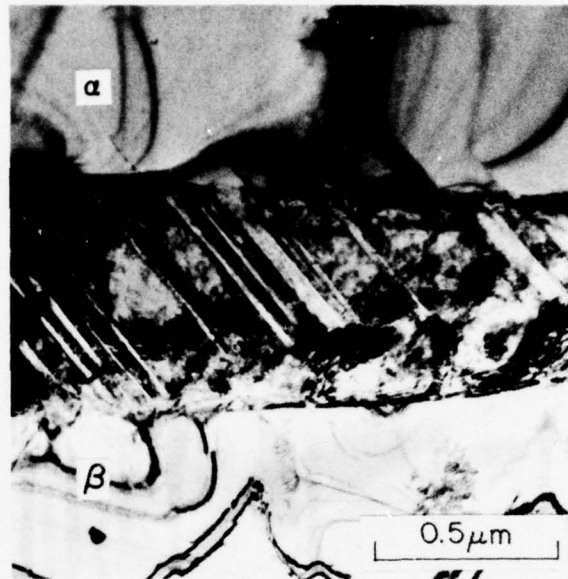


Fig. 7 TEM of Ti-6Al-4V illustrating internal striations in monolithic layer.

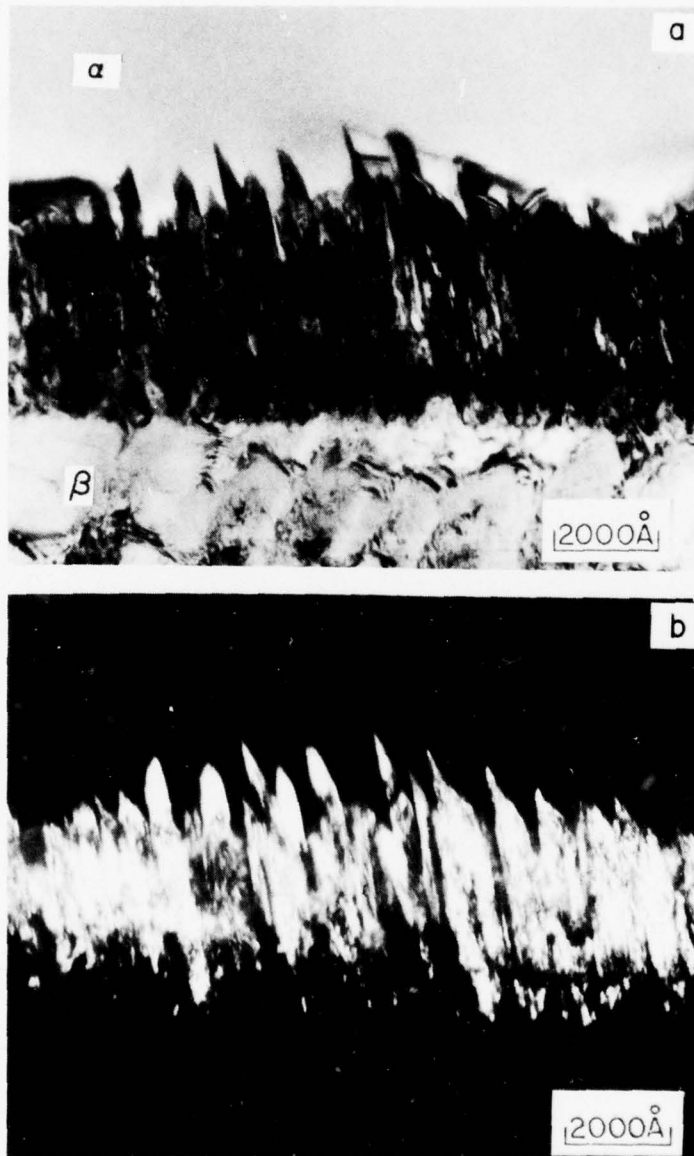


Fig. 8 TEM of Ti-6Al-4V illustrating detailed structure of striated interfacial layer: (a) bright field, (b) dark field.

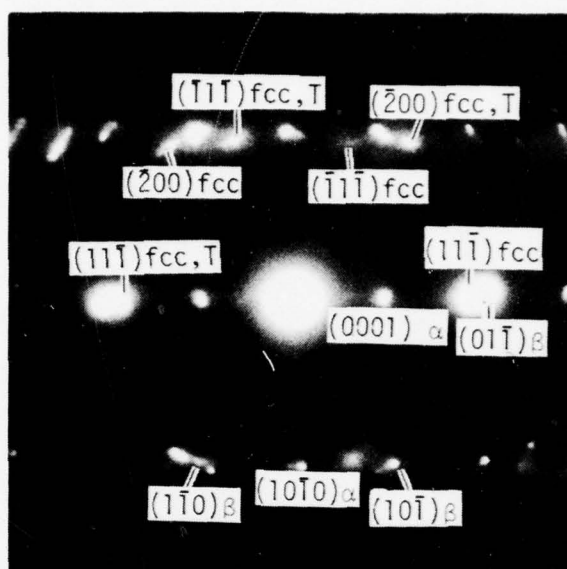


Fig. 9 Selected area electron diffraction pattern from striated interfacial layer.



SC5056.1TR

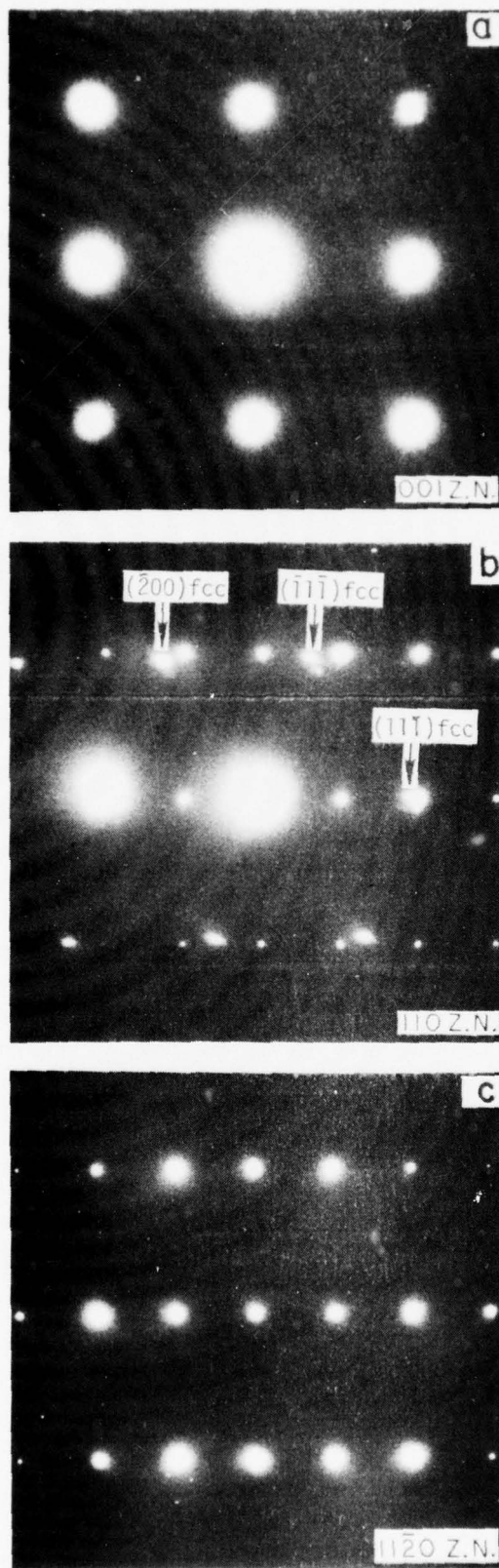


Fig. 10 Selected area electron diffraction patterns confirming orientation relation among beta phase, interface phase, and alpha phase.

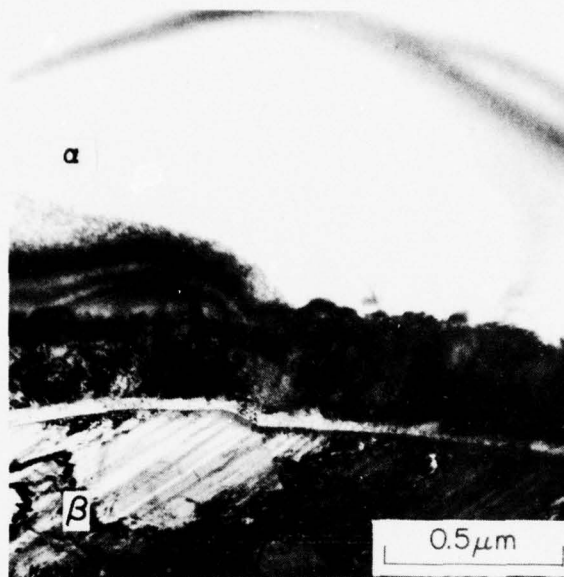


Fig. 11 TEM of Ti-6Al-4V illustrating monolithic (white) and striated (dark) interfacial layers in α/β boundary.

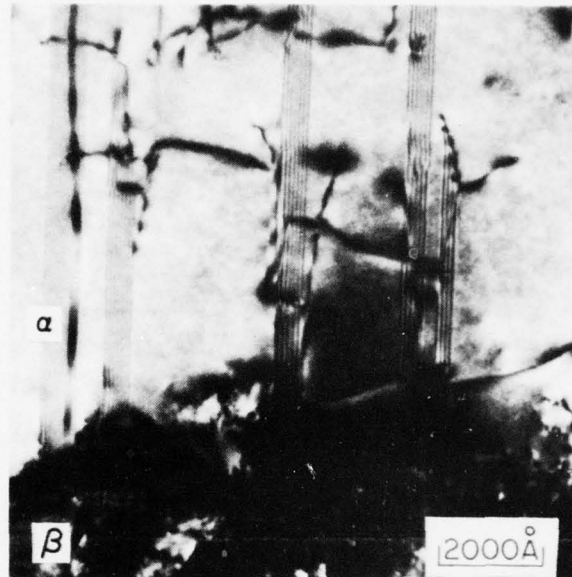


Fig. 12 TEM of Ti-6Al-4V demonstrating basal plane faults in primary alpha phase.

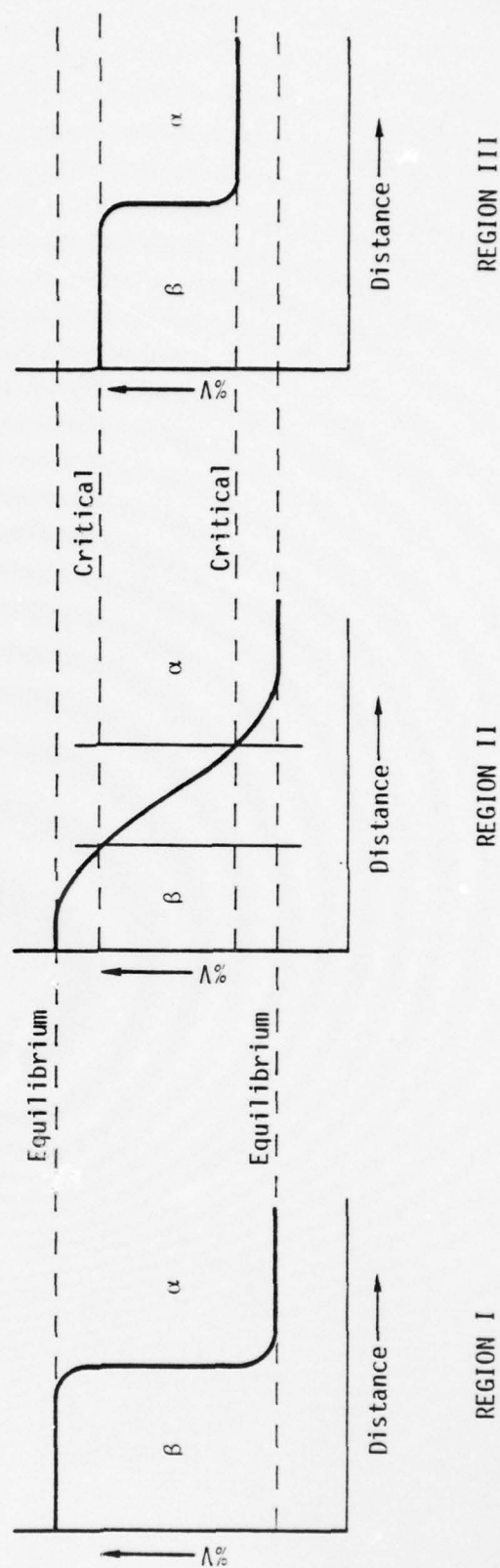


Fig. 13 Schematic description of vanadium concentration gradient in three regions of Figure 3 corresponding to (I) very slow cooling rate, (II) intermediate cooling rate, and (III) rapid cooling rate.



SC5056.2TR

7.2 THE INFLUENCE OF α/β INTERFACE PHASE ON TENSILE PROPERTIES IN Ti-6Al-4V

C.G. Rhodes and N.E. Paton
Rockwell International Science Center
Thousand Oaks, California

ABSTRACT

The effects of α/β interface phase on room temperature tensile properties in Ti-6Al-4V having an equiaxed primary α microstructure have been studied systematically. Due to the conditions under which it grows, manipulation of the interface phase width results in alteration of the volume fraction of primary α in the alloy. Tensile yield strength and elongation were correlated to interface phase width and volume fraction primary α . The relative individual influence of each of these microstructural features on properties is not unambiguously clear, but evidence indicates that yield strength increases with increasing interface phase width when the interface phase exceeds about 2500\AA and elongation decreases with increasing interface phase width when the interface phase is less than about 2500\AA . It is shown that the interface phase raises yield strength and lowers elongation by acting as a barrier to slip, intensifying planar dislocation arrangements in the primary alpha. The concepts of a "rule of mixtures" and "continuous phase" as applied to alpha plus beta phase microstructures are examined in terms of describing the tensile properties of Ti-6Al-4V.



INTRODUCTION

"Interface phase" and "interfacial layer" are terms used to describe the microstructural feature which is present under certain conditions in the α/β interfaces in two-phase titanium alloys.⁽¹⁻⁴⁾ Interface phase was previously shown to occur as an intermediate step in the $\beta \rightarrow \alpha$ transformation during slow cooling, presumably as a result of sluggish diffusion of beta stabilizers.⁽⁴⁾ Slow cooling is an integral part of many processing techniques for titanium alloys, and consequently the potential effects of interface phase on mechanical properties in these alloys warrant investigation.

The presence of a broad layer of interface phase--it has been observed as broad as 1 micron⁽⁴⁾--may lead to deleterious effects on mechanical properties. For instance, the interface phase might provide an easy crack path or crack nucleation sites in a fatigue failure or a tensile overload failure. Additionally, the interfacial layer may affect ductility by inhibiting slip between the α and β phases or by providing prolific dislocation sources for both the α and β phases.

Margolin et al.,⁽³⁾ on the other hand, have speculated that interface phase should have little or no effect on ductility. They suggest that slip is easily accommodated across α/β interfaces, however, they

cite results on alloys which have been heat treated to minimize interface phase.⁽³⁾ Margolin et al. conclude that the possible effects of interface phase on crack propagation would be, at most, only a secondary effect.



In light of the uncertainties surrounding the influence of interface phase, a study was undertaken to examine the effects of interface phase on mechanical properties in Ti-6Al-4V. This paper reports the results of the tensile properties portion of the study.

EXPERIMENTAL

Two heats of Ti-6Al-4V were used in this work, the chemical analyses are listed in Table I. The "as-received" microstructure of both heats consisted of ~90% equiaxed primary alpha particles, having approximately a 12 μ m diameter in a continuous β matrix. The heat treatments were carried out with the samples either in a dynamic inert gas atmosphere or encapsulated in evacuated ampoules. A programmable controller supplying power to the furnace was used for controlled-cooling-rate treatments.

Tensile tests were conducted on an Instron testing machine with an extensometer attached to the sample. The samples were in the form of round bars with a 6.35 mm diameter and 31.75 mm gauge length. A strain rate of $2.6 \times 10^{-4} \text{ sec}^{-1}$ was used in all tensile tests. The starting material of both heats used in the study was in the form of plate. Tensile specimens from each heat were taken such that the tensile axis corresponded to the same orientation of the plate for all samples to reduce texture effects in the tensile results.

Thin foils for transmission electron microscopy were prepared by conventional electropolishing techniques⁽⁵⁾ or by ion milling.⁽⁶⁾ The



foils were examined in a Philips EM-300 electron microscope equipped with a double tilt goniometer stage.

RESULTS

Starting Conditions

In order to determine the influence of interface phase on tensile properties in Ti-6Al-4V, the other microstructural variables must be held constant, or at least allowed to vary within a minimal range. The major microstructural feature to be controlled in α/β titanium alloys is the primary alpha, because its morphology and volume fraction can affect tensile properties.⁽⁷⁾ A fixed morphology of primary alpha was, therefore, considered necessary for this study and, inasmuch as Ti-6Al-4V is most frequently used in an α/β processed condition, an equiaxed primary alpha morphology was selected. The volume fraction of primary alpha was less easily controlled because of the condition required to vary the interface phase. It was shown previously⁽⁴⁾ that interface phase can only be altered by altering the cooling rate from temperatures high in the $\alpha+\beta$ phase field or in the β -phase field. Since the amount of primary alpha phase will be affected by cooling rates and quenching temperatures, the variety of treatments used to produce various interface phase widths resulted in volume fractions of primary alpha ranging from .73 to .90 in tensile samples.

Previous work⁽⁴⁾ showed that the interface phase width in Ti-6Al-4V can be varied from 500Å to 4500Å. The constraint of retaining a constant



volume fraction primary alpha while developing various widths of interface phase proved virtually prohibitive in the formulation of heat treatments. The heat treatments selected for tensile specimens were either single-stage (controlled-cool treatments) or two-stage (controlled-cool followed by isothermal treatments). The isothermal step in the two-stage treatments was intended to reduce the width of the interface phase which had been formed during the slow cooling step. This was based on the concept that the lower amount of equilibrium alpha phase at the isothermal step temperature would promote transformation of $\alpha \rightarrow \beta$ which would initiate at α/β boundaries and consume interface phase. These treatments were only moderately successful in significantly altering interface phase widths at isothermal-treatment temperatures of 760°C (1400°F) and below, apparently because diffusion (transformation) rates are low at those temperatures and the maximum isothermal hold time was six hours. The single-stage, controlled-cool treatments were more effective in altering the interface phase width, but at the same time these treatments produced a wider variation in volume fraction primary alpha phase.

There are other microstructural features which may vary as a result of the manipulation of the interface phase width. Two of these features which may influence properties are beta phase decomposition and Ti_3Al formation in the primary alpha. During continuous slow cooling from high in the $\alpha + \beta$ phase field, there is little likelihood of α -phase precipitation within the β -phase, but upon quenching from a predetermined temperature at the end of the controlled-cooling step, the beta phase may decompose, depending upon its



composition. There may also be decomposition of the beta phase during the isothermal step of the two-stage heat treatments, again depending upon the β -phase composition. The presence of transformed β in the microstructure can have an effect on properties.⁽⁷⁾

The formation of Ti_3Al is a sluggish reaction, but is known to occur in Ti-6Al-4V.⁽⁸⁾ The very slow cooling rates required to promote large interface layer widths are conducive to α_2 (Ti_3Al) formation. The presence of α_2 particles in α -phase has been shown to influence tensile properties.⁽⁸⁾

All of the microstructural features described here can have an effect on mechanical properties. Each has a different degree of influence on any particular property and the relative contribution of each acting singly or in concert with others can only be analyzed when all variables are controlled. In order to isolate the effects of interface phase on tensile properties, therefore, the other microstructural variables must be held reasonably constant.

Tensile Results

Room temperature tensile tests were performed on fourteen specimens given a variety of subtransus heat treatments aimed at producing a variety of interfacial layer widths. In all cases, however, the primary α particles were equiaxed. The tensile results, presented in Table II, reveal that a wide range in tensile yield strengths (from 683 to 903 MN/m²) can be developed by altering the heat treatment of α/β processed Ti-6Al-4V. The ultimate tensile



strength is influenced considerably less by heat treatment within each alloy heat, although there is a systemic difference in ultimate strength between the two alloy heats.

Tensile elongation varies from 12.6 to 18.3% among the samples with no systematic difference between the two alloy heats. Generally, the tensile ductility increases as the yield strength decreases. Table II also lists the volume fraction of primary alpha phase for each tensile test specimen. These values are seen to range from 0.73 to 0.90.

In order to determine the inherent scatter in identical samples, five tensile specimens from heat #2 were given the identical treatment of $980^{\circ}\text{C}/2$ hrs, cooled at $56^{\circ}\text{C}/\text{hr}$ to $760^{\circ}\text{C}/\text{WQ}$, which should produce a microstructure containing a narrow interface phase. These tensile results showed an average yield strength of $700.5 \pm 15.8 \text{ MN/m}^2$ and an average elongation of $15.3 \pm 1.1\%$, where the limits are 95% confidence intervals. Although this small spread may result from variations in microstructure, it is assumed that the microstructure is constant among the samples and the scatter is the statistical variation for identical samples. This means that correlations drawn between properties and microstructure must be made among samples in which yield strength varies by more than 31.6 MN/m^2 and elongation by more than 2%.

Microstructures

A typical example of the microstructure of the tensile samples is shown in Fig. 1, where the equiaxed alpha particles as mentioned earlier, are



on the order of 12 microns in diameter. The effects of volume fraction primary alpha on tensile yield strength and tensile elongation are illustrated in Figs. 2 and 3. These plots indicate that there is a correlation of the amount of primary alpha in the microstructure with these two tensile properties, although there is scatter in the data. It would be logical to assume that other microstructural features mentioned earlier would also be contributing to the yield strength and elongation of each of these samples and may, in fact, account for some of the scatter observed in the plots of Figs. 2 and 3.

Transmission electron microscopy is required for characterization of interface phase, transformed β , and α_2 particle precipitation in the 6-4 alloy specimens. Although the heat treatments were designed to preclude the precipitation of α -phase particles within the β -phase matrix, test specimens 5 and 6 were found to contain some transformed β regions. However, since α precipitation in the β -phase generally acts to strengthen the alloy⁽⁷⁾ and no apparent strengthening has occurred in tests 5 and 6 due to α -phase particle precipitation (compare tests 5 and 7 which are within scatter, or tests 6 and 3), transformed β can be ignored as a significant microstructural feature in the tensile tests.

Each of the fourteen tensile samples was examined for α_2 formation and test specimens 1, 9, and 10 were found to contain α_2 . Figure 4 illustrates a typical example of the distribution of the fine α_2 particles. Inspection of Table II reveals that test specimen 1 had the greatest yield strength of both alloy heats and the lowest elongation of heat 1. Similarly, test specimens 9 and 10 had the highest yield strength and lowest elongation



SC5056.2TR

of heat 2. It is quite likely that the presence of α_2 in the primary α has influenced the tensile properties.

In the course of this investigation, we had occasion to re-heat samples which contained α_2 particles. It was noted that reheating to temperatures as high as 760°C does not dissolve the α_2 particles, whereas 816°C is sufficient for re-resolution of the particles. This behavior is illustrated in Fig. 5.

The final microstructural feature analyzed in this study is the α/β interface phase. Before an examination of the influence of interface phase on tensile properties is made, however, the relationship between interface phase width and volume fraction primary alpha needs to be established. This relationship is presented in Fig. 6, where a least squares fit of the data indicates a positive correlation of layer width and volume fraction primary alpha. This relationship clearly arises because of the mechanism by which interface phase forms.⁽⁴⁾

Figures 2 and 3 indicated a dependence of tensile properties on volume fraction primary alpha. However, the curve in Fig. 6 leads to the conclusion that the tensile data shown in Figs. 2 and 3 might alternatively be interpreted in terms of interface phase width rather than, or in addition to, volume fraction primary alpha. If interface phase does indeed influence tensile properties, its relative effect on those properties might be dominant or it might be relatively minor when compared to the effect of volume fraction primary alpha on properties. In the following paragraphs, the tensile data will be presented alternatively in terms of, first, the assumption that the interface phase exerts only a minor influence on properties, and, second, the



SC5056.2TR

assumption that interface phase has a dominant effect on properties. This treatment of the data is made in order to assess the relative effects of interface phase and primary alpha in influencing tensile properties.

If the interface phase has only a minor effect on tensile properties, then one might expect to find that the scatter in the data points in Figs. 2 and 3 could be accounted for by the presence of interface phase. In order to examine the influence of interface phase on the scatter of the Fig. 2 and 3 data, tensile properties of test specimens having nearly identical volume fraction primary alpha ($v.f.\alpha_p$) should be compared. Inspection of Fig. 2 reveals six test results within the narrow range of $0.88 \pm 0.02 v.f.\alpha_p$. Of these six, three are samples which contained α_2 particles and, therefore, are eliminated from consideration of interface phase effects. The other three show a variation in yield strength of 83 MN/m^2 , or about a 10% variation. These data are plotted in Fig. 7 as a function of interface phase width. A least squares fit of the three data points from samples with no α_2 in the microstructure is included to show the trend of the data, not necessarily to imply a linear relationship. The plot indicates a positive correlation of tensile yield strength with interface phase width, and that, at least for interface phase widths greater than 2700\AA , interface phase can account for the scatter in the data points of Fig. 2.

In a similar manner, inspection of Fig. 3 shows four test results within the narrow range of $0.80 \pm 0.01 v.f.\alpha_p$. These data which show a wide variation in elongation are plotted in Fig. 8 as a function of interface phase width. Again, a least squares fit of the data is drawn only to indicate the trend which is a negative correlation of tensile elongation with interface



SC5056.2TR

phase width. It can be seen that at least for interface layer widths less than 2800\AA , interface phase can account for the scatter in the data points of Fig. 3.

The approach used in the generation of Figs. 7 and 8 was one that assumed the influence of interface phase on tensile properties to be minor compared to the influence of $v.f.\alpha_p$. If, on the other hand, the effect of interface phase were dominant over $v.f.\alpha_p$, the tensile data could be plotted as in Figs. 9 and 10, in which the influence of $v.f.\alpha_p$ is ignored and all data are plotted on a single graph. Figure 9 reveals that interface phase has little influence on tensile yield strength until it attains a width of greater than 2500\AA , beyond which it has a strong influence on yield strength.

The relationship between elongation and interface phase width is shown in Fig. 10. In this case, the tensile elongation decreases with increasing interface phase width until the layer reaches $\sim 2500\text{\AA}$, at which point the elongation appears to have attained a minimum value. Continued increase in interface phase width beyond $\sim 2500\text{\AA}$ has little influence on elongation.

The dependence of yield strength or elongation on interfacial layer width is different from the dependence of these properties on volume fraction primary alpha (compare Figs. 2 and 9, or 3 and 10). Although this observation is not evidence that one microstructural feature is dominant over the other as regards tensile properties, it seems to indicate that each has some effect on the properties. More will be said on this in the Discussion Section.

The gauge section of each of the tensile samples was examined by thin foil transmission electron microscopy in order to determine the influence of



samples with broad interface phase exhibited more intense planar slip in the primary α particles whereas those with narrow interface phase showed a lower density of dislocations contained in planar bands, Figs. 11 and 12. The prominent slip bands in Figs. 11(a) and 12(a) are seen to contain a high density of dislocations; trace analyses indicated that these bands lie on $\{1010\}$ planes. The samples with narrow interface phase, Figs. 11(b) and 12(b), show little indication of planar slip.

DISCUSSION

This work has shown that there is a correlation between tensile properties and either volume fraction primary alpha or interface phase width or both. In order to resolve the problem as to whether the properties are influenced by primary alpha or interface phase, the expected behavior will be examined and compared to the experimentally observed results.

In examining the influence of v.f. α_p on yield strength, Fig. 2, one must first consider the strengths of both the alpha and beta phases. It is assumed that the vanadium content of the primary alpha is unaltered from a maximum value of about 1.2 wt%⁽⁹⁾ as v.f. α_p changes, and therefore, the yield strength of the alpha phase will not be affected. The vanadium content of the β phase, however, changes as the volume fraction β -phase changes. Calculations show that the composition of the β phase is ~ 23.5 wt% V at 90% α_p and 13.8 wt% V at 80% α_p . Extrapolation of the data of



Ling et al.⁽¹⁰⁾ shows that the tensile yield strength of Ti-V (β -phase) will increase by $\sim 40\%$ as the vanadium content increases from 13.8 to 23.5 wt%.

There is some question as to whether a rule of mixtures predicts the strength of the α/β alloys or whether the strength more closely follows that of the continuous phase.⁽⁷⁾ A rule of mixtures has likely been found lacking in predicting mechanical properties in α/β alloys because of the duplex (or triplex) distribution of α -phase, for these alloys are frequently treated to produce primary alpha, secondary alpha, and finely dispersed alpha in a transformed β matrix. The (normalized) contribution of each of these to the yield strength of the alloy would not be equal because each provides a different strengthening mechanism. However, in the present study, a rule of mixtures could be applied because the microstructure consists of coarse, equiaxed primary α particles in a nontransformed β matrix; that is, the alloy is composed of a mixture of two phases in which the presence of each phase only minimally influences the properties of the other. If one assumes a rule of mixtures to account for the two-phase alloy yield strength (Fig. 2), then the increase in β -phase yield strength (based on the extrapolation of Ling et al. data) only accounts for a 20.6 MN/m^2 increase in the alloy yield strength for an increase in primary alpha from .8 to .9 volume fraction. Clearly, a rule of mixtures analysis does not account for the large increase in yield strength with $v.f.\alpha_p$.

If one assumes that the yield strength of the two-phase alloy is governed by that of the continuous phase, in this case the β -phase, it would be expected that the alloy yield strength should increase by the 40% which was shown to be the β -phase increase. The observed increase, Fig. 2, is



124 MN/m² which corresponds to about a 17% increase. In this instance, the increase in alloy yield strength is significantly overestimated by the assumption that the continuous phase dominates the tensile properties. It appears, then, that the rule of mixtures does not apply in a system where it logically could and that the continuous-phase theory does not apply, but rather the observed behavior lies somewhere between these two extremes. The observed behavior could result from β -phase solid solution strengthening which contributes to the yield strength in some modification of the rule of mixtures or it could result from the presence of an additional microstructural feature, namely interface phase.

Further evidence that the behavior observed in Fig. 2 is not necessarily the result of β -phase strengthening is seen in the data of Holden et al.⁽¹¹⁾ for β -phase alloys in the Ti-Mn system. These data, shown in Fig. 13, indicate that the yield strength of the two-phase alloy is reduced by an increase in primary alpha phase, contrary to the data in Fig. 2. The samples from which Holden et al.'s data were obtained were treated so that interface phase would be minimized or eliminated.

The rule-of-mixtures calculation predicts a very slight positive correlation of tensile yield strength with increasing v.f. α_p and the Holden et al. data predict a negative correlation of tensile yield strength with increasing v.f. α_p . Neither of these predicts the strong positive correlation observed in Fig. 2. The "continuous-phase concept" predicts the behavior of Fig. 2, but it is based on experimental observation rather than developed theory. If one rejects the "continuous-phase concept" then the shape of the curve in Fig. 2 must be addressed. If one accepts the



"continuous-phase concept" as explaining the positive correlation of yield strength with volume fraction α_p , the wide spread in yield strength values for test samples having virtually identical v.f. α_p needs to be examined. Each of these will be considered.

If one assumes that a rule-of-mixtures concept should apply, then the curve in Fig. 2, which does not follow a rule-of-mixtures prediction based on two constituents, can be explained in terms of interface phase. The data of Fig. 9 reveal that, when the interface phase width exceeds about 2500Å, it begins to exert a positive influence on tensile yield strength. It would be reasonable to assume, under these conditions, that the alloy yield strength would be predicted by a rule of mixtures including the three microstructural features: v.f. α_p , v.f. β , and interface phase width. This explains why applications of the rule of mixtures using only two microstructural constituents have failed in the past.

If, on the other hand, one accepts the "continuous-phase concept," then interface phase can account for the scatter in the data of Fig. 2. This was demonstrated in Fig. 7 where a positive correlation of tensile yield strength with interface phase width for a constant v.f. α_p (and a constant β -phase composition) is apparent. Although, under these conditions, interface phase effects were considered secondary to β -phase solid solution strengthening, the data of Fig. 7 show a significant increase in yield strength due to interface phase over the range examined. Hence, whether or not one accepts the "continuous-phase concept," interface phase is seen to exert a significant influence on tensile yield strength.



SC5056.2TR

Although the preceding discussion was limited to yield strength, a similar one can be made for tensile elongation. Analyses of Figs. 3, 8, and 10 lead to the conclusion that interface phase has a negative correlation with tensile elongation, by means of arguments similar to those applied in the yield strength discussion.

A mechanism by which interface phase increases tensile yield strength and reduces tensile elongation is indicated from the transmission electron microscopy results. The planar dislocation arrangements observed in samples with broad interface phase (and corresponding higher yield strength and lower elongation) indicate that the interface phase acts as a barrier to slip transfer from the α to β phase. The back stresses built up by the densely packed dislocations will induce more rapid strain hardening and increase the yield strength. A reduction of planar slip in the samples with narrow interface phase indicates an easier transfer of slip from the α phase, resulting in decreased strain hardening and a lower yield strength. Elongation is affected in a similar manner. The ease of slip transfer results in higher elongation in those samples with narrow interface phase widths whereas the reduced dislocation generation and motion resulting from the planar dislocation arrangement in samples with broad layers will cause a decrease in total strain.

The relationship between interface phase width and volume percent primary alpha illustrated in Fig. 6 is to be expected because of the interface phase formation mechanism.⁽⁴⁾ The interface phase forms during slow cooling simultaneously with the transformation of β to α , i.e., as the volume fraction of primary α is increasing. Although this fact makes it difficult to produce a wide range of interface phase widths for a constant volume fraction primary



SC5056.2TR

alpha, several of the samples did have a reasonable range of interface phase widths as indicated by the scatter in the data of Fig. 6. The results demonstrate that interface phase widths can be altered even within the constraints of a fixed v.f. α_p , leading to the conclusion that tensile properties in Ti-6Al-4V can be manipulated by control of interface phase widths.

The formation of α_2 (Ti₃Al) in this alloy was not unexpected for it has been observed before.⁽⁸⁾ However, it has generally been observed after long time isothermal treatments. The presence of α_2 after cooling at 56°F/hr to RT should serve as an alert to users of Ti-6Al-4V that processing conditions utilizing slow cooling rates may introduce this potentially detrimental microstructural feature.

CONCLUSIONS

This study has shown that tensile yield strength and elongation in Ti-6Al-4V containing equiaxed primary alpha are influenced by α/β interface phase and/or volume fraction primary alpha. The relative individual influence on properties of each of these microstructural features is not unambiguously clear, but evidence indicates that (1) yield strength increases with increasing interface phase width when the interface phase exceeds about 2500Å and (2) elongation decreases with increasing interface phase width when the interface phase is less than about 2500Å. Interface phase raises yield strength and lowers elongation by acting as a barrier to slip, thus, intensifying planar dislocation arrangements in the primary alpha.



ACKNOWLEDGEMENTS

We are pleased to acknowledge the experimental assistance of L.F. Nevarez, R.A. Spurling, E.H. Wright, and P.Q. Sauers. This work was supported by the Office of Naval Research (Contract N00014-76-C-0598).

REFERENCES

1. C.G. Rhodes and J.C. Williams, Met. Trans., Vol. 6A, 1975, pp. 1670-71.
2. C.G. Rhodes and N.E. Paton, Proc. 3rd Int'l. Conf. on Ti, Moscow, 1976, in press.
3. H. Margolin, E. Levine and M. Young, Met. Trans., Vol. 8A, 1977, pp. 373-77.
4. C.G. Rhodes and N.E. Paton, "Mechanical Behavior of Titanium Alloys," Contract N00014-76-C-0598, Technical Report, SC5056-1TR, 1978.
5. R.A. Spurling, Met. Trans., Vol. 6A, 1975, pp. 1660-61.
6. R.A. Spurling, C.G. Rhodes and J.C. Williams, Met. Trans., Vol. 5, 1975, pp. 2597-600.
7. R.I. Jaffee, "Ti Sci. and Tech.," R.I. Jaffee and H.M. Burte, eds., Plenum Press, NY, 1973, pp. 1665-93.
8. G. Welsch, G. Lutjering, K. Gazioghi and W. Bunk, Met. Trans., Vol. 8A, 1977, pp. 169-77.
9. F.A. Shunk, "Constitution of Binary Alloys, 2nd Suppl.," McGraw-Hill, N.Y., 1969, p. 703.
10. F. Ling, E.A. Starke, Jr., and B.G. Lefevre, Met. Trans., Vol. 5, 1974, pp. 179-87.
11. F.C. Holden, H.R. Ogden and R.I. Jaffee, J. of Metals, Vol. 6, 1954, pp. 169-84.



TABLE I
COMPOSITION OF T1-6Al-4V, BY WEIGHT PERCENT

Heat	Ti	Al	V	Fe	C	O	H	N
#1	Bal	6.15	4.09	0.18	0.011	0.129	0.0067	0.019
#2	Bal	6.1	4.0	0.19	0.02	0.122	0.0088	0.018



TABLE II
ROOM TEMPERATURE TENSILE TEST RESULTS FOR TWO HEATS OF Ti-6Al-4V

Test No*	Heat Treatment	Interface Phase Width	Vol.Fract. Primary α	Y.S. MN/m ²	U.T.S. MN/m ²	Elong. (%)
1	980°C/2hrs <u>56°C/hr</u> RT +540°C/4 hrs/WQ	2370Å	0.88	903	972	12.9
2	925°C/2hrs <u>56°C/hr</u> 650°C/WQ	3480	.87	876	931	14.6
3	925°C/2hrs <u>56°C/hr</u> 705°C/WQ	3910	.86	855	903	15.2
4	925°C/2hrs <u>56°C/hr</u> 815°C/WQ	950	.79	745	986	18.3
5	980°C/2hrs <u>56°C/hr</u> RT + 815°C/4hrs/WQ	0	.76	731	986	16.3
6	980°C/2hr <u>56°C/hr</u> RT + 760°C/6hrs/WQ	2760	.81	724	972	14.4
7	870°C/2hrs <u>28°C/hr</u> 805°C/WQ	0	.77	710	958	16.4
8	980°C/2hrs <u>56°C/hr</u> 760°C/WQ	Not Meas	.73	683	965	16.2
9	980°C/2hrs <u>56°C/hr</u> RT +540°C/30min/WQ	2970	.90	834	869	12.6
10	980°C/2hrs <u>56°C/hr</u> RT +540°C/30min/AC	2420	.87	820	848	15.2
11	980°C/2hrs <u>56°C/hr</u> RT +540°C/30min/WQ	2730	.89	793	827	15.2
12	980°C/2hrs <u>56°C/hr</u> RT +730°C/30min/WQ	600	.76	710	910	16.2
13	980°C/2hrs <u>56°C/hr</u> 815°C/WQ	640	.79	703	910	16.6
14	980°C/2hrs <u>56°C/hr</u> RT <u>25°C/hr</u> 815°C/WQ	710	.80	689	903	17.0

* Tests 1-8 are Heat #1, Tests 9-14 are Heat #2.



FIGURE CAPTIONS

- Fig. 1 Scanning electron micrograph of Ti-6Al-4V depicting typical microstructure of samples used in this study.
- Fig. 2 Tensile yield strength as a function of volume percent primary alpha.
- Fig. 3 Tensile elongation as a function of volume percent primary alpha.
- Fig. 4 Thin foil transmission electron micrograph of tensile test #1 specimen revealing Ti_3Al particle formation within primary alpha. Dark field, $g(1011)\alpha_2$.
- Fig. 5 Selected area electron diffraction patterns demonstrating the stability of Ti_3Al . (a) as slow cooled, $980^\circ C \xrightarrow{56^\circ C/hr}$ room temperature; (b) as in (a) plus $760^\circ C/30min/WQ$; (c) as in (a) plus $816^\circ C/5min/WQ$.
- Fig. 6 Interface phase width as a function of volume percent primary alpha.
- Fig. 7 Tensile yield strength as a function of interface phase width for samples containing 88 ± 2 volume percent primary alpha.
- Fig. 8 Tensile elongation as a function of interface phase width for samples containing 80 ± 1 volume percent primary alpha.
- Fig. 9 Tensile yield strength as a function of interface phase width.
- Fig. 10 Tensile elongation as a function of interface phase width.
- Fig. 11 Thin foil transmission electron micrographs of two Ti-6Al-4V tensile tested specimens. $[11\bar{2}0]$ α zone normal in both micrographs. (a) test specimen #11, $\sigma_{ys} = 115$ ksi, $\epsilon = 15.2\%$, $\vec{g} = 1\bar{1}01$; (b) test specimen #12, $\sigma_{ys} = 103$ ksi, $\epsilon = 16.2\%$, $\vec{g} = 1\bar{1}01$.
- Fig. 12 Thin foil transmission electron micrographs of two Ti-6Al-4V tensile tested specimens, $[11\bar{2}3]$ α zone normal in both micrographs. (a) test specimen #11, $\sigma_{ys} = 115$ ksi, $\epsilon = 15.2\%$, $\vec{g} = 10\bar{1}1$; (b) test specimen #12, $\sigma_{ys} = 103$ ksi, $\epsilon = 16.2\%$, $\vec{g} = 10\bar{1}1$.
- Fig. 13 Tensile yield strength as a function of volume percent primary alpha in Ti-Mn alloys. Data from Holden et al.(11).



SC5056.2TR

▲ SC78-1606

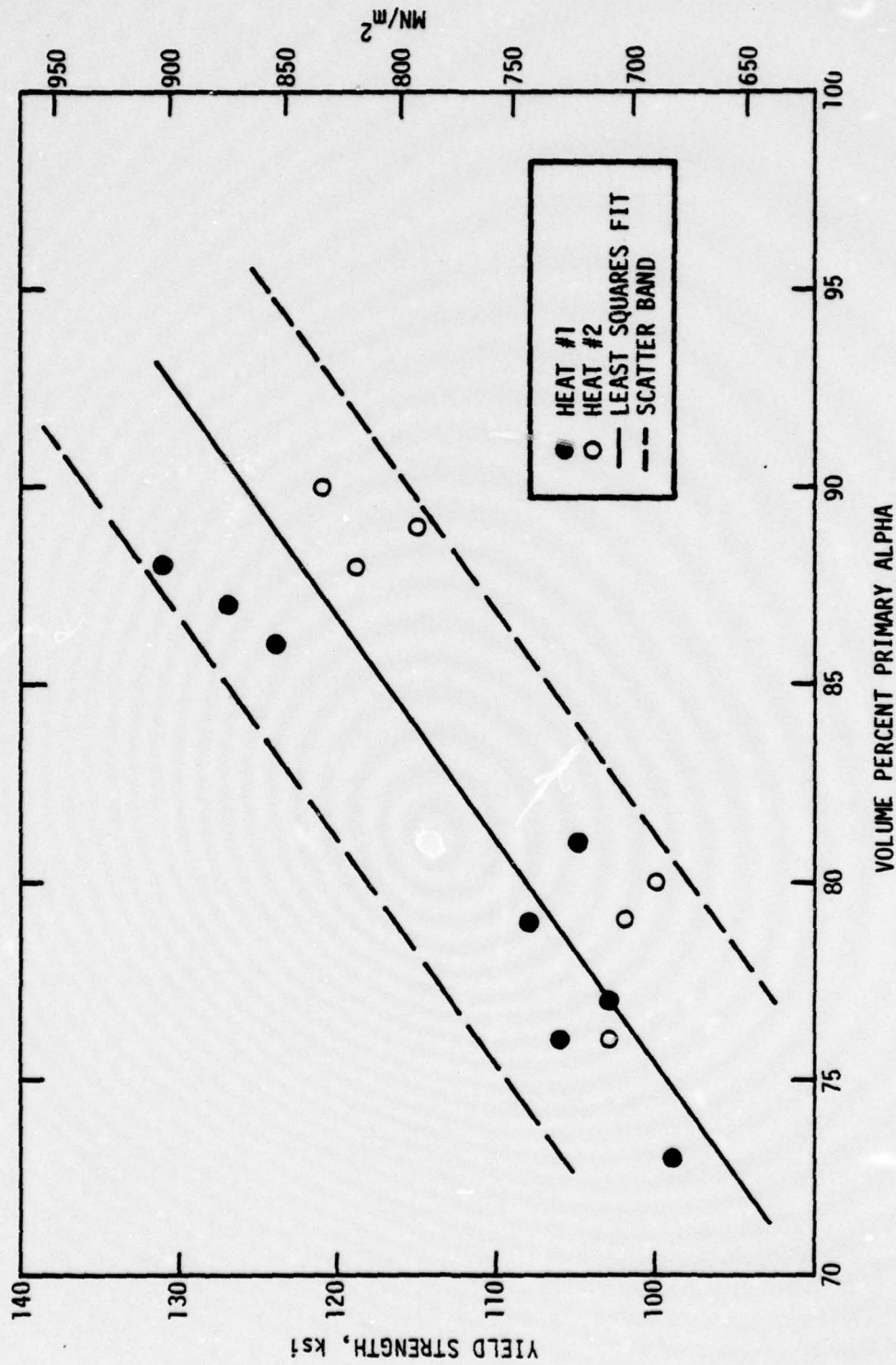


Fig. 2 Tensile yield strength as a function of volume percent primary alpha.



SC5056.2TR

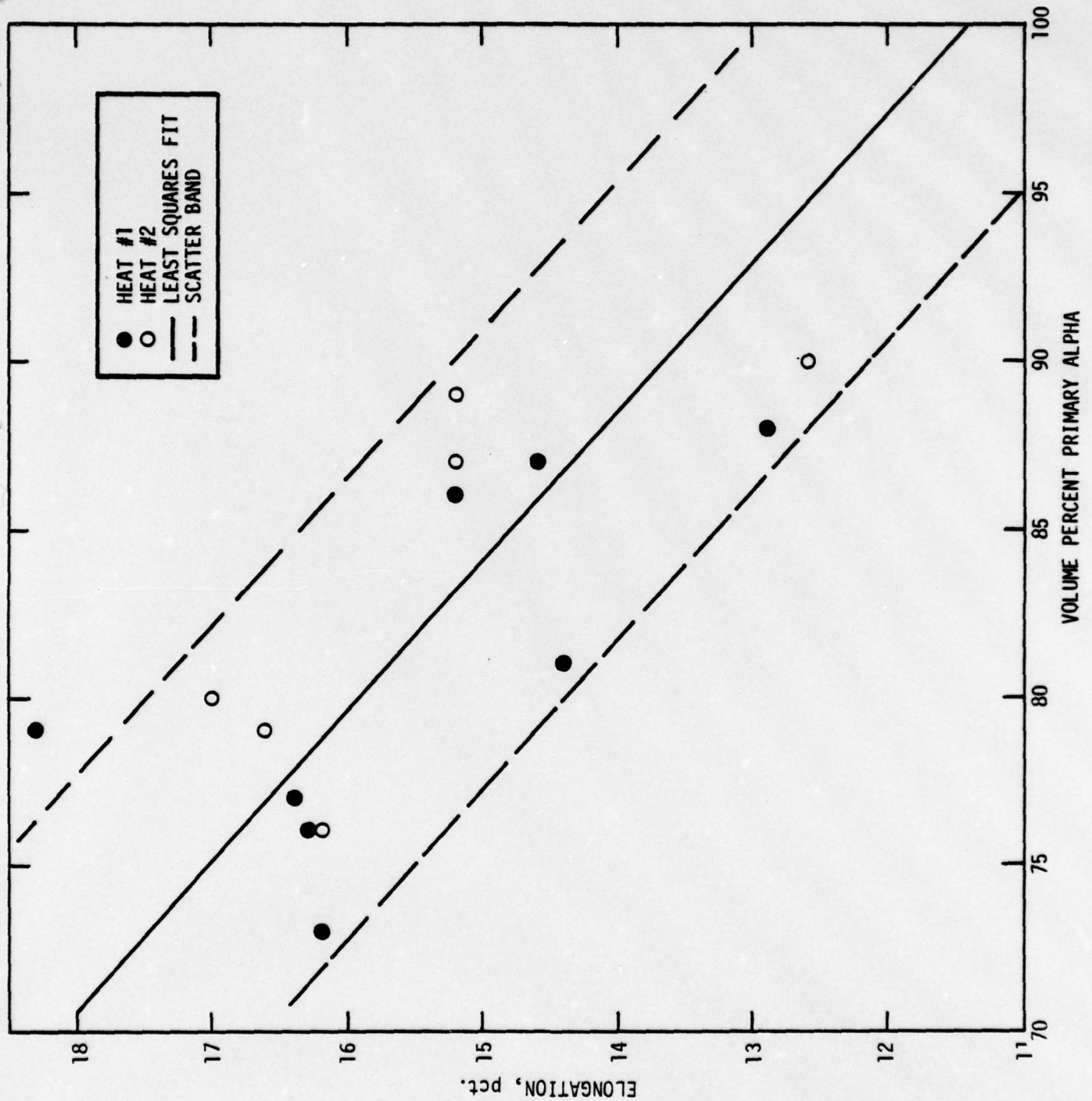


Fig. 3 Tensile elongation as a function of volume percent primary alpha.



Rockwell International

Science Center

SC5056.2TR



Fig. 4 Thin foil transmission electron micrograph of tensile test #1 specimen revealing Ti_3Al particle formation within primary alpha. Dark field, $g(1011)\alpha_2$.

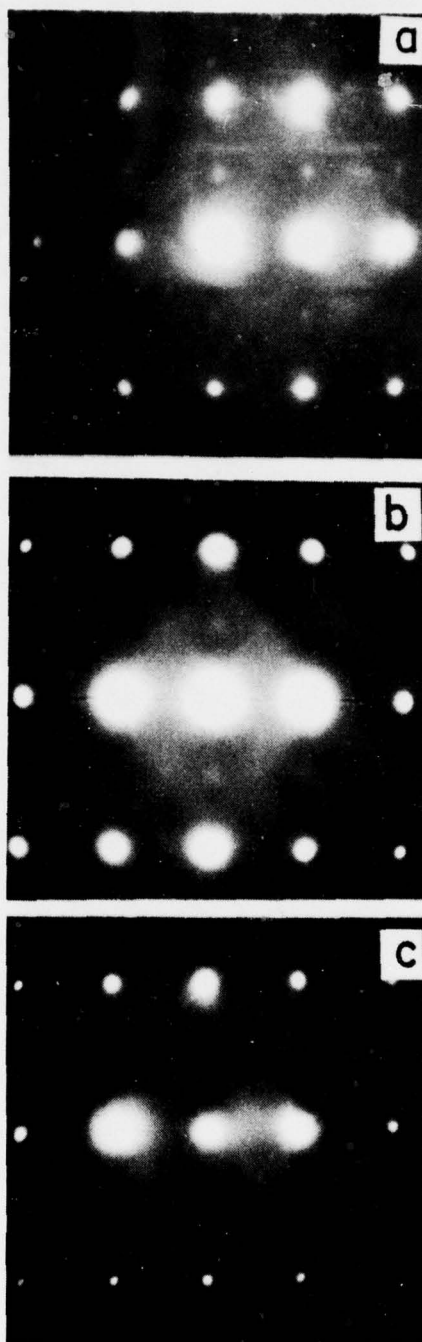


Fig. 5 Selected area electron diffraction patterns demonstrating the stability of Ti_3Al . (a) as slow cooled, $980^{\circ}C$ $56^{\circ}C/hr$ room temperature; (b) as in (a) plus $760^{\circ}C/30min/WQ$; (c) as in (a) plus $816^{\circ}C/5min/WQ$.



SC5056.2TR

SC78-1008

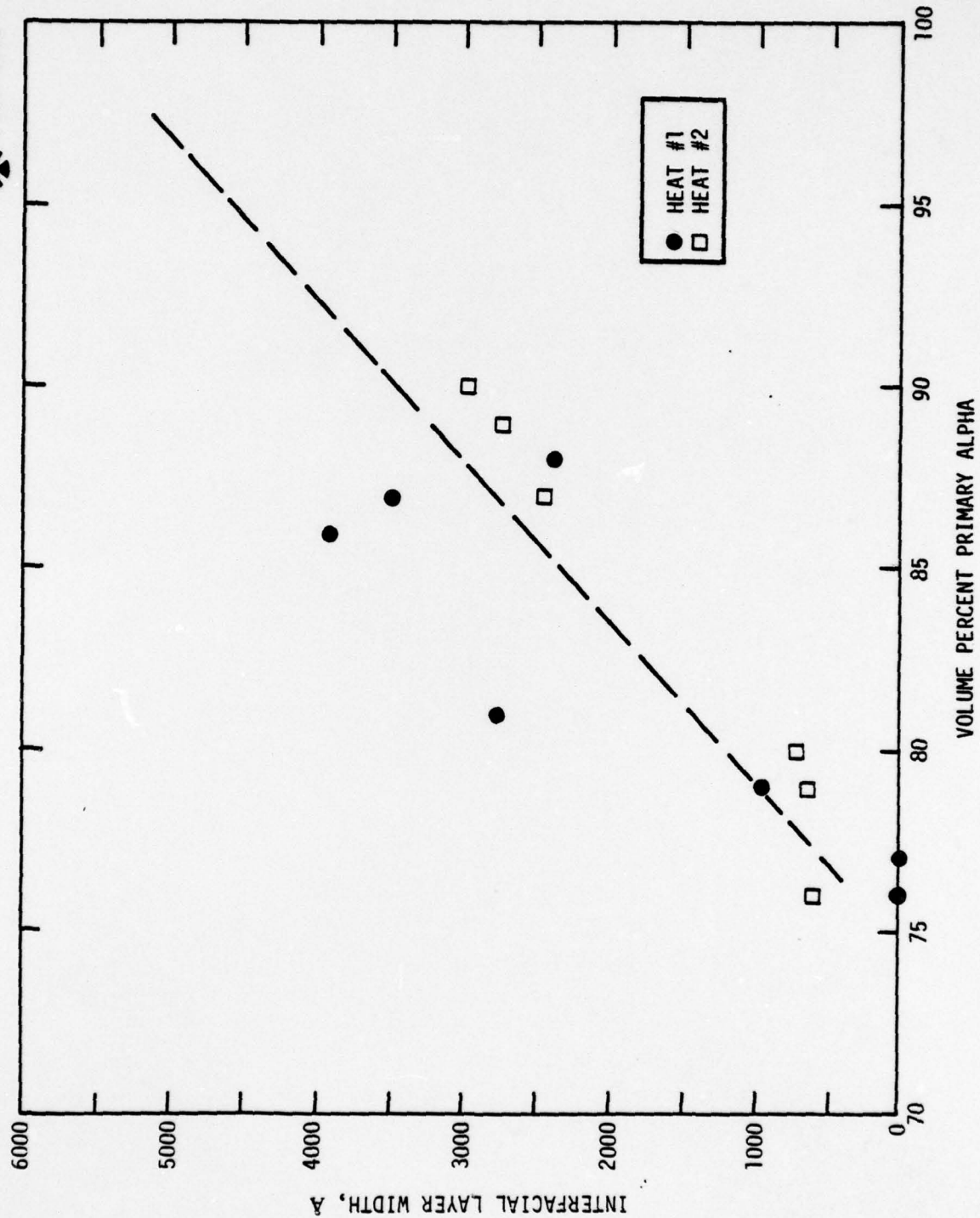


Fig. 6 Interface phase width as a function of volume percent primary alpha.

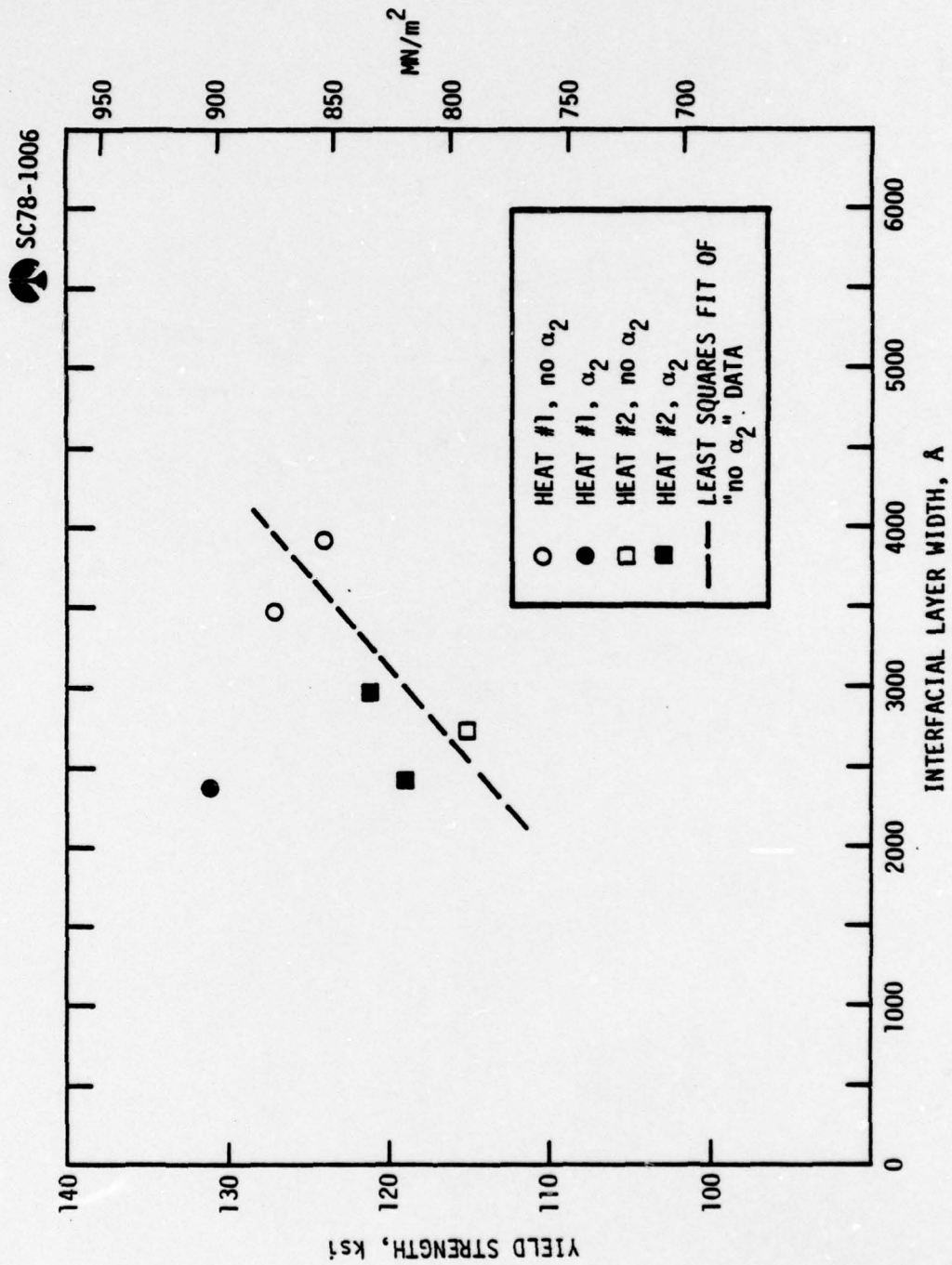


Fig. 7 Tensile yield strength as a function of interface phase width for samples containing 88±2 volume percent primary alpha.



SC5056.2TR

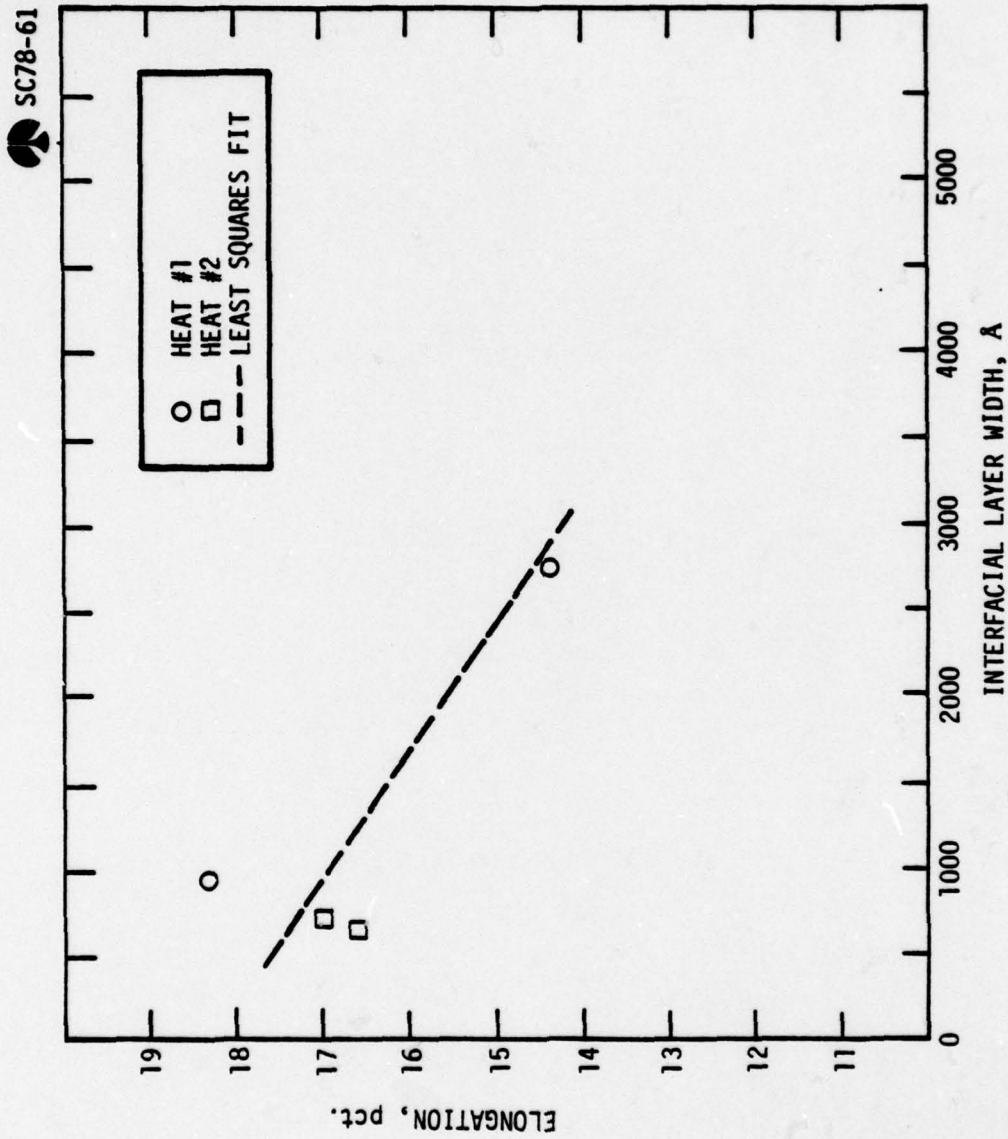


Fig. 8 Tensile elongation as a function of interface phase width for samples containing 80 ± 1 volume percent primary α phase.

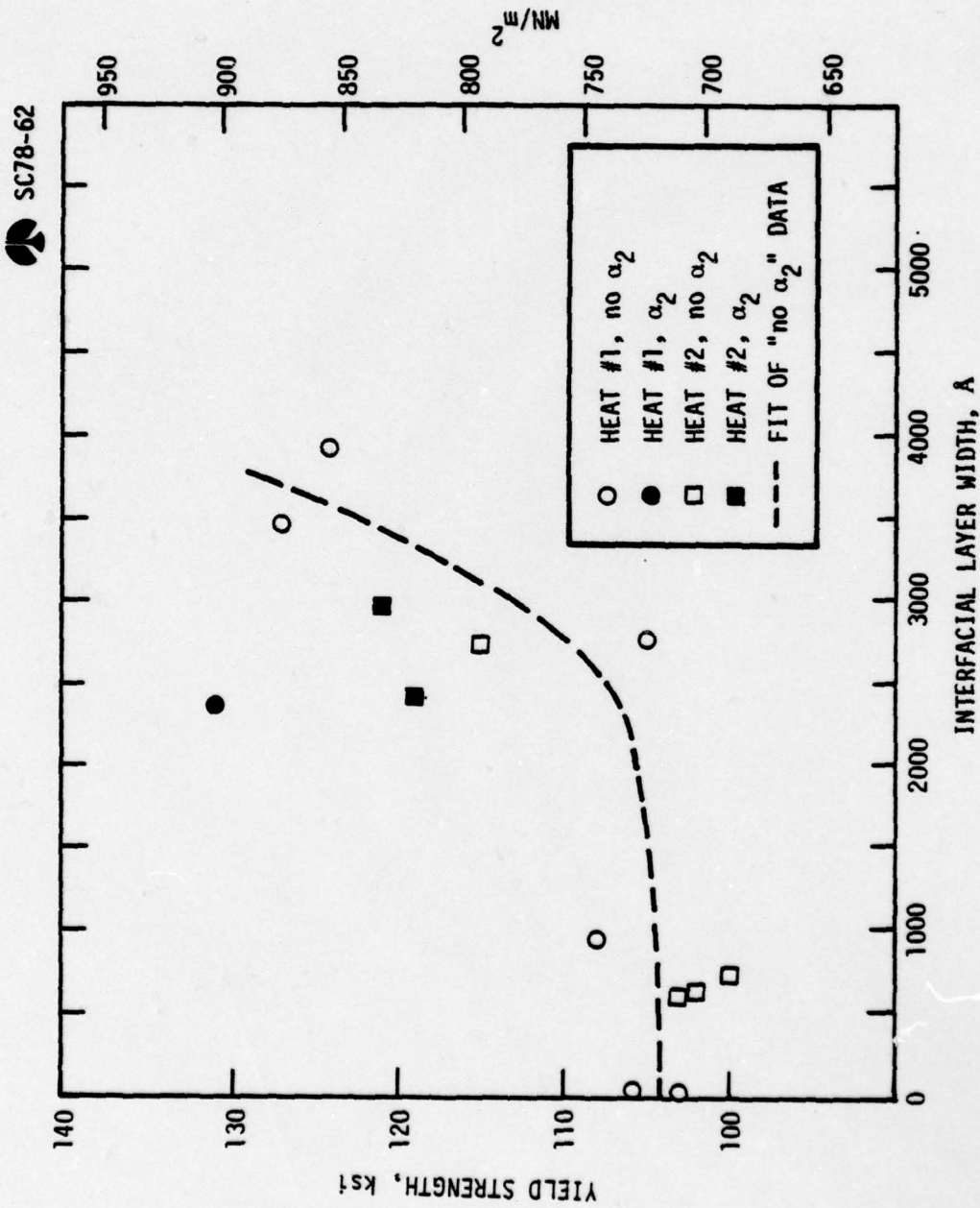


Fig. 9 Tensile yield strength as a function of interface phase width.



SC5056.2TR

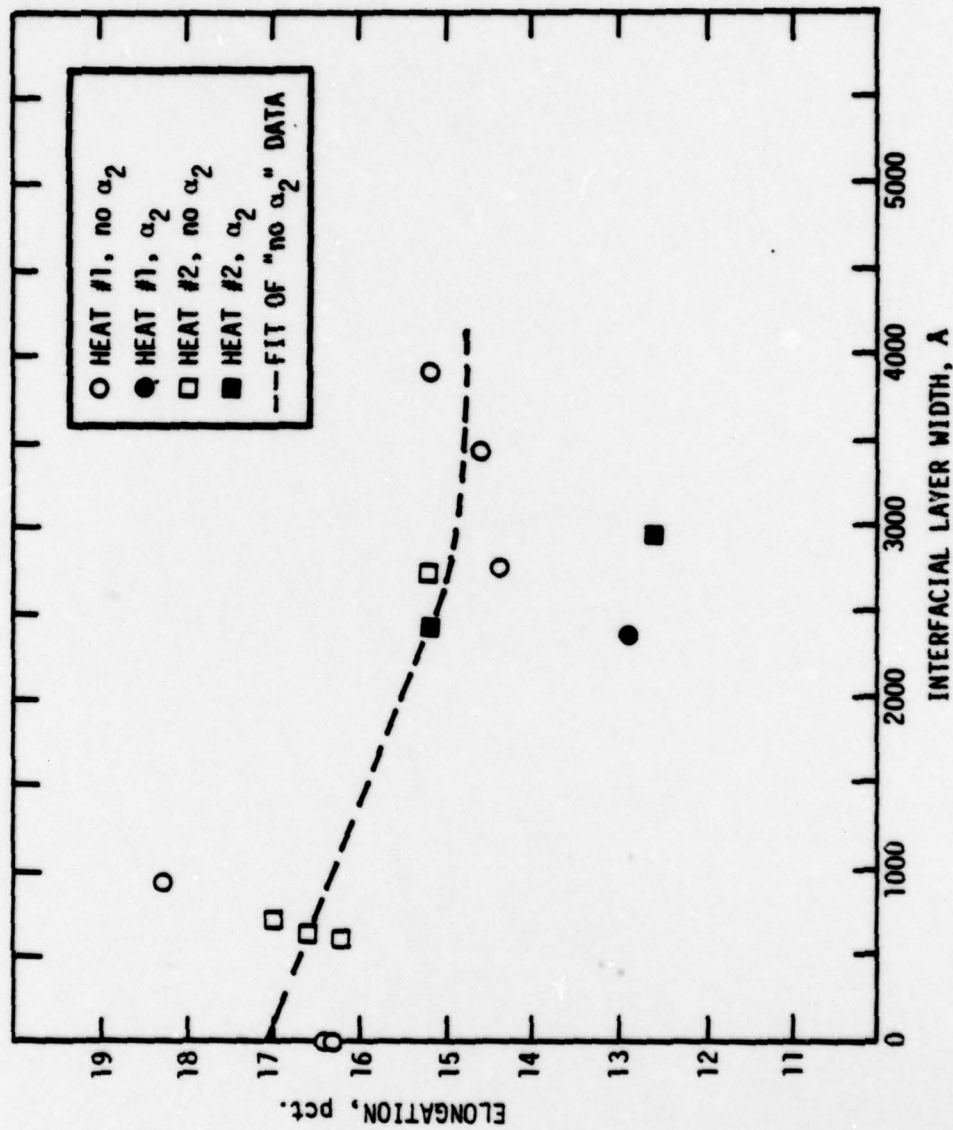


Fig. 10 Tensile elongation as a function of interface phase width.

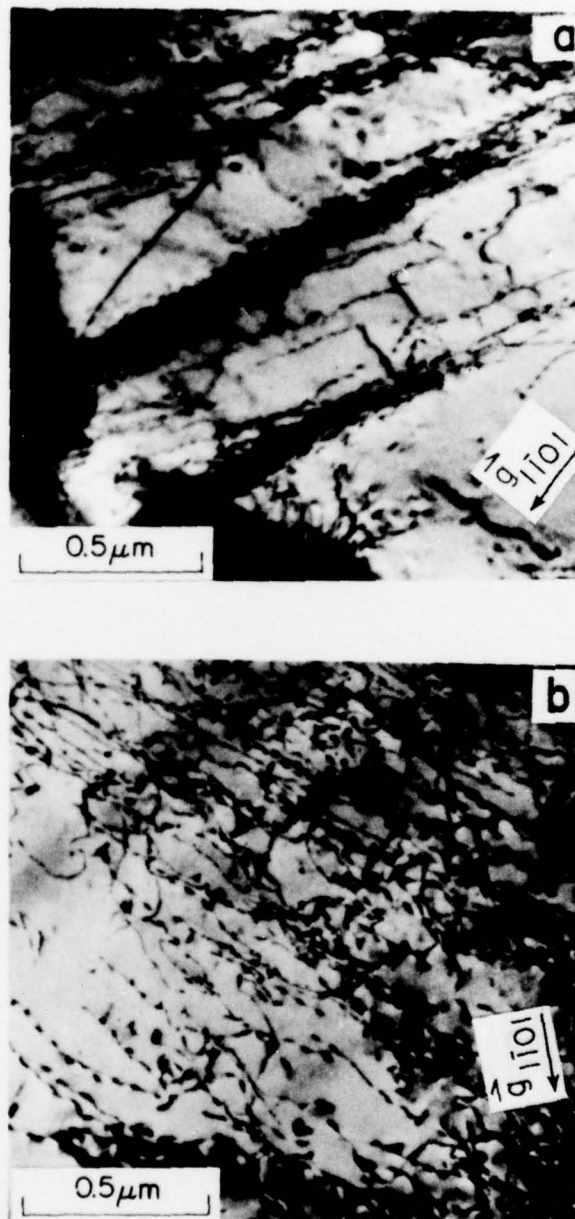


Fig. 11 Thin foil transmission electron micrographs of two Ti-6Al-4V tensile tested specimens. $[1120]$ α zone normal in both micrographs. (a) test specimen #11, $\sigma_{ys} = 115$ ksi, $\epsilon = 15.2\%$, $\bar{g} = 1101$; (b) test specimen #12, $\sigma_{ys} = 103$ ksi, $\epsilon = 16.2\%$, $\bar{g} = 1101$.

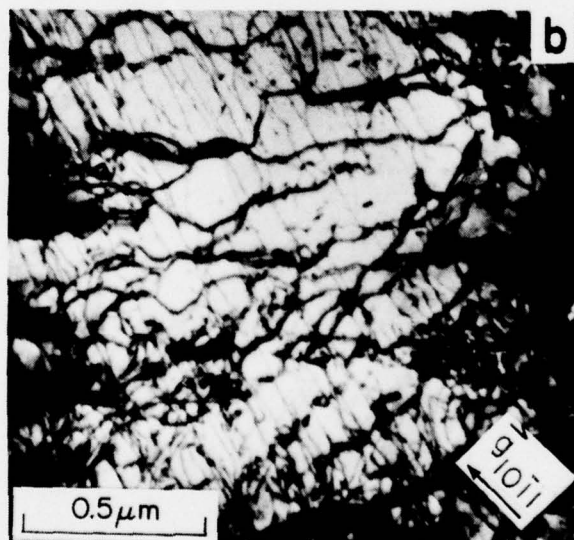
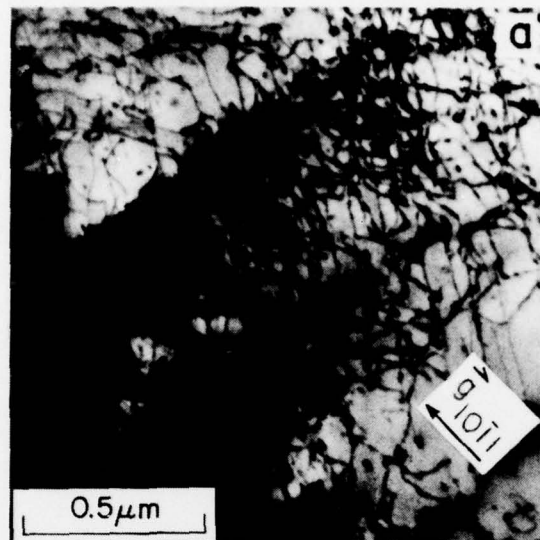


Fig. 12 Thin foil transmission electron micrographs of two Ti-6Al-4V tensile tested specimens, $[11\bar{2}3]$ α zone in both micrographs. (a) test specimen #11, $\sigma_{ys} = 115$ ksi, $\epsilon = 15.2\%$, $\vec{g} = 10\bar{1}1$; (b) test specimen #12, $\sigma_{ys} = 103$ ksi, $\epsilon = 16.2\%$, $\vec{g} = 10\bar{1}1$.

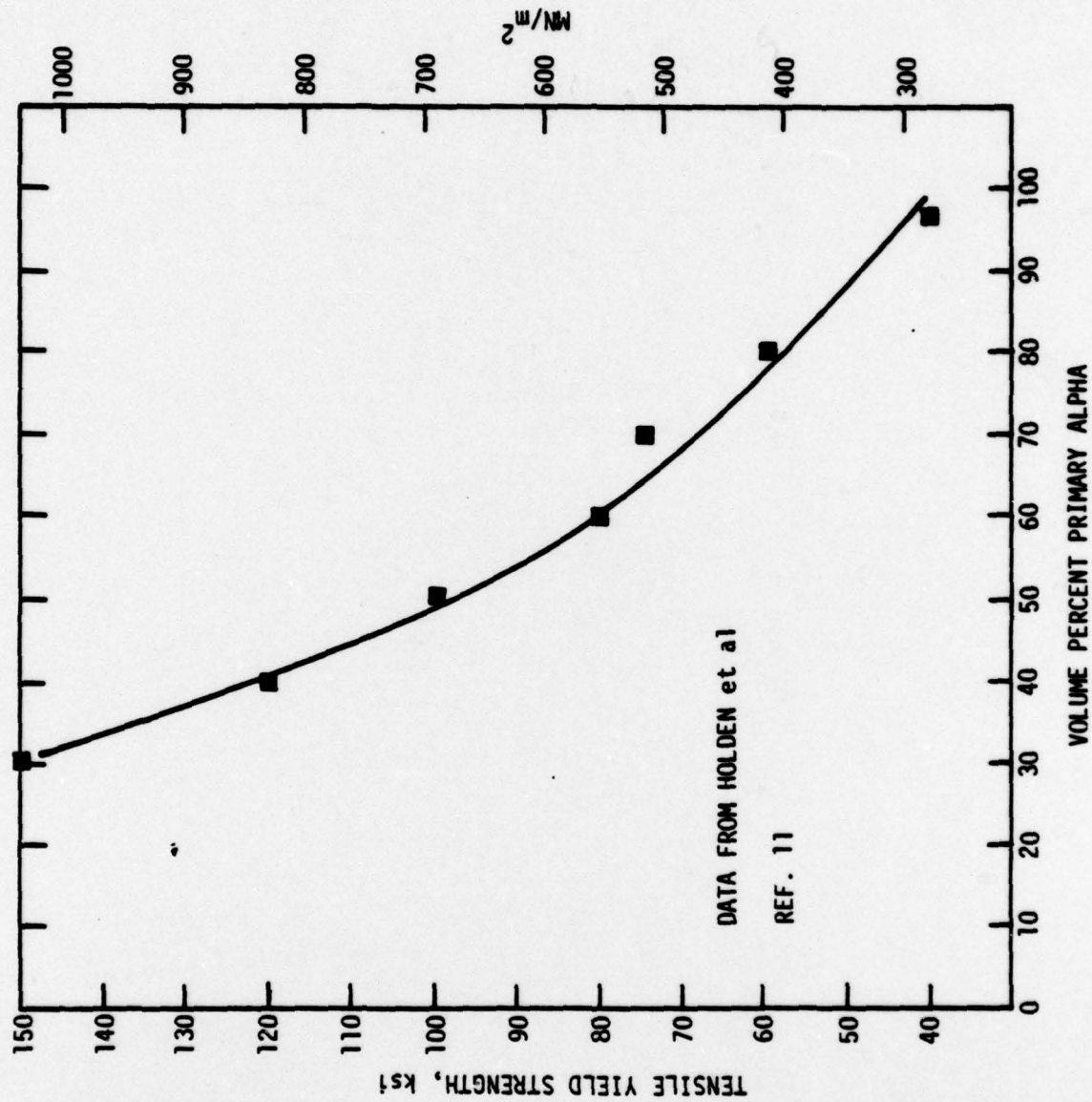


Fig. 13 Tensile yield strength as a function of volume percent primary alpha in Ti-Mn alloys. Data from Holden et al. (11).



SC5056.3TR

7.3 EFFECTS OF HYDROGEN ON ANISOTROPIC ELASTIC PROPERTIES OF bcc Ti-ALLOYS

L. A. Ahlberg, O. Buck, and N. E. Paton
Rockwell International Science Center
Thousand Oaks, California 91360 USA

The relatively large effects of hydrogen on yield strength, Young's modulus (and its temperature dependence) and the lattice parameter of metastable (bcc) Ti-alloys have been known for some time.¹⁻⁴ In this class of materials, the room temperature solubility of H is quite large, so that hydride formation does not interfere with the measurements. Some of the work² showed that both yield strength and Young's modulus decrease with increasing H content, while the lattice parameter increases. These results have been interpreted in terms of a predominantly electronic interaction between H and the host lattice. It is now known⁵ from the H dependence of second order elastic constants and the lattice parameter, as well as third order elastic constants, that the observed changes in second order constants can be separated into those due to volume changes and those from intrinsic alloying modifications of the interatomic forces, the latter being basically electronic in nature. Since third order elastic constants for the Ti-V system have been determined recently,⁶ it seemed worthwhile to measure the hydrogen sensitivity of the (anisotropic) second order elastic constants (a combination of which determines the Young's modulus). Such information would allow us to obtain insight into the physical effects of H on the alloy system and its effect on the plastic deformation of bcc metals.⁷ The present note reports on some of our observations on the Ti-V-H system.

As described earlier,⁸ an ultrasonic phase comparison technique was



SC5056.3TR

used to determine both the values of the pure-mode ultrasonic sound velocities (at about 12 MHz) and their dependence on H and temperature. From these data, the second order elastic constants C_{ij} can be determined.⁹ The specimen used for these measurements was a single crystal of Ti-40V alloy which was cut to expose a parallel pair of {100} faces (0.516 cm apart) and a parallel pair of {110} faces (0.848 cm apart). This specimen was charged in a micro-Sieverts apparatus with various amounts of H at 800°C.

Table I summarizes the second order elastic constants C_{11} and C_{44} , as well as important combinations of C_{ij} such as $C' = (C_{11} - C_{12})/2$ (a shear constant) and $B = (C_{11} + 2 C_{12})/3$ (the bulk modulus), as a function of four hydrogen levels. Furthermore, the anisotropy factor $A = C_{44}/C'$, which is a measure of the lattice instability, is given in Table I. This quantity A is of some interest to the present studies since the metastable Ti-V alloys undergo a lattice transformation [the athermal $\beta \rightarrow \omega$ transformation¹⁰] at low temperatures, which seems to be affected by the presence of H³. As was pointed out by Zener,¹¹ bcc lattices with a large A tend to be unstable and effects of H on A should give an indication of the transformation behavior of the alloy. As seen from Table I, C' is the elastic property that is most severely affected by H (in the average about -2.6% per a/o H). Therefore, A is rapidly increasing with H, indicating that the lattice becomes more unstable. We also noticed that the attenuation of the acoustic signal, that is used to determine C, increases sharply with increasing H concentration. This attenuation is caused by the $\beta \rightleftharpoons \omega$ transformation, as discussed earlier.¹⁻⁴ Thus, the large changes in A, C' , and the attenuation suggest strongly that the $\beta \rightleftharpoons \omega$ transformation temperature is raised with increasing H concentration.



SC5056.3TR

Table II summarizes the temperature dependence of the quantities given in Table I. Particularly noticeable is the change in sign for dC_{11}/dT and dC/dT (and therefore dA/dT) with increasing H concentration. It is now clear that the change in temperature behavior of the Young's modulus with increasing H, as observed on both Ti-V³ and Ti-Mo^{2,4} alloys at room temperature, is mainly due to either the contribution from dC_{11}/dT or dC'/dT or both.

Based on the present second order elastic constants data and their changes with H concentration, we can now separate the extent to which the observed changes are caused by the intrinsic alloying effect (isovolumetric changes) from those due to the lattice parameter change, which accompanies the addition of hydrogen. This was recently demonstrated for the NbH system,⁵ where it was postulated that any elastic modulus M is a function of H concentration, c, and the average lattice spacing, a, so that the total change with c can be written as

$$\frac{dM}{dc} = \left. \frac{\partial M}{\partial c} \right|_a + \left. \frac{\partial M}{\partial a} \right|_c \frac{da}{dc} \quad (1)$$

Rewriting Eq. (1) yields the relative intrinsic alloying effect

$$\left. \frac{1}{M} \frac{\partial M}{\partial c} \right|_a = \frac{1}{M} \frac{dM}{dc} - \left. \frac{1}{M} \frac{\partial M}{\partial a} \right|_c \frac{da}{dc} \quad (2)$$

with

$$\left. \frac{1}{M} \frac{\partial M}{\partial a} \right|_c \frac{da}{dc} = - \frac{B}{M} \frac{dM}{dp} \frac{3}{a} \frac{da}{dc} \quad (3)$$

where dM/dp is the pressure derivative of a modulus M and a the lattice parameter. dM/dp have been measured recently⁶ for 0 a/o H and are given in Table



SC5056.3TR

III. da/adc was determined in the present investigation to be $da/adc = 6.9 \times 10^{-4}$ per a/o H. We thus are able to estimate the intrinsic alloying effect for $M = C_{11}$, C_{44} , and C' with the results given in Table IV. Those effects due to the lattice parameter change are all negative, and those due to intrinsic effects (electronic in nature) of H on the moduli M turn out to be positive for C_{11} and C_{33} , but the isovolumetric change, $(1/C')$ ($\partial C'/\partial C'/\partial c$) at constant a_0 in Ti-40V (bcc phase) becomes large and, more important, negative. It is also noted that the $(1/M)$ (dM/dC) values for C_{44} and C' are very similar to those respective values reported for pure V.¹² This correspondence indicates that the $\Delta C'$ observed in the Ti-40V alloy is also a manifestation of the stress-induced relaxation associated with the hydrogen atoms, as suggested by Fisher et al.¹² and as indicated in the results of the acoustic phonon frequency measurements in Nb¹³ and Ta.¹⁴ The evidence for a Snoek type of relaxation is even more apparent in the substitutional solid-solution matrix, where 1) the acoustic attenuation associated directly with H is apparent here, but not in pure V, and 2) the temperature dependence of C' changes very significantly, from a negative to positive dC'/dT .

The apparent absence of a significant effect of H on dC'/dT in pure V, Nb, or Ta has been the primary argument against general acceptance of the Snoek model for explaining the decrease in C' with increasing H.¹⁵ For an interstitial of concentration N in either an octahedral or tetrahedral position within a bcc lattice of atomic volume V_0 , the $\Delta C'$ within the Snoek model is derived from a stress-induced depopulation of one set of tetragonal dipoles, with a $1/T$ dependence as follows:



SC5056.3TR

$$\frac{\Delta C'}{C'_0} = \frac{C'_H - C'_0}{C'_0} = -C'_H \frac{2}{3} (V_0/KT)(\lambda_1 - \lambda_2)^2 N \quad (4)$$

where $(\lambda_1 - \lambda_2)$ is the tetragonal strain distortion associated with the interstitials in a bcc lattice. For the Ti-40V alloy, the data obtained¹² between 275 and 311K clearly show that $(\Delta C'/C'_0)$ becomes more negative with decreasing T ; however, a simple $1/T$ dependence with a constant $(\lambda_1 - \lambda_2)$ is not observed for any of the three ternary alloys. We note, however, that the $\Delta C'$ data for the 2.4 a/o and 3.6 a/o H alloys follow a $1/(T - T_C)$ dependence quite closely with T_C values of 176 and 128K, respectively. Although the fit to a $1/(T - T_C)$ dependence indicates that an interaction between interstitial and solute atoms is somehow involved in the relaxation,¹⁶ the absence of terminal solubility data for H as a function of temperature precludes any interpretation of the T_C values. The larger T_C for the smaller H content is not consistent with expected solubility data and clearly indicates that further measurements with much improved precision are necessary to obtain a better comparison with either Eq. (4) or a similar version with a non-zero T_C term.

It should also be emphasized that dC_{11}/dT in this alloy (Table II) is also very significantly affected by the increase in H concentration, although the change in C_{11} with H is small. This suggests that the effects on dC'/dT may not be purely relaxation associated, but may also possibly be related to effects of H on the $\beta \rightarrow \omega$ transformation.

These results open up further avenues of research. For instance, the authors believe that an accurate knowledge of the anisotropic elastic moduli will be useful to determine the H dependent shear stress τ , necessary to move a dislocation on the appropriate slip plane.¹⁷ On the other hand, the data



SC5056.3TR

may give us a better understanding on the effects of H on the $\beta \rightleftharpoons \omega$ transformation. Our results show that the anisotropy factor A increases with increasing H concentration. As indicated in Fig. 1 plotting A as a function of V concentration and as a function of H in Ti-40V, yields (at low H concentrations) basically the same slope for both curves if the addition of 1 a/o H is equivalent to the extraction of 1 a/o V. Such an equivalence was speculated about earlier³ without quantitative proof. The meaning of this observation would be that the hydrogen attracts basically one electron from the vanadium. Furthermore, we should note that the effects of H on C are so large [in particular in respect to NbH⁽⁵⁾] that there is good reason to believe that the H (actually H⁻, if the previous statement is valid) gives rise to a large tetragonal distortion of the Ti-V lattice.¹³

ACKNOWLEDGMENTS

This work was supported by the Office of Naval Research under Contract No. N00014-76-C-0598. Consultations with E.S. Fisher, D.G. Westlake and J. Miller are gratefully appreciated.



SC5056.3TR

REFERENCES

1. A.W. Sommer, S. Motokura, K. Ono and O. Buck, *Acta Met.*, 21, 489 (1973)
2. N.E. Paton, O. Buck and J.C. Williams, *Scripta Met.*, 9, 687 (1975)
3. O. Buck, D.O. Thompson, N.E. Paton, and J.C. Williams, in Internal Friction and Ultra-sonic Attenuation in Crystalline Solids, Vol. 1, D. Lenz and K. Lucke, Eds., Springer Verlag, Berlin, p. 451 (1975).
4. N.E. Paton and O. Buck, in Effects of Hydrogen on Behavior of Materials (A.W. Thompson and I.M. Bernstein, Eds.), AIME, New York, p. 83 (1976).
5. O. Buck, L.A. Ahlberg, L.J. Graham, G.A. Alers and C.A. Wert, submitted to *J. Phys. Chem. Sol.*
6. K.W. Katahara, Ph.D. Thesis, Geology and Geophysics Department, University of Hawaii (1977).
7. J.W. Christian in Proceedings II Conf, on the Strength of Metals and Alloys, Am. Soc. for Metals, p. 51 (1970).
8. L.J. Graham, H. Nadler and R. Chang, *J. Appl. Phys.*, 39, 3025 (1968).
9. H.J. McSkimin, *J. Acoust. Soc. Am.*, 22, 413 (1950).
10. D. deFontaine, N.E. Paton and J.C. Williams, *Acta Met.*, 19, 1153 (1971).
11. C. Zener, Elasticity and Anelasticity of Metals, University of Chicago Press, Chicago (1948).
12. E.S. Fisher, D.A. Westlake and S.T. Ockers, *Phys. Stat. Sol. (a)* 28, 591 (1975)
13. N. Stump, A. Magerl, G. Alefeld and E. Schedler, *J. Phys. F: Metal Physics* 7, L1 (1977).
14. A. Magerl, W.D. Teuchert and R. Scherm, *J. Phys. C: Sol. State Physics* 11, 2175 (1978).
15. A. Magerl, B. Berre and G. Alefeld, *Phys. Stat. Sol. (a)* 36, 161 (1976).
16. R.W. Powers and M.V. Doyles, *J. Appl. Phys.* 30, 514 (1959).
17. A. Seeger and G. Schock, *Acta Met.* 1, 519 (1953).



SC5056.3TR

TABLE I

Anisotropic second order elastic constants of Ti-40V, doped with H, at 22.5°C.

All values, except A (dimensionless), in 10^{11} dyn/cm².

	0 a/oH	2.4 a/oH	3.6 a/oH	4.8 a/oH
C ₁₁	14.88	14.77	14.65	14.45
C ₄₄	4.053	4.076	4.085	4.104
C	2.399	2.293	2.223	2.114
B	11.68	11.710	11.690	11.630
A	1.690	1.780	1.840	1.940

TABLE II

Temperature derivatives of the second order elastic constants of Ti-40V doped with H, at 22.5°C. Units of first four derivatives in 10^7 dyn/cm²/°C. dA/dT: in 10^{-4} /°C.

	0 a/oH	2.4 a/oH	3.6 a/oH	4.8 a/oH
dC ₁₁ /dT	-17.84	-10.43	-4.37	+9.33
dC ₄₄ /dT	-4.18	-4.04	-3.77	-2.88
dC'/dT	-6.71	-1.60	+0.44	+7.88
dB/dT	-8.89	-8.30	-4.96	-1.18
dA/dT	+2.99	-0.52	-2.06	-8.60



SC5056.3TR

TABLE III

Pressure derivatives of second order elastic constants of Ti-38.5V,
from Reference 6 (all units dimensionless).

dC_{11}/dP	dC_{44}/dP	dC'/dP	dB/dP
4.63	0.431	0.533	3.92

TABLE IV

The effects of H on the moduli on Ti-40V (all units in 10^{-3} per a/oH)

1st column: measured values.

2nd column: changes due to lattice expansion.

3rd column: Changes due to intrinsic effects.

M	$\frac{1}{M} \frac{dM}{dc}$	$\frac{1}{M} \frac{\partial M}{\partial a}$	$\frac{da}{dc}$	$\frac{1}{M} \frac{\partial M}{\partial c}$	a
C_{11}	-6.02	-7.65		+1.63	
C_{44}	+2.42	-2.62		+5.04	
C'	-2.47	-5.46		-19.2	



SC5056.3TR

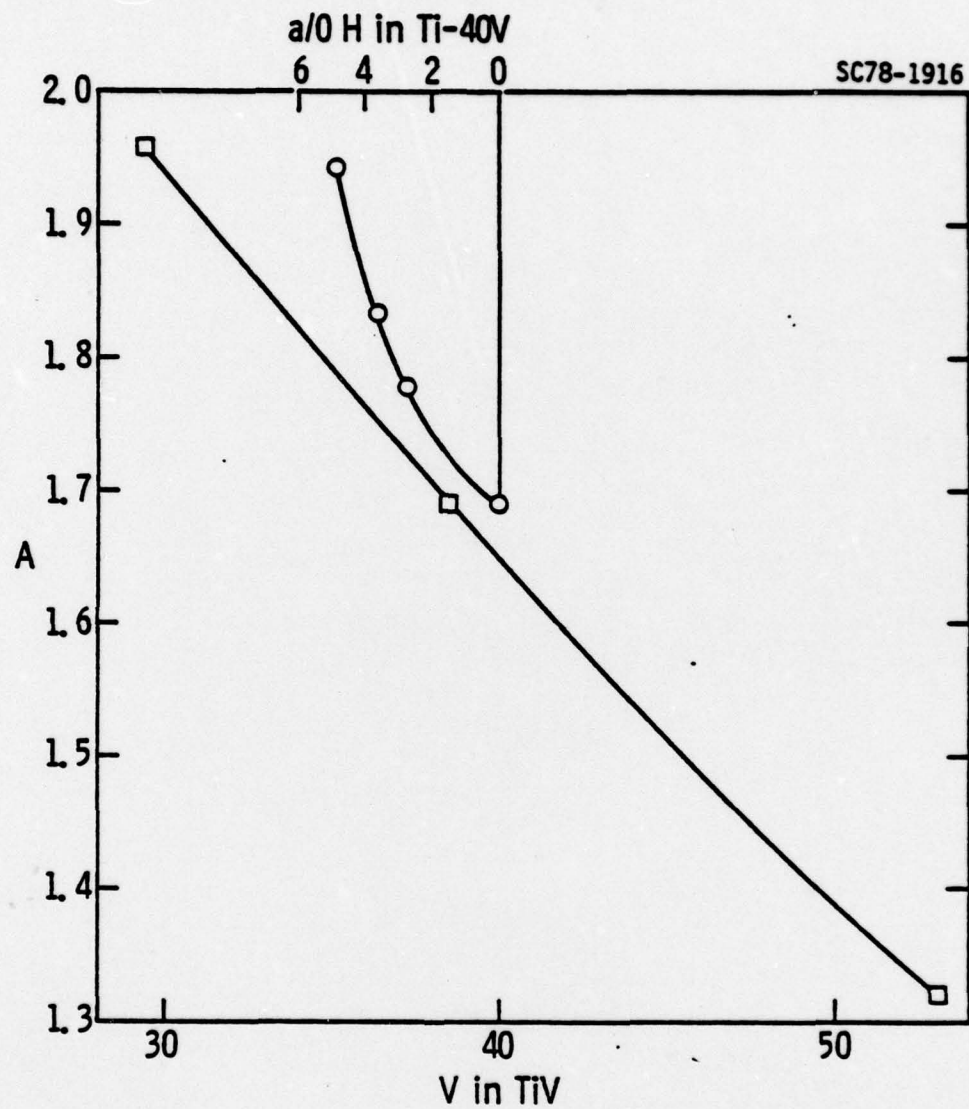


Fig. 1. The change of anisotropy factor with vanadium in Ti-V (6) and hydrogen concentration in Ti-40V.